Optimised Label-Free Biomarker Assays with Electrochemical Impedance Spectroscopy

A thesis submitted for the degree of

Masters of Science (by Research)

Trinity 2013



Mengyun Xu

St Hilda's College

Optimised Label-Free Biomarker Assays with Electrochemical Impedance Spectroscopy

Mengyun Xu

St Hilda's College, University of Oxford
Masters of Science (by research) in Inorganic Chemistry
Trinity 2013

ABSTRACT

There is huge academic interest and clinical need associated with the development of biomarker immunoassays where general aims are the generation of highly specific, convenient and sensitive sensing formats. In this project, a powerful electrochemical technique, electrochemical impedance spectroscopy (EIS), is applied in the establishment of powerful biomarker detecting protocols. Firstly, ultrasensitive, label-free and reusable insulin sensors, based on an antibody-PEGylated thiol self-assembly monolayer (PEG thiol SAM) interface, were produced and characterised *via* Faradaic EIS, presenting a detection limit (LOD) of 1.2 pM, a linear range across four orders of magnitude, and high sensitivity in even 50 % serum. By applying similar surface chemistry, a label-free biosensor, specific for the detection of α-synuclein antibodies, was fabricated. The α-synuclein interfaces used enabled the reliable detecting of this biomarker in patient sample serum. The concentration levels in the control and a patient group were determined to be significantly different, and, significantly, this difference was consistently across two different cohorts. Strikingly, this could potentially underpin an entirely new means of early Parkinson's disease (PD) diagnosis. Non-Faradaic EIS methods were additionally applied to label-free insulin assays at both PEG thiol SAM and zwitterionic polymer film interfaces. The latter presented not only an exceptionally non-fouling interface, but also one seemingly both highly biocompatible and facilitating enhanced receptor: target binding. Finally, impedance assays, though potent, generally, operate by sampling only one of a limited number of available experimental variables, typically, R_{ct} for Faradaic EIS, or C or Z for non-Faradaic EIS. Work carried out herein also explores the generation and utility of a portfolio of mathematically derived immittance functions all obtained from the same raw data sets. A particular focus was the examination of whether these were capable of increasing assay sensitivity and efficiency above normal impedance treatments.

ACKNOWLEDGEMENT

Firstly, I would like to thank Dr Jason J Davis for offering this opportunity to work on such an exciting and state-of-the-art project, and for the support and supervision he has provided throughout my programme.

I am also grateful for the support and help from the present and former members of the JJD group, and in particular for the expertise and advice from Dr Xiliang Luo, Dr Wen-Yen Huang, Dr Joshua Lehr, Dr Gemma-Louise Davies, and Mr Matthew Cunningham.

I would also like to thank the Professor Ludmilla Morozova-Roche from Umeå University, Sweden, and Dr Richard Wade-Martins from University of Oxford, United Kingdom, for providing the patient sera samples used in this project.

Finally, I would like to express my gratitude to my family for their support and encouragement.

Contents

CHAPTER 1. INTRODUCTION ---- 1

1.1 IMMUNOASSAYS ---- 1
1.1.1 Typical Techniques for Labelled Immunoassays ---- 1
1.1.2 Typical Techniques for Label-Free Immunoassays ---- 4
1.1.3 Anti-Fouling Interfaces ---- 7
1.2 ELECTROCHEMICAL IMPEDANCE SPECTROSCOPY (EIS) ---- 8
1.2.1 Faradaic & Non-Faradaic EIS ---- 9
1.2.2 Electrical Equivalent Circuits (EECs) ---- 10
1.2.3 Parameters & Data Presentation for EIS ---- 12
1.3 BIOMARKERS ---- 16
1.3.1 Insulin ---- 17
1.3.2 α-Synuclein Auto-Antibody ---- 22
1.4 CHALLENGES & OBJECTIVES ---- 24

CHAPTER 2. EXPERIMENTAL SECTION ---- 26

2.1 MATERIALS & REAGENTS ---- 26
2.2 APPARATUS ---- 27
2.3 PRE-TREATMENT OF GOLD ELECTRODES ---- 27
2.4 FABRICATION OF BIOSENSORS ---- 30
2.4.1 The PEGylated Thiol Self-Assembled Monolayer (PEG Thiol SAM) ---- 30
2.4.2 The Zwitterionic Polymer Film ---- 31
2.4.3 Immobilisation & Characterisation of Receptor Interfaces ---- 32
2.5 *IN SITU* & *EX SITU* DETECTION ---- 34
2.6 FARADAIC EIS MEASUREMENTS ---- 34
2.6.1 The Concentration of The Redox Probe ---- 35
2.6.2 Data Processing ---- 36
2.6.3 Incubation Time ---- 37
2.6.4 Assay Performances ---- 39
2.6.5 Regeneration of Receptor Interfaces ---- 39
2.7 NON-FARADAIC EIS MEASUREMENTS ---- 40
2.7.1 Data Processing ---- 40
2.7.2 Stability Test of Polymer Film ---- 41
2.7.3 Assay Performances ---- 41
2.8 ANALYTICAL CURVES & LANGMUIR PLOTS ---- 42
2.9 THE DETECTION OF PARKINSON'S DISEASE PATIENT SAMPLES ---- 44
2.9.1 Patient Samples ---- 44
2.9.2 Self-Calibration Method ---- 45
2.9.3 Standard Addition Method ---- 46
2.9.4 Box-And-Whisker Plots ---- 47
2.10 ELECTROCHEMICAL IMMITTANCE ANALYSIS ---- 49
2.10.1 Data Source ---- 49
2.10.2 Definitions of Investigated Parameters ---- 50

2.10.3 Data Processing ---- *51*

CHAPTER 3. INSULIN ASSAY *VIA* FARADAIC EIS ---- 53

3.1 OBJECTIVES ---- 53
3.2 BIOSENSOR FABRICATION ---- 54
3.3 THE DETECTION OF INSULIN IN A BUFFER SOLUTION ---- 56
3.4 THE DETECTION OF INSULIN IN COMMERCIAL BLOOD SERUM ---- 58
3.5 REGENERATION OF THE SENSOR SURFACE ---- 61
3.6 CONCLUSIONS ---- 62

CHAPTER 4. A-SYNUCLEIN ANTIBODY ASSAY *VIA* FARADAIC EIS ---- 63

4.1 OBJECTIVES ---- 63
4.2 BIOSENSOR FABRICATION ---- 64
4.3 DETECTION OF COMMERCIAL A-SYNUCLEIN ANTIBODY IN A BUFFER SOLUTION ---- 65
4.4 DETECTION OF COMMERCIAL A-SYNUCLEIN ANTIBODY IN HUMAN SERUM ---- 67
4.5 DETERMINING THE ACCURACY OF THIS METHODOLOGY ---- 69
4.6 DETECTION OF A-SYNUCLEIN AUTO-ANTIBODY IN PATIENT SAMPLES ---- 71
4.7 CONCLUSIONS ---- 75

CHAPTER 5. INSULIN ASSAY *VIA* NON-FARADAIC EIS ---- 77

5.1 OBJECTIVES ---- 77
5.2 ZWITTERIONIC POLYMER INTERFACES ---- 78
5.2.1 Stability Test ---- *78*
5.2.2 Biosensor Fabrication ---- *80*
5.2.3 Frequency-Dependent Response ---- *81*
5.2.4 Concentration-Dependent Response ---- *83*
5.2.5 Characterisation of Anti-Fouling Property ---- *85*
5.3 PEG THIOL SAM INTERFACES ---- 86
5.3.1 Biosensor Fabrication ---- *86*
5.3.2 Frequency-Dependent Response ---- *87*
5.3.3 Concentration-Dependent Response ---- *88*
5.3.4 Characterisation of Anti-Fouling Property ---- *90*
5.4 CONCLUSIONS ---- 91

CHAPTER 6. ELECTROCHEMICAL IMMITTANCE ANALYSIS ---- 94

6.1 OBJECTIVES ---- 94
6.2 FREQUENCY SPECTRA (FS) ---- 95
6.3 FREQUENCY-DEPENDENT ANALYSIS ---- 96
6.4 CONCENTRATION-DEPENDENT ANALYSIS ---- 99
6.5 CONCLUSIONS ---- 101

CHAPTER 7. CONCLUSIONS & FUTURE WORK ---- 103

CHAPTER 8. REFERENCES: ---- 106

APPENDIX A. FREQUENCY SPECTRA (FS) ---- 112

APPENDIX B. TABLE OF FIGURES ---- 116

ABBREVIATIONS

AC:	Alternating Current
BSA:	Bovine Serum Albumin
C_{DL}:	Double Layer Capacitance
CE:	Counter Electrode
CPE:	Constant Phase Element
CV:	Coefficient of Variation
DC:	Direct Current
EEC:	Electrical Equivalent Circuits
EIS:	Electrochemical Impedance Spectroscopy
ELISA:	Enzyme-Linked Immuno Sorbent Assay
FRA:	Frequency Response Analyser
FS:	Frequency-Dependent Spectra
GCE:	Glassy Carbon Electrode
H-Y:	Hoehn and Yahr Scale
K_D:	Dissociation Constant
LOD:	Limit of Detection (or Detection Limit)
PBS:	Phosphate Buffered Saline
PBST:	Phosphate Buffered Saline Tween-20
PCBMA:	Poly (Carboxybetaine Methacrylate)
PD:	Parkinson's Disease
PEG:	Polyethylene Glycol
pI:	Isoelectric Point
QCM:	Quartz Crystal Microbalance
R_{ct}:	Charge Transfer Resistance
R_s:	Resistance of Solution
RS:	Relative Sensitivity
SAM:	Self-Assembled Monolayer
SPR:	Surface Plasmon Resonance
WE:	Working Electrode
Z^*:	Complex Impedance

Chapter 1. Introduction

1.1 Immunoassays

Immunoassays are chemical analyses of the presence or concentration of substances (*e.g.* antibodies, antigens and hormones), which make use of immunological reactions. For over 40 years, immunoassays have been used in hospitals for the diagnosis of medical condition, as well as in the food industry for quality-control assessment. Generally, based on their sensing performances, immunoassays can be subdivided into labelled and label-free. There are different categories of immunoassays and various anti-fouling interfaces, which have been applied to reduce non-specific binding.

1.1.1 Typical Techniques for Labelled Immunoassays

Labelled immunoassays are performed by conjugating analytes or a third reagent with a special label, which can convert the changes, induced by binding between the receptor and target, into detectable signals. The first example can be traced back to 1959, when a radioimmunoassay of iodine-131 labelled bovine insulin, in human blood plasma, was conducted by Yalow and Berson.[1] Since then, a wide variety of labels have been used for immunoassays, including radioactive,[1] fluorescent,[2] and luminescent transduction.[3] However, the application of directly labelled assays is severely constrained, due to the difficulties and inaccuracy arising from the requirement of labelling all the analytes. Therefore, labelled sandwich assays, where secondary

antibodies, instead of analytes, are labelled, have been presented to address this problem. The typical approach to conduct this technique is to firstly capture the analyte with a primary antibody, before adding a labelled secondary antibody, which can specifically bind to the analyte and generate an observable signal. In 1975, the discovery of producing monoclonal antibodies specific to certain binding sites (epitopes) considerably increased the applicability of labelled sandwich assays.[4] Based on this protocol, primary and secondary antibodies can be and have been designed, so that they, like monoclonal antibodies, are specific to two different epitopes on the same antigen, resulting in a considerable reduction in the cross-reactivity of a secondary antibody and hence increased specificity.

The enzyme-linked immune sorbent assay (ELISA), first developed in the early 1970s as a replacement of the radioimmunoassay (which suffers from serious hazards associated with the preparation and handling of the radioactive reagents), has been commonly used, not only for antibody concentration determination[5] and virus testing,[6, 7] but also in home pregnancy tests[8] and the food industry.[9] In general, ELISA is significantly less harmful and more user-friendly than the radioimmunoassay (Figure 1.1). Typically, a layer of receptor (antigen or antibody) is firstly constructed in a sample well, followed by treatment with a blocking buffer solution (mostly BSA solution, this prevents unwanted adsorption onto the substrate). The quantification of the binding signals is achieved by conjugating the target with enzymes (*i.e.* alkaline phosphatise [10]), which can specifically effect the changes in the colour and the darkness of the substrates (such as *para*-nitrophenyl phosphate, pNPP), allowing measurement of the intensity of the light transmission at a certain wavelength (405 nm for pNPP).

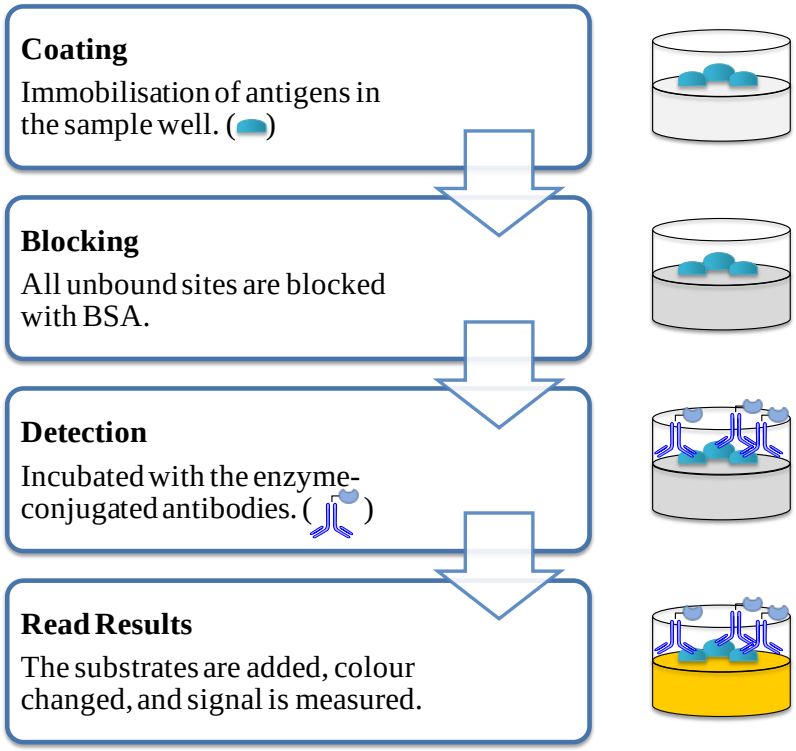


Figure 1.1. Enzyme-linked immune sorbent assay (ELISA) overview flowchart and scheme.

In addition to the typical format of ELISA (direct assays) describe above, techniques providing indirect and sandwich assays have also been developed (Figure 1.2). The latter two follow the same basic procedure as that of a direct assay with some additions, such as capturing an antibody and a secondary antibody. Direct and indirect assays have the advantage of fewer operational steps, while sandwich assays offer improved efficiency, sensitivity and specificity over ELISA.[6, 11]

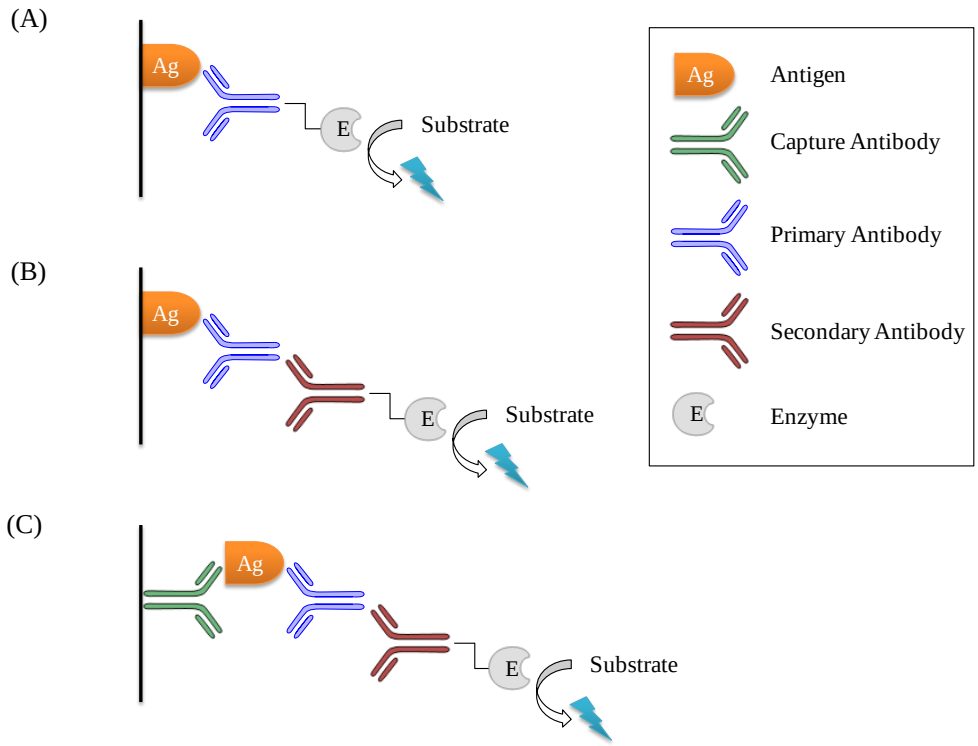


Figure 1.2. The three types of enzyme-linked immune sorbent assay (ELISA). (A) Direct assay, (B) Indirect assay, (C) Sandwich assay.

1.1.2 Typical Techniques for Label-Free Immunoassays

Although labelled assays have been well established and applied on a great number of assays, their disadvantages are clear. They require the conjugation of antibodies with labels for each individual experiment; considerably increasing the cost and preparation time. Furthermore, this modification is potentially destructive to the structure and function of target, reducing its efficiency and efficacy.

Therefore, there has been a strong demand for the development of label-free assays, a technique that detects a specific analyte without labelling the analyte or adding a third labelled reagent. Due to the lack of indication and amplification of the labels, it is of great importance to find an appropriate method of measurement, which is high

throughput and particularly sensitive. To date, mass transduction, optical and electrochemical techniques have been developed for label-free immunoassays, and widely reported in the literature.[12-14]

Quartz crystal microbalance (QCM) is the representative mass transduction method for immunoassays. Shons and co-workers reported the first BSA-antibody biosensor, characterised by QCM.[15] The measurements were achieved by recording the mass-induced changes in the oscillator-produced frequency, when antigens are bound to antibodies on a chip.[16] Recently, in order to improve its real-time measurement capabilities, QCM has been combined with flow-injection analysis (FIA).[17] One of the most powerful optical techniques, surface plasmon resonance (SPR) characterises the antigen-antibody interaction by recording the refractive index, which alters upon binding.[18] Based on this principle, some upgraded SPR techniques have been developed; for example, multi-channel SPR has been applied for multi-detection of various target in human serum.[12]

Both QCM and SPR demonstrate the great advantages of conducting label-free, real-time measurements over a variety of molecules with diverse binding affinities.[19] However, their application has been severely limited by the concern of the low throughput.[19] Though it seems that merging traditional SPR technique with protein arrays could be a potential solution, outstanding improvement of the throughput has not been reported in the literature to date.[20]

Electrochemical methods, which utilise electrical signals to characterise the binding of analytes, are promising for use in performing label-free, sensitive, robust and

rapid detections.[21-25] Based on the differences of measured electrical signals, electrochemical measurement methods can be further divided into five categories, amperometry or voltammetry (measuring current), potentiometry (measuring potential or charge accumulation), conductometry (measuring the conductivity inter-electrode medium), field-effect-transistor-based method (measuring current or potential going through a semiconductor), and impedance spectroscopy (measuring the variation of the ratio of a sinusoidal potential to the induced current, discussed further in Section 1.2).[26]

A preferred method for label-free detection is electrochemical impedance spectroscopy (EIS), measuring the electrical impedance of an interface in various alternative current (AC) steady states (by varying the frequency of the sine wave). During the EIS measurements, a relatively small amplitude perturbation (typically 5 – 20 mV) is applied together with a constant mild direct current (DC) bias (0 mV for non-Faradaic EIS and generally < 250 mV for Faradaic EIS); this mild condition can ensure the minimum effect on the target. Considering its sensing ability, EIS is powerful in analysing the complex electrical resistance of a system and is highly sensitive to interface phenomena, and minute changes in target binding to an interface can be directly detected, without an additional label.[27] Furthermore, EIS is an exceedingly informative technique, since each measurement can collect responses at tens of frequencies spanning several orders of magnitude; it provides abundant options for the selection of the optimum (most responsive) data.

In years to come, the target of developing immunoassays is likely to be producing point-of-care devices, which are designed to be easy to use, inexpensive, portable, rapid and sensitive, and are ideal for non-professional patient use. EIS, with features of high

sensitivity, non-destructive effect on analytes and high throughput, has the potential to meet all of the above requirements and to achieve this transfer with ease. This technique will be further introduced in Section 1.2.

1.1.3 Anti-Fouling Interfaces

For the purpose of clinical applications, it is highly desirable, though challenging, to perform immunoassays in complex bio-fluids, such as blood, serum, cerebrospinal fluid (CSF) and urine, due to the extremely complicated components; for example, plasma contains > 30,000 proteins, various enzymes and ions.[28] The selectivity in recorded signals, differentiating the antigen-antibody binding and non-specific interference, is in particular a concern for label-free immunoassays, which are performed by measuring the changes in mass, refractive index, current, *etc*; any adsorption of non-specific components (some of which can be electroactive) can result in noticeable false signals. One possible approach to increase the selectivity of label-free immunoassays is to improve the anti-fouling ability of the biosensing interfaces, by the addition of inert proteins (*e.g.* BSA), surfactants (*e.g.* Tween-20), or by constructing a hydrophilic and neutrally-charged interface, which is the most efficient and the most common approach.[26]

Non-specific bindings, mostly electrostatic, and hydrogen bonding, can be considerably reduced by the formation of a hydrophilic and neutral interface. To date, the formation of an oligoethylene glycol (OEG) or a polyethylene glycol-based (PEG) monolayer has successfully provided an effective anti-fouling interface for biomedical applications.[29] The anti-fouling properties of these PEG interfaces have been

characterised by many methods, such as X-ray photoelectron spectroscopy (XPS) and atomic force microscopy (AFM).[30] The PEG monolayer has been reported to resist non-specific adsorption in 10 % serum.[31]

In addition to anti-fouling materials based on PEG and its derivatives, some biocompatible polymers have attracted attention. In 2006, Zhang and co-workers characterised the anti-fouling properties of a zwitterionic polymer, poly (carboxybetaine methacrylate) (PCBMA), which was thought would make a significant contribution at improving the surface resistance, due to its neutral surface charge and high hydrophilicity.[32] In 2010, the high anti-fouling ability of the PCBMA was further characterised by determining the protein adsorption of this polymer film, utilising SPR. Since an efficient assay of a cancer biomarker in 100 % serum was achieved, this PCBMA has been regarded as a promising anti-fouling material.[33] However, this polymer has not yet been applied in the fabrication of label-free electrochemical biosensors.

1.2 Electrochemical Impedance Spectroscopy (EIS)

Electrochemical impedance spectroscopy (EIS), as a powerful tool for performing assays, has been used for the detection of a variety of substances, such as antibodies and antigens,[34] peptides,[35] nucleic acids,[36] aptamers,[37] and cells.[38] Depending on the presence or absence of a redox process near the electrode / electrolyte interface, EIS can be subdivided into two categories, Faradaic and non-Faradaic EIS. This section will

introduce previous studies, electrical equivalent circuit models, and graphical representations of the data collected by both techniques.

1.2.1 Faradaic & Non-Faradaic EIS

Faradaic EIS measurements are performed in the presence of a redox probe, such as $[Fe(CN)_6]^{4-/3-}$ [36] and ferrocene.[39] The redox probe is responsible for the redox-related charge transfer in solution and across the electrode / electrolyte interface. In order to prevent depletion of this Faradaic process, a direct current (DC) bias is always applied, which is typically the halfway potential of the chosen redox couple. Faradaic EIS is used in a great number of reported EIS experiments, and it is very promising for point-of-care applications because of its remarkable sensitivity and ease of performance. Immunoassays utilising Faradaic EIS mostly show a detection limit (LOD) at sub nanomolar level.[26] In 2013, Elshafey and co-workers reported a label-free impedimetric biosensor for Murine double minute 2, a brain cancer biomarker, with an outstanding LOD of 5.2 fM.[40]

However, as a result of the extra addition of redox probes, Faradaic EIS is considered to be less transferable to point-of-care devices.[27] The upgraded technique is non-Faradaic EIS, which works in the absence of redox probes, at zero DC bias voltage. In 1996, Rickert and co-workers attempted to perform the non-Faradaic detection of an antibody immobilised on a mixed alkane thiol self-assembled monolayer by measuring capacitance signals. It was claimed that reliable evidence of target binding were witnessed.[41] After that, a variety of studies on non-Faradaic EIS have been reported.[42-44] Similarly low LOD at nanomolar levels can still be achieved without redox probes,[45, 46]

however, fewer examples of performing assays in complex solutions have been seen, probably due to the difficulties of reducing non-specific bindings.

1.2.2 Electrical Equivalent Circuits (EECs)

EIS involves monitoring the change in surface impedance, as electrochemical reactions occur at the electrode / electrolyte interface. Electrical equivalent circuits (EECs) are commonly used to describe these reactions occurring at the electrified interfaces. The typical EEC model for Faradaic EIS is Randles equivalent circuit, while the EECs for non-Faradaic are relatively diverse, however, all are broadly based on Randles equivalent circuit with some variations. Thus, in this section, firstly, the standard Randles equivalent circuit will be discussed.

Figure 1.3 demonstrates the elements of a Randles equivalent circuit, with an illustration of the representative electrified interface below, to aid understanding of each element. A double layer, which consists of a Helmholtz plane and a diffusion layer, is formed close to the electrified interface, where the working electrode (WE) is positively charged. The Helmholtz plane normally refers to the dense monolayers of cations and anions, forming a capacitor near the WE surface, known as a double layer capacitor (C_{DL}). When electrochemical reactions take place on this interface, the electron transfer process across this interface can be triggered by overcoming an activation barrier; described as the charge transfer resistance (R_{ct}). Similarly, this barrier of charge transfer exists in the bulk solution between the WE and the counter electrode (CE); this is described as solution resistance (R_s). The Warburg impedance (Z) is regarded as an

element that characterises the one-dimensional diffusion process of components, such as cations and anions, from the bulk solution to the WE.[47]

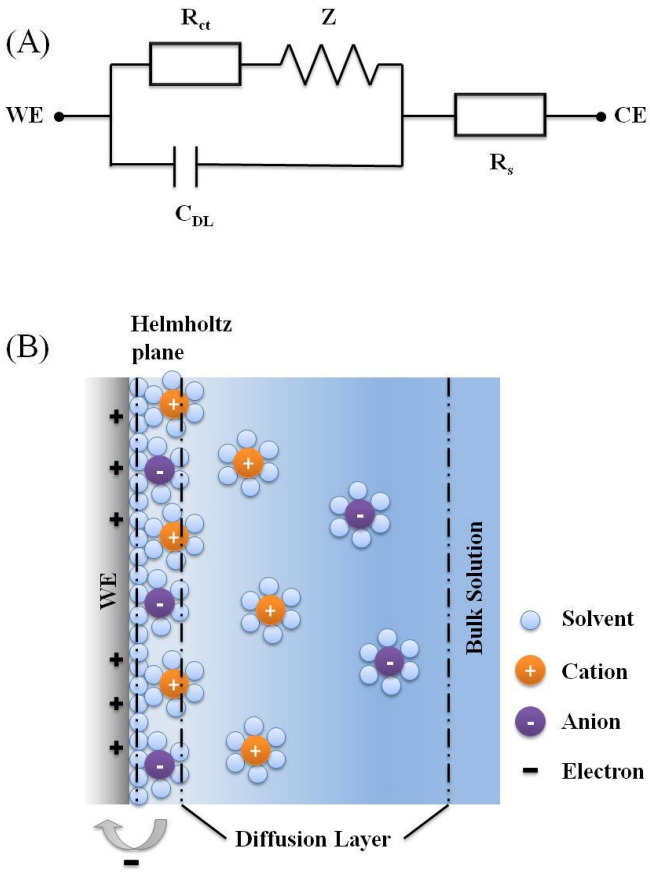


Figure 1.3. (A) The Randles equivalent circuit of an electrified interface. Elements in the circuit correspond to each interfacial component; (WE) working electrode, (C_{DL}) double-layer capacitor, (R_{ct}) charge transfer resistor, (Z) Warburg impedance, (R_s) resistor of the bulk solution, (CE) counter electrode. (B) Scheme of the double layer which focuses at an electrified interface, where the working electrode (WE) is positively charged. The monolayers of ions absorbed onto the surface, in Helmholtz plane, can be considered as a simple capacitor.

However, for non-Faradaic EIS, due to the absence of redox probes, a more complicated unknown process is happening between the WE and CE, instead of the Faradaic redox process. Therefore, modelling a proper EEC that can accurately describe the situation in solution is extremely difficult. Various EEC models have been

discussed.[48, 49] However, it remains inconclusive that which one is the most applicable EEC model.

1.2.3 Parameters & Data Presentation for EIS

To perform EIS, Faradaic and non-Faradaic, an alternative voltage is usually applied between the WE and CE; there is a shift of the sine wave between the voltage and the induced alternative current, namely phase (ϕ) (Figure 1.4).

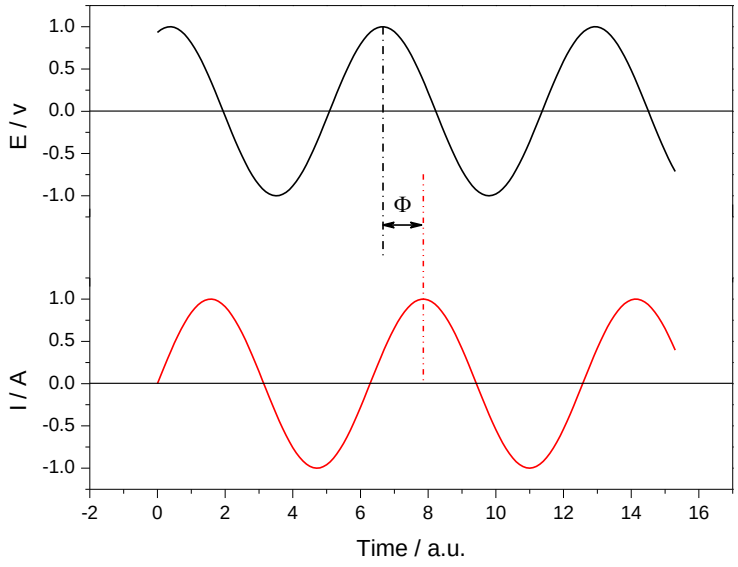


Figure 1.4. A diagram of alternative voltage and alternative current. There is a shift between these two sine waves, namely phase (ϕ).

The impedance, a frequency-related complex function, is mathematically defined as the ratio of alternative voltage (V^*) to current (I^*). The equations for voltage (V^*), current (I^*) and complex impedance (Z^*) are shown as follows:

$$V^*(\omega t) = |V| \exp(j\omega t) \quad \textbf{1.1}$$

$$I^*(\omega t) = |I| \exp[j\omega(t-\phi)] \quad \textbf{1.2}$$

$$Z^* = \frac{V^*(\omega t)}{I^*(\omega t)} = |Z| \exp(j\omega\phi) \qquad \left(j = \sqrt{-1}\right) \quad \textbf{1.3}$$

where t is the time and ω is the angular velocity, a frequency-related parameter.

In an electrolytic cell, the current is generated by the diffusion process of components, such as cations and anions, from the bulk solution to the WE, and the redox reactions near the electrode / electrolyte interface. When an alternative voltage is applied, either a change of frequency or an alteration at the electrified interface can give rise to the changes in the sine wave of current, namely phase shift. Accordingly, since the complex impedance (Z^*) is a phase-related function, phase shift can result in changes in Z^* (Equation 1.3). This complex function (Z^*) can be further mathematically distributed to two parameters; real impedance (Z') and imaginary impedance (Z''), as follows:

$$Z^* = |Z| \exp(j\omega\phi) = |Z| \cos\phi + j|Z| \sin\phi \quad \textbf{1.4}$$

$$Z' = |Z| \cos\phi \quad \textbf{1.5}$$

$$Z'' = |Z| \sin\phi \quad \textbf{1.6}$$

There are various ways of presenting EIS data; amongst them, Nyquist and Bode plots are the most common. The Nyquist plot, plotting the real impedance (Z') on the x

axis and the imaginary impedance (Z'') on the y, across a certain range of frequencies, is typically used to present Faradaic EIS data, shown in Figure 1.5. In the Nyquist plot, the Faradaic EIS data can be fitted by Randles equivalent circuit, and critical information can be read out, such as modulus impedance ($|Z|$, $|Z|^2 = |Z'|^2 + |Z''|^2$), phase (ϕ, $\tan \phi = |Z''| / |Z'|$), and more importantly the charge transfer resistance (R_{ct}, the diameter of the semi-circle), which is the major parameter allowing data processing of Faradaic EIS. For immunoassays, signals in R_{ct} arise as a result of the binding of targets, which effectively changes the activation barrier of electron transfer from the redox probe to the electrode. Although in certain cases, a drop in R_{ct} was observed, responsible for the binding of a target,[50] the majority of Faradaic EIS studies report an increase in R_{ct}.

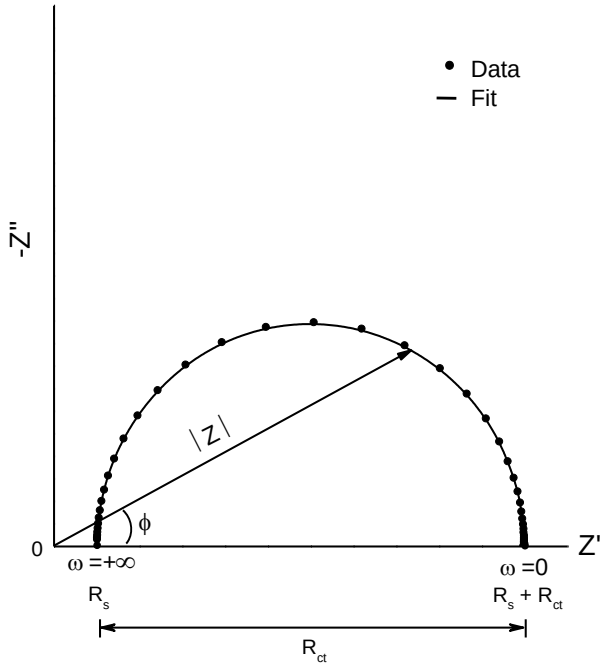


Figure 1.5. A representative example of the Nyquist plot.

For Faradaic EIS, the Nyquist plot is a powerful tool, since the values of R_{ct}, the most important parameter, can be directly calculated. However, this plot is not ideal to demonstrate the relationship between the frequency and the responses in impedance (Equation 1.3). Furthermore, for non-Faradaic EIS, due to the absence of charge transfer process, R_{ct} is not an applicable parameter, and the Nyquist plot loses its advantage of data presentation. In this instance, the Bode plot is preferred.

Typically, the Bode plot displays the modulus values of impedance ($|Z|$) and phase (ϕ) along with the logarithmic frequencies (from left to right going from zero to infinite), shown in Figure 1.6. Theoretically, the response in $|Z|$ is dominated by solution resistance (R_s) at high frequencies, and the phase varies in the range from 0° to 90°. However, this curve has been seen to be distorted to various degrees.[51, 52] In the cases of non-Faradaic EIS studies, in addition to the typical Bode plot, responses in other parameters, such as capacitance (C, $C = 1 / (\omega Z^*)$) and admittance (Y, $Y = 1/Z^*$), were also presented in the format of Bode plots to investigate the frequency dependence.[53]

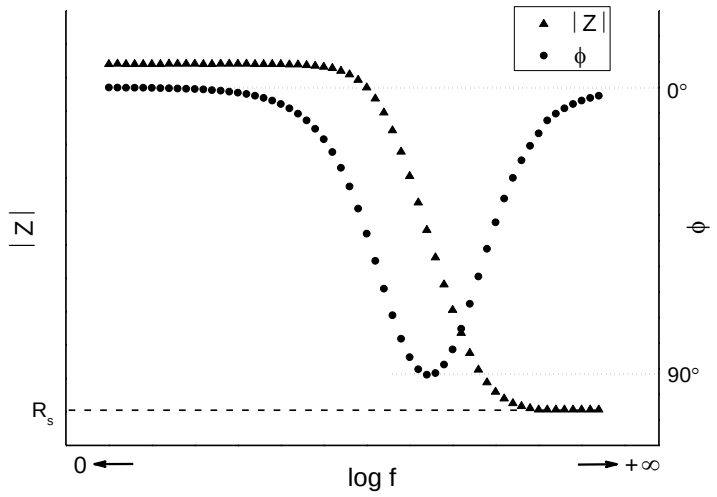


Figure 1.6. A representative example of the Bode plot.

In summary, for Faradaic EIS, charge transfer resistance R_{ct} is the most frequently used parameter, and it can be simply calculated by fitting the data with the Randles equivalent circuit in a Nyquist plot. However, for non-Faradaic EIS, frequency-dependent responses, presented in the format of Bode plots, are mostly studied. Utilisations of various parameters, such as capacitance (C) and admittance (Y), have been seen in the literature.[53]

1.3 Biomarkers

A biomarker, or biological marker, is an indicator which characterises a biological process, a pathogenic process, or pharmacological response.[54] In recent years, there has been constant development of protein biomarkers, for the diagnosis of various diseases, such as cancer,[55] diabetes,[56] and neurodegenerative diseases.[57, 58] In this thesis, two of

the most important disease biomarkers, insulin and α-synuclein auto-antibody, were assessed. In this section, their structures and some essential previous studies are introduced.

1.3.1 Insulin

Insulin is a vital peptide hormone, converting glucose to glycogen in the liver, and balancing carbohydrate and fat metabolism.[59] *In vivo*, the dimer and hexamer insulin can be generated by hydrophobic interactions, but the active form of insulin is the monomer, which is formed by two chains linked by two disulfide bonds, containing 51 amino acids (21 residues in Chain A, 30 residues in Chain B) (Figure 1.7).[60] The monomer insulin is a small-sized protein with a negative surface charge in pH 7.4 solutions (molecular radius is ca. 1.3 nm, pI ca. 5.3).[61, 62]

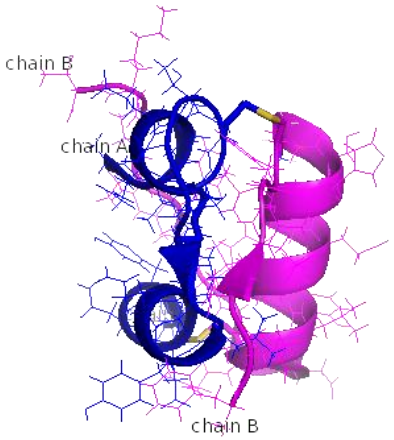


Figure 1.7. The insulin monomer, formed by Chain A (blue) and Chain B (magenta), is presented. The backbone is shown with ribbon, side-chains with lines. Two disulfide bounds are labelled in yellow, shown with sticks.

Insulin is a useful biomarker in monitoring and controlling blood glucose levels of athletes, so that their performance can be improved.[63] In addition, the amount of

insulin in the human body is related to the occurrence of Type II diabetes, which develops when the body generates an insufficient amount of insulin to maintain a normal blood glucose level.[64, 65] With an increase in the incidence of this disease,[66] the development of an ultrasensitive, efficient and accurate diagnostic method would be highly valuable, and insulin is a promising biomarker to achieve this.

However, since insulin is a small-sized target with a weak negative surface charge in pH 7.4 solutions,[61, 62] it is particularly difficult to perform efficient label-free assays. As introduced previously (Section 1.1.2), electrochemical methods have demonstrated great advantages (*e.g.* rapid, low-cost) on label-free assays; therefore, various electrochemical label-free insulin assays have been reported, in Table 1.1.

Most of them are irreversible amperometric assays, collecting signals of current changes induced by the direct oxidation of insulin (details see Table 1.1).[67-69] For the clinical applications of biosensors, not only a low LOD but also the ability to perform detection in complex fluids (*e.g.* serum) is important. This electrochemical oxidation method, although reported to achieve a LOD at pico-molar levels,[70] the detection cannot be performed in serum, since it can generate significant background by oxidising all the electroactive substances without specificity.

In 2007, Gobi and co-workers reported detection of insulin on insulin antibody and PEG thiol-modified gold chips *via* SPR in 10 % and 25 % serum samples,[71] followed by another SPR insulin immunoassay in 10 % serum, based on similar surface chemistry,[72] where the LOD was reduced dramatically through the addition of functionalised gold (Au) nanoparticles. Although the signal was significantly amplified,

multi-step modification and detection are time-consuming and labour-intensive. Overall, all the previous studies mentioned suffer from either inapplicability for detection in serum, or complicated and tedious modification and detection processes; therefore they are not likely to meet the requirements for point-of-care devices. EIS, on the other hand, is a preferred electrochemical method for the performance of efficient and rapid label-free assays, thus, attempts towards conducting insulin assays *via* EIS can be a promising solution to address this problem.

Table 1.1. Previous insulin detection systems.

Method	Surface	LOD	Linear range	Tests in Serum	Ref
Amperometry (measuring current)	GCE[a]	46 nM	189 nM – 4.7 µM	/	73
PSA[b]	SCE[c]	20 nM	20 – 100 nM	/	74
Amperometry (measuring current)	GCE modified with CNT[d]	14 nM	14 nM – 1 µM	/	75
Hydrodynamic voltammetry	GCE modified with CNT	30 nM	0.10 – 3.0 µM	/	69
CV[e]	CCE[f] modified with $K_4[Mo(CN)_8]$ and nickel powder	0.45 nM	0.5 – 500 nM	/	76
FIA[g]	CCE modified with nickel powder	2 pM	15 pM – 1 µM	/	70

[a] Glassy Carbon Electrodes
[b] Potentiometric Stripping Analysis
[c] Screen-Printed Carbon Electrodes
[d] Carbon Nanotubes
[e] Cyclic Voltammetry
[f] Carbon Ceramic Electrode
[g] Flow Injection Amperometry

SPR	Au chips modified with PEG monolayer	0.17 nM	0.17 – 0.52 nM	< 25 %	71
CV	GCE modified with nickel oxide nanoparticles and guanine	22 pM	22 pM – 4 µM	/	77
CV	GCE modified with CNT	1 µM	/	/	78
CV	GCE modified with CNT	1.3 nM	3.4 – 68 nM	/	79
CV, DPV[h], FIA	GCE modified with SiC[i]	3.3 pM	3.3 – 600 pM	/	80
SPR[j]	Au electrodes modified with OEG thiol, thiol modified AuNP[k] were added	0.5 pM	2 – 43 pM	10 %	72
CV	SPE modified with nickel-cobalt oxide powder and CNT	38 nM	17.3 nM – 5.4 µM	/	67
Hydrodynamic voltammetry	CPE[l] modified with silica gel	36 pM	90 pM – 1.4 µM	/	68
Chronoamperometry, EIS	SPE modified with nickel oxide nanoparticles and CNT	6.1 nM	20 – 260 nM	/	81

[h] Differential Pulse Voltammetry
[i] Silicon Carbide Nanoparticles
[j] Surface Plasmon Resonance
[k] Au Nanoparticles
[l] Carbon Paste Electrode

1.3.2 α-Synuclein Auto-Antibody

Parkinson's disease (PD), a protein distortion and aggregation induced, chronic and age-dependent disease,[82, 83] is the second most common neurodegenerative disease in Europe.[84] Currently, the presence of Lewy bodies is the major characterisation of this disease.[85] The major component of Lewy bodies is α-synuclein, which consists of 110 amino acids (14 kDa), shown in Figure 1.8.[86]

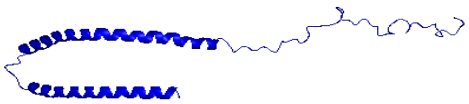


Figure 1.8. Structure of α-synuclein in sodium dodecyl sulphate.

The natural form for α-synuclein is an unfolded monomer. However, in the cerebrospinal fluid (CSF) and plasma of PD patient, soluble oligomers and insoluble fibrils have been observed.[86] Among these three conformations, the soluble oligomeric α-synuclein is reported to be the most toxic species.[87]

Although the function of α-synuclein in the pathology of PD remains unclear, this protein, as a biomarker for PD, has been widely studied,[88] and a variety of measurement methods have been applied to perform α-synuclein assays, such as NMR spectroscopy,[89] fluorescence measurements,[90] western blot,[91] ELISA,[92] size exclusion chromatography (SEC),[93] and photoelectrochemical measurements.[94] However, these previous studies present several drawbacks. Firstly, most of these assays either detect pre-labelled targets or use signal amplification to achieve a relatively low LOD. Though there is one work reporting an LOD of 1.79 pM, [94] this is labelled and multi-step

detection. Secondly, techniques, such as NMR and SEC, require sophisticated instrumentation, as well as specific professional skills, which largely limit their applications. Thirdly, none of these examples is able to conduct an early-stage diagnosis of PD.

Diagnosis of PD in early stages is essentially desirable, since earlier treatment can potentially be more effective,[95] but difficult, due to the restriction of neural damage and less distinguishable symptoms.[96] For the diagnosis of the early onset of neurodegenerative diseases, naturally occurring antibodies (auto-antibodies) to amyloid structures, such as amyloid β-peptide$_{(25\text{-}35)}$, have been observed to be the sensitive biomarkers.[97, 98] Following this concept, the detection of natural immunity was also applied in the diagnosis of PD, by determining the amount of α-synuclein auto-antibody. The multi-epitopic auto-antibody against α-synuclein was firstly found to be strongly correlated in familial PD; occurring percentages in healthy controls and familial patient samples are 31 % and 90 % respectively.[99] After that, Yanamandra and co-workers observed the correlation of the specific auto-antibody level, against α-synuclein monomers, and the stage of PD.[84] In the same year, more detailed concentration levels of auto-antibody, against α-synuclein monomers, were reported to be increasing in early stage, then decreasing to control levels at the 10-year disease stage.[100] However, contrary results, decreasing responses in early stage have also been reported,[85] and the variability of the auto-antibody concentration level and its dependence on the stage of PD remains inconclusive.

1.4 Challenges & Objectives

In summary, this project will explore label-free impedimetric immunosensors, which are capable of performing sensitive assays, both in simple buffer solutions and in complex fluidic systems (*e.g.* human serum). This section introduces the main perspectives of each results chapter, and highlights the main challenges.

Since insulin is a small-sized target with a weak negative surface charge in pH 7.4 solutions (molecular radius of the monomer is ca. 1.3 nm, pI ca. 5.3),[61, 62] label-free immunoassay of insulin has been a great challenge, and most previous detection was conducted by irreversible oxidation of insulin, instead of performing immunoassays with insulin antibody. EIS has been reported as a powerful technique for label-free immunoassays. This work describes the first attempt to develop a highly sensitive label-free impedimetric insulin biosensor, using Faradaic and non-Faradaic EIS. Furthermore, for non-Faradaic EIS, to improve the selectivity and the anti-fouling ability in complex fluid, two anti-fouling interfaces, PEG and a zwitterionic polymer (PCBMA), were examined thoroughly (Chapter 3 & Chapter 5).

It is essential for biosensors to be able to efficiently detect the marker for which they have been designed in real patient samples. Since PD is the second most common neurodegenerative disease in Europe,[84] the importance of discovering an accurate diagnostic method is clear. This is of particularly importance for early stages, since earlier diagnosis and hence treatment is likely to be more beneficial to patients.[95] The auto-antibodies against α-synuclein have demonstrated promise as biomarkers for the diagnosis of early onset PD, by western blot[84] and ELISA,[85] however there is currently

a lack of agreement of the correlation between the concentration of auto-antibodies and the stage of PD. Thus, a label-free impedimetric biosensor was fabricated, and applied on the early-stage diagnosis of PD (Chapter 4).

Although both Faradaic and non-Faradaic EIS have been applied to characterise various biosensors,[101] there is no systematic comparison of sensing performances of these two EIS techniques, detailed quantitative analysis of different EIS parameters, or investigation of the sensitivity dependence of different parameters on frequency. Since the biosensor performances, such as measuring time, sensitivity and linear range are variable across different EIS parameters, it is important to find the optimum frequencies and parameters, so as to achieve high efficiency assays for protein biomarker screening with satisfactory performances. In the development of an EIS protein biosensor, there is a lack of general guidance on whether to choose a Faradaic or non-Faradaic EIS, and further how to choose a specific parameter for analysis once the EIS technique is determined. Herein, the performances of various insulin biosensors with respect to different Faradaic and non-Faradaic EIS parameters were investigated and compared, with the aim of providing some useful suggestions or indications on how to choose appropriate methods and parameters for the development of impedimetric protein biosensors (Chapter 6).

Chapter 2. Experimental Section

2.1 Materials & Reagents

The diamond sprays (1/10, 1/4, 1 micron), used for mechanical polishing, were purchased from Kemet International Ltd, while the polishing cloth (MicroCloth) was purchased from Buehler, UK. Human insulin, human blood serum, bovine serum albumin (BSA), ethanolamine (98 %), 1-ethyl-3-(3-dimethylaminopropyl) carbodiimide (EDC), N-hydroxysuccinimide (NHS), dimethyl sulfoxide (DMSO), glycine hydrochloride (Gly-HCl), and phosphate buffered saline (PBS, 10 mM, pH 7.4) tablets were purchased from Sigma Aldrich. Mouse monoclonal insulin antibody (IgG_1) and mouse monoclonal α-synuclein antibody raised against human-origin α-synuclein were purchased from Santa Cruz Biotechnology, Inc. The human monomeric α-synuclein and patient serum samples were supplied by *Professor Ludmilla Morozova-Roche's group at the Department of Medical Biochemistry and Biophysics, Umeå University, Sweden*, and by *Dr Richard Wade-Martins' group at the Department of Physiology, Anatomy and Genetics, University of Oxford, United Kingdom*. Polyethylene glycol (PEG) containing thiol HS–$(CH_2)_{11}$–$(EG)_3$–OCH_2–COOH (PEG thiol) was purchased from Prochimia Surfaces, Poland. The washing solution for receptor interfaces was prepared by dissolving PBS tablets (Sigma Aldrich) in ultrapure water with the addition of 0.05 % v/v Tween-20 (PBST). 2-(*N*,*N'*-dimethylamino)ethyl methacrylate (DMAEM, 98 %), β-propiolactone (95 %), ethylene glycol dimethacrylate (EGDM, ≥ 97.0 %), and 2-hydroxy-2-methylpropiophenone (97 %) were purchased from Sigma Aldrich. All

other solvents, such as ethanol, acetone, and ether were of analytical grade. Ultrapure water (18.2 MΩ/cm) was obtained from an Ultrapure (Elga Water Flex3) system and used throughout.

2.2 Apparatus

Electrochemical experiments, cyclic voltammetry (CV) and electrochemical impedance spectroscopy (EIS) were performed on an Autolab Potentiostat equipped with an FRA2 module (Metrohm Autolab B.V.). A conventional three-electrode system with a Teflon-sealed gold working electrode (99.99 % purity, 1.6 mm diameter, BASi), a platinum wire counter, and a silver/silver chloride (Ag / AgCl, filled with 1.0 M KCl, +0.236 Vs SHE) reference electrode (CH Instruments) was used. All potentials reported are relative to the Ag / AgCl reference electrode. All data was further processed with OriginPro 8.5.1 or MATLAB R2011b.

2.3 Pre-Treatment of Gold Electrodes

Prior to the fabrication of biosensors, it is essential to refresh and polish gold surfaces. In this section, some critical steps of the polishing process will be introduced.

Initially, the electrodes were mechanically polished to flat and mirror-like surfaces, with diamond sprays in three successive sizes (3, 1, and 0.25 micron), on polishing cloths. This was followed by rinsing and ultra-sonic washing with ultrapure water (18.2 MΩ/cm) and absolute ethanol (analytical grade) to remove the physically adsorbed substances. A treatment of hot piranha solution (concentrated H_2SO_4: 30 %

H_2O_2, v/v 3:1. Caution: please treat with extreme care!) was performed to the electrodes for about 15 min, followed by rinsing and ultra-sonic washing with ultrapure water for 1 – 2 min.

The subsequent electrochemical polishing protocol is generally based on Xiao's work with some alterations.[102] First of all, a number of negative cyclic voltammetry scans were performed in 0.5 M KOH aqueous solution, until stable, smooth curves were obtained. This step is performed to remove the trace substances, such as segments of thiol and protein, which have not been removed by hot piranha solution. Subsequently, a series of scans, from -0.35 to 1.5 V, were conducted in 0.5 M H_2SO_4 at a scan rate of 4 V/s. This step needs to be repeated until the height and shape of peaks are constant. After that, determinations of the effective surface area were accomplished at a scan rate of 100 mV / s, in 0.5 M H_2SO_4. From the cyclic voltammetry in Figure 2.1, the effective surface area can be calculated by assessing the charges of the sharp cathodic peak in coulombs, and then applying this number into the following equation:

$$A\left(cm^2\right) = \frac{Q\left(\mu C\right)}{482\left(\mu C / cm^2\right)} \qquad \textbf{2.1}$$

where *A* represents the effective area and *Q* is the area of the cathodic peak in coulombs. 482 μC is the average charge needed to reduce one cm^2 of polycrystalline gold.[103]

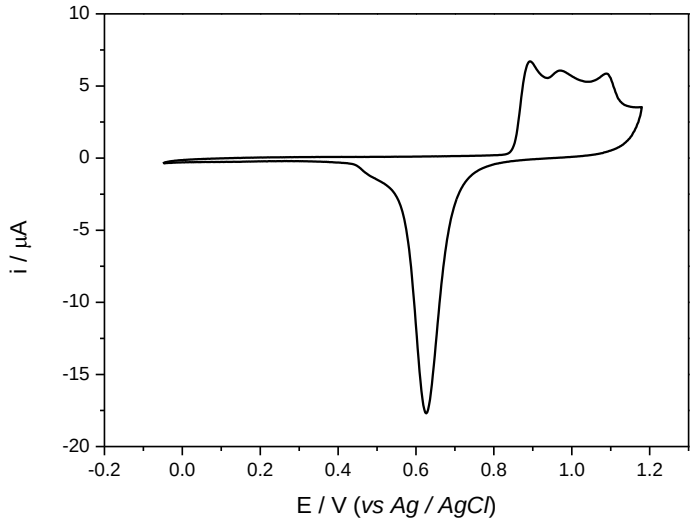


Figure 2.1. Determination of the effective surface area of a gold surface by CV scans in 0.5 M H_2SO_4.

According to the polishing techniques and experimental performance, the effective surface area can mostly be controlled at around 0.03 cm^2. This effective surface area were used in later experiments to normalise the values for Nyquist and Bode plots, in order to eliminate the variation induced by effective surface areas across different electrodes.

To perform Faradaic EIS, it is necessary to apply an initial potential to maintain constant oxidation and reduction reactions of redox probes. This initial potential is commonly set as the halfway potential ($E_{1/2}$, $E_{1/2} = (E_{pa} + E_{pc}) / 2$) of the redox species. Figure 2.2 is a representative cyclic voltammetry of bare gold, measured in 10 mM PBS containing 0.1 M KCl and 1.0 mM $[Fe(CN)_6]^{3-/4-}$, the halfway potential of which is normally determined as 0.21 V. This halfway potential was set as the initial bias for Faradaic EIS measurements.

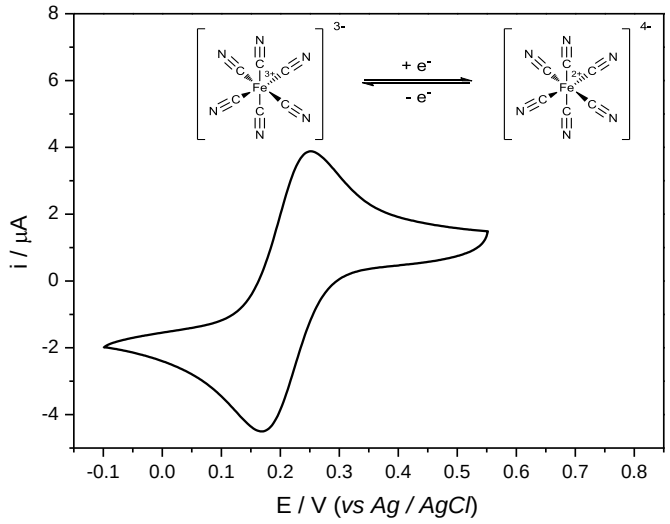


Figure 2.2. Representative CV curve of a bare gold surface recorded in 10 mM PBS containing 1.0 mM $[Fe(CN)_6]^{3-/4-}$ and 0.1 M KCl. The difference between the anodic and the cathodic peak is around 85 mV, and the halfway potential is about 0.21 V.

2.4 Fabrication of Biosensors

Two different categories of interfaces are discussed here: one is a PEG thiol formed self-assembled monolayer (SAM); the other is a zwitterionic polymer film, poly (carboxybetaine Methacrylate) (PCBMA). The fabrication processes of biosensors based on these two interfaces will be described in the following sections.

2.4.1 The PEGylated Thiol Self-Assembled Monolayer (PEG Thiol SAM)

The pre-treated gold electrodes were immersed in 1 mM PEG thiol absolute ethanol solution for 12 h at 4 ^{o}C to ensure the assembly process is long enough to form a well-ordered monolayer. Then they were washed with absolute ethanol (HPLC grade) and dried in a flow of nitrogen gas. The PEG thiol used in this thesis is a carboxyl group terminated thiol with three ethylene glycol groups [HS-$(CH_2)_{11}$-$(EG)_3$-OCH_2-

COOH, structural formula shown in Figure 2.3]. PEG thiol self-assembled monolayers (SAMs) are reported as biocompatible[104] and highly anti-fouling.[105, 106]

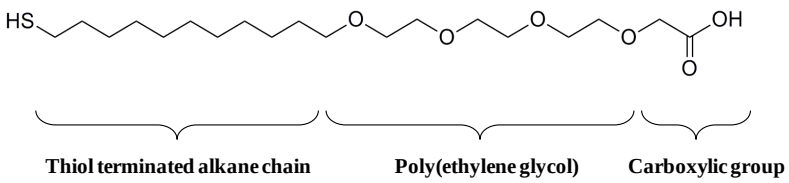


Figure 2.3. Structural formula of PEG thiol

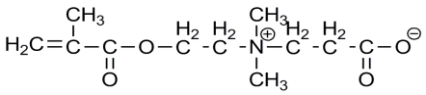
2.4.2 The Zwitterionic Polymer Film

The preparation of the monomer, 2-carboxyl-*N*,*N*-dimethyl-*N*-(2′-methacryloyloxyethyl) ethanaminium inner salt (CBMA), was carried out following a previous study.[32] Initially, 10 mL of β-propiolactone (0.86 g, 12 mM) in anhydrous acetone was added drop-wise to 50 mL of 2-(*N*,*N'*-dimethylamino)ethyl methacrylate (DMAEM) (0.79 g, 10 mM) anhydrous acetone solution with stirring. Then, the mixture was reacted at about 15 °C for 5 h under a blanket of nitrogen. Eventually, the white precipitate was successively washed with 50 mL of anhydrous acetone, 100 mL of anhydrous ether, and dried with a vacuum desiccator. The monomer was preserved at 4 °C before further polymerisation. The structural formula of CBMA is shown in Figure 2.4 (A).

The polymerisation was conducted directly on the gold surface, according to Yang's work in 2011.[107] Initially, the gold surface was covered with 1 μL aqueous solution containing 172 g/L CBMA (monomer), 2 g/L ethylene glycol dimethacrylate (crosslinker) and 11.7 g/L 2-hydroxy-2-methylpropiophenone (photoinitiator). Then, the surface was exposed to 254 nm UV light to initiate the reaction, and left for 30 min

to proceed (structure in Figure 2.4 (B)). Freshly prepared electrodes were immersed in 10 mM PBS (pH 7.4) before further experiment.

(A)



(B)

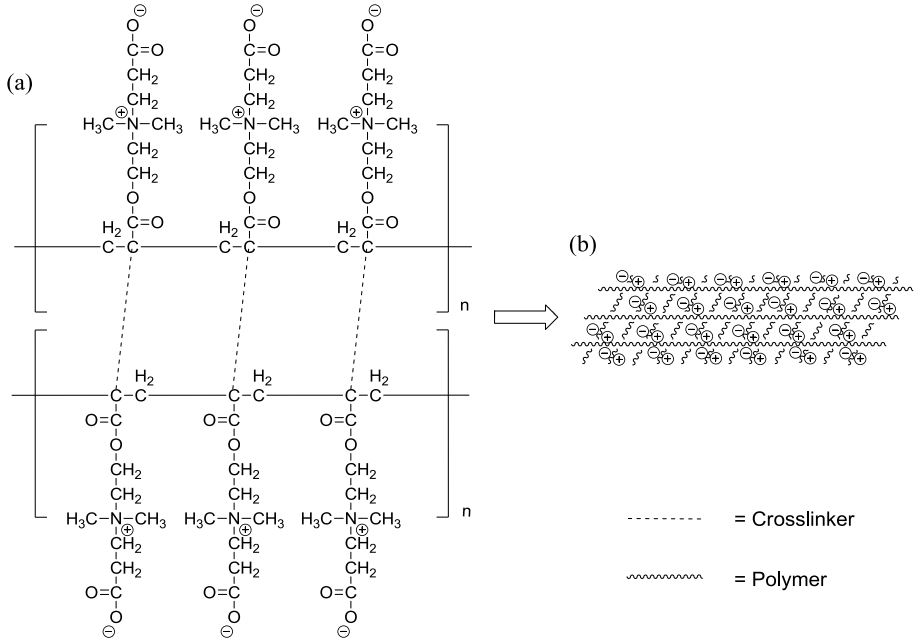


Figure 2.4. (A) The structure of 2-carboxyl-*N*,*N*-dimethyl-*N*-(2′-methacryloyloxyethyl) ethanaminium inner salt (CBMA). It is a zwitterionic compound terminated with a carboxylic acid group. (B) The structure of its polymeric material (PCBMA) is shown in (a). The representative illustration in (b) will be used throughout this thesis.

2.4.3 Immobilisation & Characterisation of Receptor Interfaces

The fabrication of receptor interfaces is schematically shown in Figure 2.5. Both the PEG thiol monolayer and the zwitterionic polymer film have carboxyl groups, which can be activated *via* a carbodiimide reaction, allowing coupling to amino groups on proteins. The thiol or polymer-modified gold surface was first reacted with a mixture of 0.4 M EDC and 0.1 M NHS in ultrapure water (18.2 MΩ/cm) for 40 min at room

temperature. After rinsing with water, the activated probes were immediately immersed in 1.0 μM receptor PBS solution (insulin antibody or α-synuclein) for 4 h at room temperature. Finally, for PEG thiol SAM, the treatment with 1 M ethanolamine (pH was adjusted to 8.5 with 0.5 M KOH) aqueous solution for 1 h was used to deactivate the extra carboxyl groups which are still active, and to neutralise the surface charge of the thiol monolayer. For the zwitterionic polymer film, which is originally neutrally charged, instead of the treatment of deactivation reagent, the extra activated carboxyl groups were quenched with water (in PBS for 1 h).

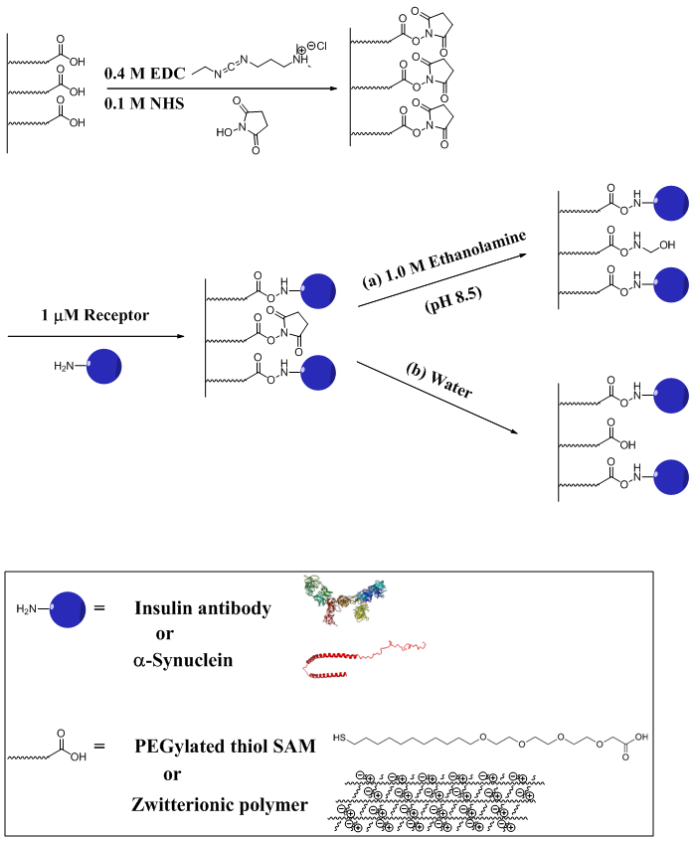


Figure 2.5. Scheme for the process of the EDC / NHS activation and subsequent immobilisation of receptors (insulin antibody or α-synuclein). The antibody interface based on the PEG thiol SAM was deactivated with 1.0 M ethanolamine (pH 8.5) aqueous solution, while the antibody interface based on polymer film was quenched with water (in PBS).

2.5 *In Situ* & *Ex Situ* Detection

Two terms: *in situ* and *ex situ*, are mentioned throughout this thesis; they refer to two different approaches of performing incubation and measurements. *In situ* describes the analyses that conduct both incubation and measurement in the same solution. More precisely, the analytes existed in the measuring system, when the EIS measurements were carried out. This method is suitable for detections in simple solutions, such as insulin assays in buffer solutions, where the composition of the solution was relatively simple (10 mM PBST with 1.0 mM $[Fe(CN)_6]^{3-/4-}$ and 0.1 M KCl), and the presence of insulin would have little interference in the signals. The advantage of this method is that analytes can be directly injected into the system, which minimises the error caused by changes in the arrangement of three electrodes. However, when it comes to detections in complex fluid, the components of which are more highly varied, to perform *in situ* detection could result in significant distortion in signals . Therefore, *ex situ* analyses, whereby the incubation and measurements were performed in separate solutions, were used.

2.6 Faradaic EIS Measurements

Faradaic EIS measurements were applied for insulin assays (Chapter 3) and α-synuclein antibody assays (Chapter 4) based on PEG thiol SAM. Signals were recorded across a wide range of frequencies from 0.01 Hz to 1000 kHz. The amplitude of the applied sine wave was 10 mV with the direct current potential set at 0.21 V, which is the halfway potential of the used redox species, $[Fe(CN)_6]^{3-/4-}$ (Section 2.3).

2.6.1 The Concentration of The Redox Probe

In order to find the best concentration of the redox probe ($[Fe(CN)_6]^{3-/4-}$), presenting the most responsive signals to the target, three concentrations of $[Fe(CN)_6]^{3-/4-}$, 1.0 mM, 2.0 mM and 4.0 mM, were investigated. The investigation was conducted by using the freshly-prepared biosensor to detect 50 pM insulin. The response in R_{ct} was measured before and after the incubation (Figure 2.6). The results indicate that 1.0 mM of $[Fe(CN)_6]^{3-/4-}$ is the most responsive concentration. 1.0 mM $[Fe(CN)_6]^{3-/4-}$ solution was used in the later experiment of Faradaic EIS.

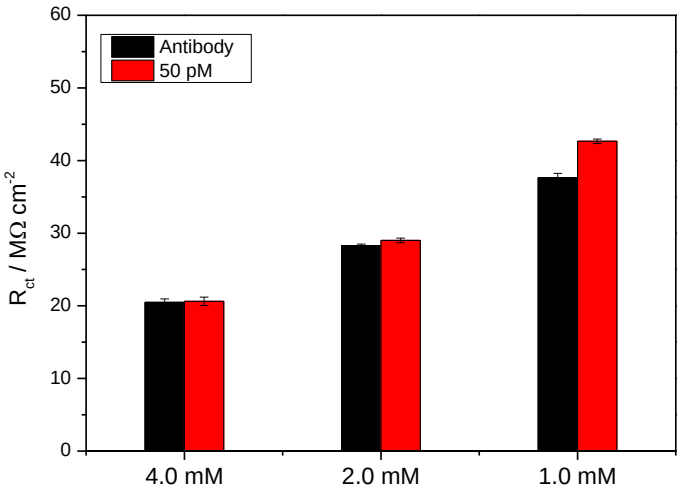


Figure 2.6. The concentration of the redox probe ($[Fe(CN)_6]^{3-/4-}$) was optimised by performing the detection of 50 pM insulin with freshly-prepared biosensor. Three concentrations, 1.0 mM, 2.0 mM and 4.0 mM, were investigated. The response in R_{ct} was recorded before (black) and after (red) the incubation (n = 3 for each test). The results demonstrate that the most responsive signals were observed for 1.0 mM $[Fe(CN)_6]^{3-/4-}$.

2.6.2 Data Processing

For all the Faradaic EIS studies in this thesis, the parameter, charge transfer resistance (R_{ct}), is calculated by fitting the data with the Randles equivalent circuit (as introduced in Section 1.2.3). This fitting was processed in the Frequency Response Analysis (FRA) programme with the 'Find circle' function (Figure 2.7), allowing the semi-circle (blue curve) to be fitted, and the key information, such as R_s, R_{ct} (R_p), and *CPE*, to be determined. This fitting operation can be repeated until an appropriate fitting curve that evenly crosses every data point was observed.

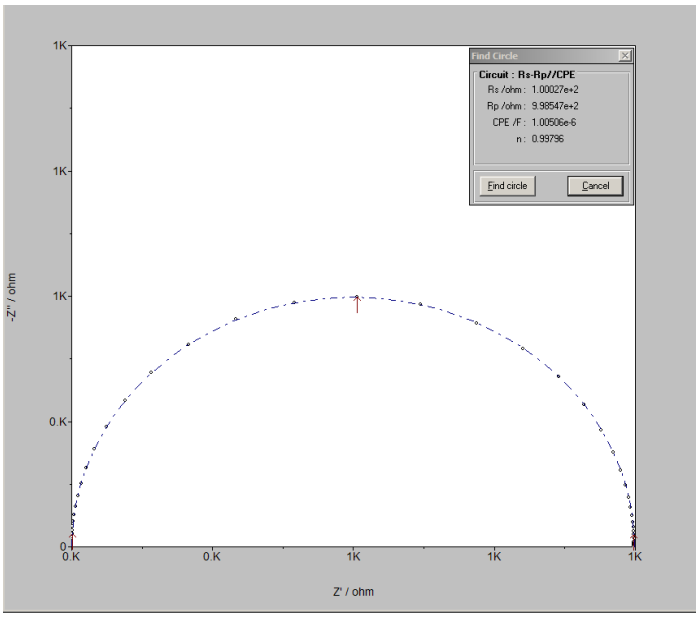


Figure 2.7. A representative example of data fitting in FRA. The blue fitting curve was obtained by marking the beginning, centre, and ending point of the semi-circle, and meanwhile, the values of R_s, R_{ct} (R_p), and *CPE* were shown in the corner window.

When the binding occurs between an antibody and its antigen, a change in R_{ct} can be observed, due to electrostatic interaction, and, more importantly, steric hindrance; they raise the energy barrier of the diffusion of the redox couple, from bulk solution to

the gold surface, and increase the potential energy of oxidation and reduction reactions.[27] Thus, the change in R_{ct} is strongly associated with the binding of targets. R_{ct} was measured when incubating with varying concentrations of targets (from pM to several hundred nM). Raw data were normalised as follows:

$$R_{ct}'\,\% = \frac{R_{ct}^{\,n} - R_{ct}^{\,0}}{R_{ct}^{\,0}} \times 100\,\% \qquad \textbf{2.2}$$

where $R_{ct}^{\,n}$ is the raw signal in R_{ct} obtained by incubating with different concentrations of targets. $R_{ct}^{\,0}$ is the R_{ct} measured on the receptor interfaces.

This normalised R_{ct} (R_{ct}' *%*) is widely used in this thesis to define all the key properties of biosensors, such as sensitivity, LOD, linear range, K_D, and so on. Error bars were obtained by three successive measurements on one electrode, and each experiment has been repeated across at least three electrodes individually.

2.6.3 Incubation Time

The incubation process was monitored by conducting Faradaic EIS measurements every 10 or 20 min. This is to investigate the optimum incubation time, when the binding of antigen and antibody reaches equilibrium.

For insulin assays, the most significant increase in charge transfer resistance (R_{ct}) was occurred in the first 10 min (Figure 2.8). However, in order to ensure that the binding mostly reaches equilibrium, the incubation time was extended to 20 min.

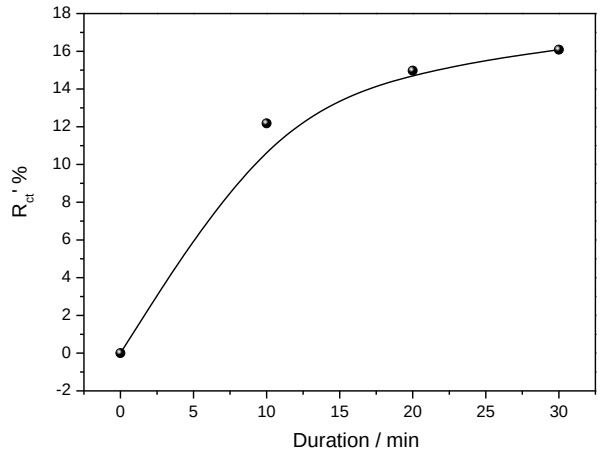


Figure 2.8. Incubation time analysis for insulin assays. Twenty minutes was chosen to be the incubation time.

For α-synuclein assays, though there is slight increase in R_{ct} after 30 min, the most significant increase was observed in the first 20 min, which is considered to be the most efficient and appropriate incubation time (Figure 2.9).

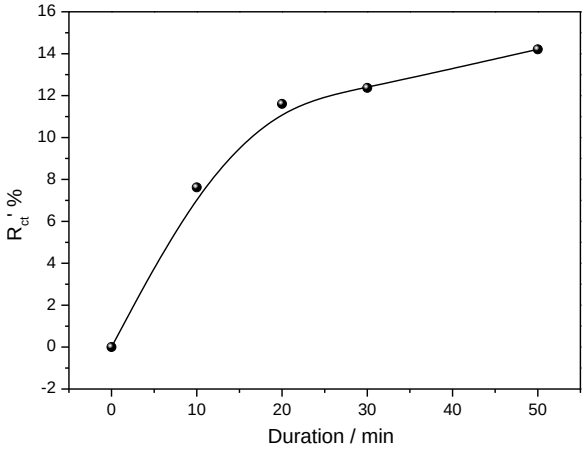


Figure 2.9. Incubation time analysis for synuclein assays. Twenty minutes is adopted as the incubation time.

2.6.4 Assay Performances

The detection was initially performed in PBS buffer solutions, varying the concentration of targets (*in situ* for insulin assays, *ex situ* for α-synuclein antibody assays). Subsequently, to investigate the selectivity, the same biosensor was incubated with various concentrations of control solutions of BSA in 10 mM PBS.

The performance of assays in complex bio-fluid (*e.g.* human serum) were characterised by recording changes in R_{ct}, before and after the *ex situ* incubation with different volume percentages of commercial human serum in PBS. For insulin assays, it is worth mentioning that there is noticeable amount of insulin in human serum (fasting concentration ~ 60 pM).[108] Therefore, a correction was conducted by subtracting the responses in R_{ct}' *%*, contributed by the serum insulin. For the clinical application, 50 pM is considered to be a relatively low concentration. Compared to the specific response to 50 pM of target, the normalised responses (corrected responses for insulin assays), which were lower than 10 % of that, were regarded as insignificant.

2.6.5 Regeneration of Receptor Interfaces

The regeneration ability of biosensors was investigated for Faradaic insulin assays. Initially, a freshly prepared insulin biosensor was incubated with 100 pM insulin in 10 mM PBS, and the R_{ct} was recorded before and after the incubation in 10 mM PBST (10 mM PBS with 0.05 % v/v Tween-20) solution with 1.0 mM $[Fe(CN)_6]^{3-/4-}$ and 0.1 M KCl. Subsequently, targets bound to the sensor surface were removed with a treatment of 0.2 M Gly–HCl aqueous solution containing 1 % DMSO for 5 min, followed by a

further incubation with 100 pM insulin PBS solution. This step was repeated, and EIS measurements were applied to monitor the changes.

2.7 Non-Faradaic EIS Measurements

Non-Faradaic measurements were applied for insulin assays based on PEG thiol SAM and zwitterionic polymer (PCBMA) films (Chapter 5). They were performed on the same module and three-electrode system as Faradaic measurements in 10 mM PBS (pH 7.4) with zero initial bias.

2.7.1 Data Processing

Real impedance (Z'), which is one of the most commonly investigated parameters for non-Faradaic EIS studies, was used. The raw values of real impedance (Z') were normalised as follows:

$$Z'\% = \left| \frac{Z'_{antigen} - Z'_{antibody}}{Z'_{antibody}} \right| \times 100\ \% \qquad \textbf{2.3}$$

where $Z'_{antigen}$ is the original Z' obtained by incubating with different concentrations of insulin. $Z'_{antibody}$ is the original Z' obtained by measuring the freshly prepared antibody interfaces. In order to avoid confusion, the absolute values were used, due to the fact that the binding of different targets can induce increasing or decreasing responses.[109, 110] The error bars were derived by performing three successive measurements on the same electrode, and each experiment has been repeated three times individually.

2.7.2 Stability Test of Polymer Film

In this thesis, the polymer film is constructed by physical attachment, without specific cross-linkers; compared to building chemical bound films (which takes 2 days), this is a faster method of fabrication (taking 12 hours). However, this physical construction of the polymer films led to concerns that the film may decompose during measurement, and thus, it is of great importance to estimate its stability. The stability test was carried out with non-Faradaic EIS measurements on the same Autolab Potentiostat as Faradaic ones, equipped with an FRA module using a three-electrode system in 10 mM PBS (pH 7.4). The amplitude of the applied sine wave was 10 mV with 0 V DC bias. The well-prepared electrodes were stored in fresh 10 mM PBS solution during the interval periods between tests. The relative response of real impedance (*RZ'*) at four selected frequencies, 0.9, 0.5, 0.1 and 0.01 Hz were used to show the stability of the polymer films over 24 days. The definition of relative response is shown below:

$$RZ' = \frac{Z'_n}{Z'_0} \qquad \textbf{2.4}$$

where Z'_n represents the response in Z' tested on the n^{th} day, while Z'_0 is the response in Z' of freshly-prepared polymer film. Error bars are the standard deviation of RZ' at four frequencies, on the same day.

2.7.3 Assay Performances

The assay performances *via* non-Faradaic EIS are generally the same as *via* Faradaic EIS, with some alternative. The *ex situ* detection was initially performed in

PBS buffer solutions, varying the concentration of insulin. Then, detection of various concentrations of control solutions of BSA in 10 mM PBS was performed as control. Since the incubation time is mostly decided by the nature of target and receptor, the same 20 min was also used for the insulin assays *via* non-Faradaic EIS. The performances of assays in various concentrations (% v/v) of serum were carried out in the same way, introduced in Section 2.6.4.

2.8 Analytical Curves & Langmuir Plots

Analytical curves (or calibration curves) and Langmuir plots illustrate how the analytical signal changed with the concentration of the analyte. However, for an analytical curve, the concentration is logarithmic, while it is normal scale for a Langmuir plot. The data in an analytical curve can be fitted to a straight line by using linear regression analysis, which generated a model described by the equation:

$$y = Sx + I \quad (y = R_{ct}'\% \; or \; Z'\%) \tag{2.5}$$

where y is the normalised response ($R_{ct}'\%$ for Faradaic EIS, $Z'\%$ for non-Faradaic EIS); S is the slope, which represents the sensitivity of a biosensor normally expressed in % per decade concentration, x is the logarithmic concentration of analyte, and I is the x-intercept, which is a constant that associates with the background. Detection limit (LOD) is the corresponding concentration, 10^x, where x is calculated *via* Equation 2.5, when taking three times of the error of the receptor-interface responses as y.

The dissociation constant (K_D) is an equilibrium constant that indicates the affinity of the target and receptor. The Langmuir adsorption isotherm was used to determine the K_D of antigen-antibody binding, and it is assumed that each antibody can only accept one antigen.[111] The Langmuir adsorption isotherm is as follows:

$$\Delta R = \frac{[A] \times \Delta R_{max}}{K_D + [A]} \quad \textbf{2.6}$$

where ΔR represents the changes of signals (R_{ct}' *%* for Faradaic EIS, Z' *%* for non-Faradaic EIS), in regard to the signals recorded on receptor interfaces; $[A]$ represents the concentration of target (insulin or α-synuclein antibody). ΔR_{max} is the maximum of signal change; it is the response of an ideal situation, where each immobilised receptor is bound to a target.

The Langmuir adsorption isotherm equation, shown in Equation 2.6, is converted to the equation for Hanes-Woolf plot as follows:

$$\frac{[A]}{\Delta R} = \frac{1}{\Delta R_{max}}[A] + \frac{K_D}{\Delta R_{max}} \quad \textbf{2.7}$$

Hanes-Woolf plot is generated by plotting [*A*] on the *x* axis and [*A*] / ΔR on *y* axis. K_D can be calculated by dividing the *y*-intercept by slope:

$$K_D = \frac{K_D / \Delta R}{1 / \Delta R} = \frac{y - Intercept}{Slope} \qquad \textbf{2.8}$$

2.9 The Detection of Parkinson's Disease Patient Samples

2.9.1 Patient Samples

The Hoehn and Yahr scale (H-Y) is a commonly used staging scale, which defines general categories of the degrees of movement disorder in PD.[112] Two cohorts of patient samples were examined. One was supplied by *Professor Ludmilla Morozova-Roche's group at the Department of Medical Biochemistry and Biophysics, Umeå University, Sweden*; the other was from *Dr Richard Wade-Martins' group at the Department of Physiology, Anatomy and Genetics, University of Oxford, United Kingdom.* Initially, fourteen known early stage patient samples (H-Y 2 stage) and fourteen known control samples from *Umeå* cohort were tested to investigate variability of the concentration levels of α-synuclein auto-antibody, in patients and healthy controls (Table 2.1).

Table 2.1. Group characteristics of tested population

Group Characteristics	PD Patients	Healthy Controls
No. of Subjects	14	14
Age (years)	64.3 ± 10.5	/
Gender (Male : Female)	9 : 5	/
H-Y	2	0

To investigate the applicability of the biomarker, α-synuclein auto-antibody, in various PD patient cohorts, blind detection of another five unknown samples, provided by *the University of Oxford*, were carried out. The information for these patient samples was revealed after the determination and shown in Table 2.2.

Table 2.2. Group characteristics of tested population

Catalogue	**RH / 101**	**RH / 103**	**RH / 104**	**RH / 105**	**JR / 045**
Age	50	77	64	56	77
Sex	Male	Female	Female	Male	Female
H-Y	2	2	2	2	3

2.9.2 Self-Calibration Method

The *ex situ* (see Section 2.5) detection of patient and control samples, supplied by *Umeå University* (see Table 2.1), was performed *via* Faradaic EIS, with 50 % dilution of the samples in PBS (see Section 2.6). The biosensors were controllably prepared according to Section 2.3 & 2.4.

Since EIS is a highly sensitive technique, for the determination of concentration, any slight variation of the surface coverage could give rise to noticeable errors. Thus, self-calibration analyses were applied. After the primary detection of concentrations of α-synuclein auto-antibody in patient samples, three relatively low concentrations (50, 100 and 200 pM for patient samples, 50, 80 and 100 pM for controls) were chosen to produce the individual calibration curve for each biosensor. The concentrations of samples (x in Figure 2.10) can be calculated by calibrating the normalised R_{ct} response

(R_{ct}' %(x) in Figure 2.10) into the specific calibration curve. Triplicate tests on one electrode were applied for all samples, and out-of-range values were confirmed by replications on at least two individual electrodes.

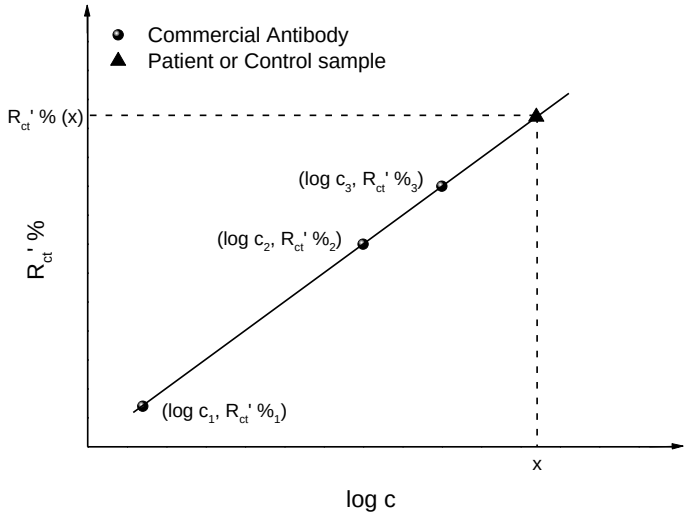


Figure 2.10. Scheme of the self-calibration method.

2.9.3 Standard Addition Method

The *ex situ* (see Section 2.5) detection of unknown samples, supplied by *University of Oxford* (see Table 2.2), were performed in 10 % samples, by using Faradaic EIS measurements (see Section 2.6). Since the detections are blind, it is impossible to select the proper calibrating concentrations. Thus, standard addition analyses were conducted (shown in Figure 2.11). Three concentrations of commercial α-synuclein antibody in the linear range, 50 pM, 100 pM, 150 pM, were selected. Triplicate tests on one electrode were applied for all samples, and each sample was replicated on at least two individual electrodes.

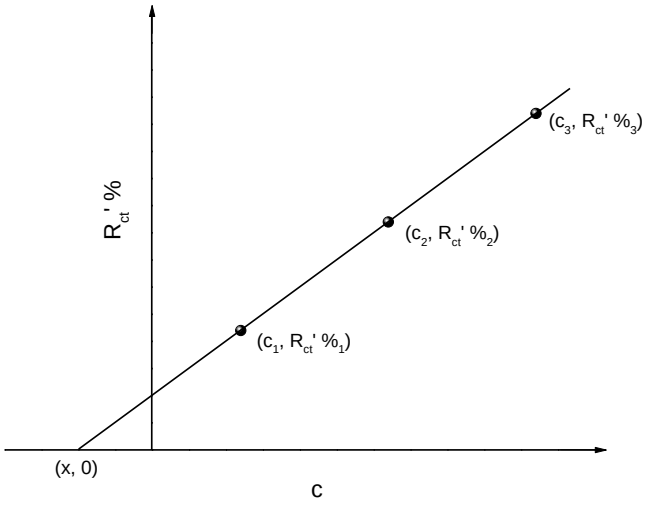


Figure 2.11. Scheme of the standard addition method.

2.9.4 Box-And-Whisker Plots

For the *Umeå University* patient samples, box-and-whisker diagrams were used to plot the results, in OriginPro 8.5.1. Box-and-whisker plots consist of six parts; minimum, lower quartile, median, mean, upper quartile, maximum, and outliers, which can display detailed information about the statistical distribution of each population (Figure 2.12).

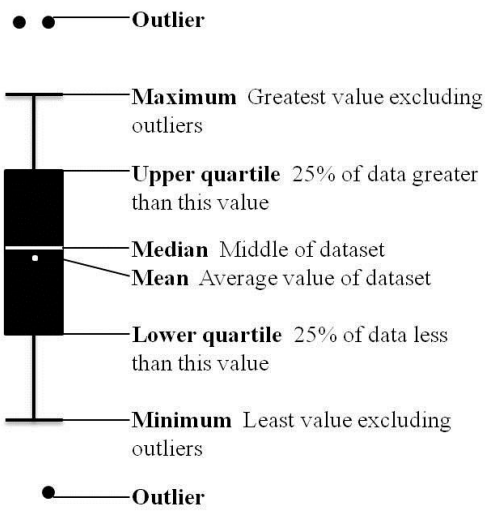


Figure 2.12. The explanation of box-and-whisker plot.

In OriginPro 8.5.1, outliers are defined as follows:

$$\text{Upper Outliers} = \text{Upper Quartile} + \left[1.5\times\left(\text{Upper Quartile}-\text{Lower Quartile}\right)\right] \quad \textbf{2.9}$$

$$\text{Lower Outliers} = \text{Lower Quartile} + \left[1.5\times\left(\text{Upper Quartile}-\text{Lower Quartile}\right)\right] \quad \textbf{2.10}$$

A Student's *t*-test was performed to investigate the significance of the difference between control and H-Y 2 patient groups, with the exclusion of outliers, in Microsoft Office Excel. The concentrations of patient samples will be considered to be significantly higher than those of control samples, if the two-tailed *p* value is lower than 0.05.

2.10 Electrochemical Immittance Analysis

The objectives of electrochemical immittance analysis is to select the optimum parameters and frequencies, presenting the most sensitive responses The analysis based on Faradaic and non-Faradaic insulin EIS assays will be described in this section.

2.10.1 Data Source

The electrochemical immittance analysis was conducted based on the data of Faradaic and non-Faradaic insulin EIS assays. Both Faradaic and non-Faradaic EIS measurements were carried out on an Autolab Potentiostat equipped with an FRA2 module using the same three-electrode system (see Section 2.2). The responses in a wide range of frequencies, from 0.01 Hz to 1000 kHz (40 data points were evenly selected) were measured. The error bars are the standard deviations of three successive measurements on the same electrode, and each experiment was repeated three times individually across different electrodes. Faradaic EIS measurements were performed in 10 mM PBS solution containing 1.0 mM $[Fe(CN)_6]^{3-/4-}$ and 0.1 M KCl, with the initial DC bias set at 0.21 V, while non-Faradaic measurements were carried out simply in 10 mM PBS buffer solution with zero initial bias. Detection of insulin by using both Faradaic and non-Faradaic EIS was carried out *in situ*. A special code for MATLAB R2011b was written to calculate and convert the raw data, in impedance (Z), into other various parameters. OriginLab 8.5.1 was used to do further data processing.

2.10.2 Definitions of Investigated Parameters

In this work, parameters, based on a complex impedance function (Z^*), a complex capacitance function (C^*), a complex modulus function (M^*) and a complex admittance function (Y^*), were chosen to perform the analysis. The definition of Z^* is the same as introduced previously (Section 1.2.3). The mathematical relationships between the other three functions and Z^* are as follows:

$$C^* = \frac{1}{j\omega Z^*} \quad \textbf{2.11}$$

$$M^* = \left(j\omega\varepsilon_0 x \right) Z^* \quad \textbf{2.12}$$

$$Y^* = \frac{1}{Z^*} \quad \textbf{2.13}$$

where ε_0 is the dielectric permittivity in vacuum, and x, assumed to be 1, is a geometric parameter of the film on the surface.

According to the Equation 1.4, this complex function Z^* can be mathematically distributed to two components, real impedance (Z') and imaginary impedance (Z''), both of them were used as parameters. Similarly, there is a real and an imaginary part for each of the other three complex functions, C^*, M^* and Y^*. In addition to the real and imaginary component of each function, the ratios of the imaginary to its real part were also selected as investigated parameters. In total, twelve parameters were analysed (Table 2.3).

Table 2.3. Investigated parameters of four functions

Function	Real	Imaginary	Ratio
Z	Z'	Z''	Z'' / Z'
Y	Y'	Y''	Y'' / Y'
C	C'	C''	C'' / C'
M	M'	M''	M'' / M'

2.10.3 Data Processing

The variability of responses in all parameters was systematically evaluated across forty frequencies spanning 0.01 Hz – 1 M Hz. In defining a useful normalised response that accounts for spectral noise, the binding-induced response is initially specified as:

$$R_n\,\% = \frac{R_n - R_0}{R_0} \times 100\,\% \qquad \textbf{2.14}$$

where R_0 is the signal of the receptor interface in the absence of target. R_n is the response of specific target. R represents any of the twelve investigated parameters in Table 2.3.

The noise is taken as the coefficient of variation (*CV*) of signals measured on three different bare gold electrodes on three different days (Equation 2.15):

$$CV = \left| \frac{SD^{n}_{Bare\ Gold}}{\overline{A}^{n}_{Bare\ Gold}} \times 100\% \right| \qquad \textbf{2.15}$$

where CV is the absolute value of the ratio of the standard deviation of all measurements to its average, and is expressed as a percentage. This noise represents the overall errors caused by the variations of electrodes and instability of instruments.

Both the optimum frequency and parameter require a relatively high sensitivity and relatively low noise. Thus, the relative sensitivity (*RS*) is defined as the ratio of response (R_n *%*) to noise (*CV*):

$$RS = \frac{R_n\ \%}{CV} \qquad \textbf{2.16}$$

An optimum parameter, at the optimum frequency, can be defined as one where *RS*, a dimensionless parameter, is the maximum, according to Equation 2.16.

For Faradaic EIS, a comparison between all twelve investigated parameters (Table 2.3) and charge transfer resistance (R_{ct}) was conducted. The normalised response of R_{ct} (R_{ct} *%*) is calculated in the same way as Equation 2.14. Since R_{ct} is a frequency-independent parameter, the noise, $CV(R_{ct})$, is defined as the average of the coefficients of variation that were determined on three different bare gold electrodes on different days. $RS(R_{ct})$ refers to the relative sensitivity of R_{ct}, which is the ratio of R_{ct} *%* to $CV(R_{ct})$.

Chapter 3. Insulin Assay *via* Faradaic EIS

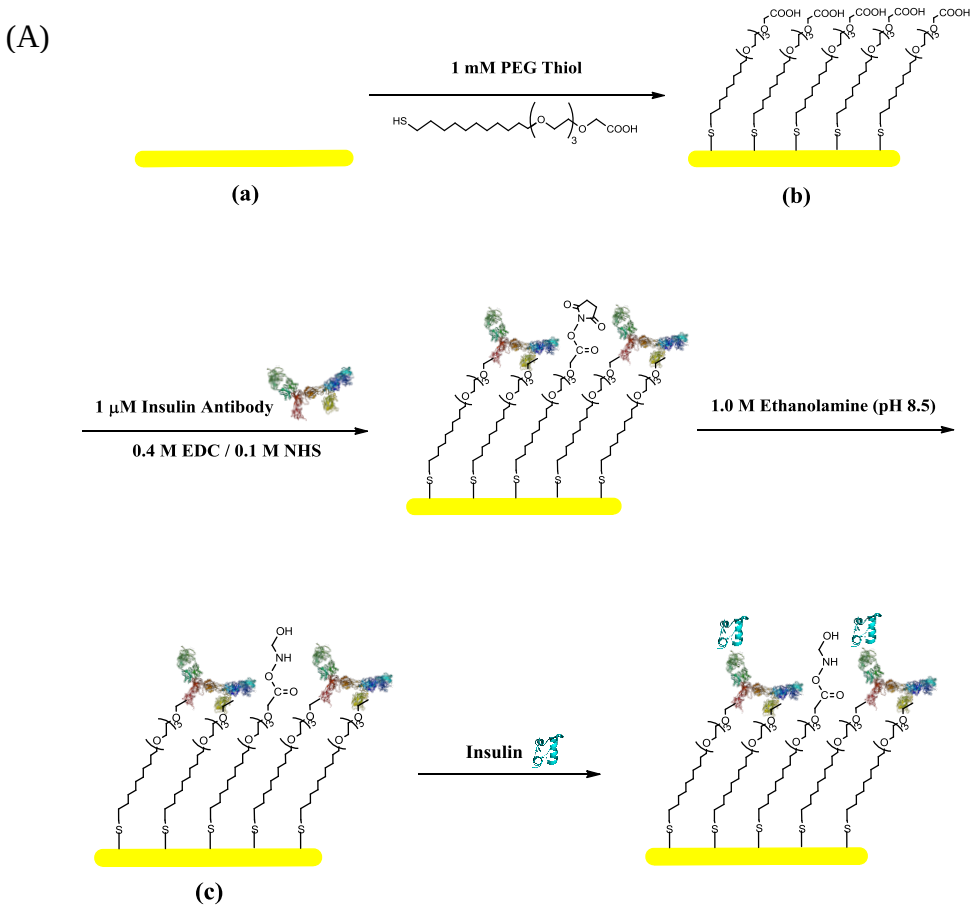
3.1 Objectives

Performing sensitive label-free insulin immunoassay has been an enormous challenge, since insulin is a small target with weak negative charge.[61, 62] Previously, electrochemical detection was performed by the irreversible oxidation of insulin, where amperometric conditions were ultilised.[67, 81, 113] Disadvantages in using the oxidation process as a signature of detection lie with the relatively low sensitivity (LOD at nM level), poor repeatability, complicated assembly process, and the impossibility of detection in serum, *etc*.[77] Faradaic EIS has been reported to be an effective method in performing efficient label-free immunoassays.[114-116] However, this technique has not been applied in the label-free immunoassays of insulin.

Herein, a label-free insulin biosensor will be characterised by means of Faradaic EIS, with the aim of generating a highly sensitive and selective biosensor. The biosensor should have a linear range wide enough to cover a clinical concentration range (three orders of magnitude), and should be able to perform detections in complex fluids, such as blood serum. The anti-fouling ability of this biosensor will be determined by measuring the response, when incubating with different dilutions of human serum. Attempts to regenerate and reuse the biosensor will also be described.

3.2 Biosensor Fabrication

The label-free insulin biosensor was fabricated by initially forming PEG thiol SAM, coupling insulin antibodies by activating the carboxyl groups with EDC / NHS, and then deactivating with ethanolamine, in Figure 3.1 (A). Faradaic EIS measurements were used to monitor the assembly process. Nyquist impedance plots (Figure 3.1 (B)) reported a change in R_{ct}, as various reagents were coupled to the surface. For a freshly cleaned bare gold surface (Figure 3.1 (B), (a)), the Nyquist plot is almost a linear line, with a considerably small R_{ct} (~ 160 Ω cm^{-2}). Prior to antibody modification, due to the strong electrostatic repulsion and steric hindrance of the monolayer, the barrier to charge transfer from the modified gold surface to $[Fe(CN)_6]^{3-}$, increased. Thus, there was an increase in R_{ct} after the formation of PEG thiol SAM (Figure 3.1 (B), (b)); a change, from 160 Ω cm^{-2} to 4 MΩ cm^{-2}, was seen. Similarly, the electrostatic repulsion and steric hindrance of the insulin antibody layer, severely blocks the electron transfer process. This change was also confirmed by EIS; an increase of 50 % in R_{ct} (from 4 MΩ cm^{-2} to 6 MΩ cm^{-2}) was seen (Figure 3.1(B), (c)). These observations are consistent with what has been previously documented.[117-120]



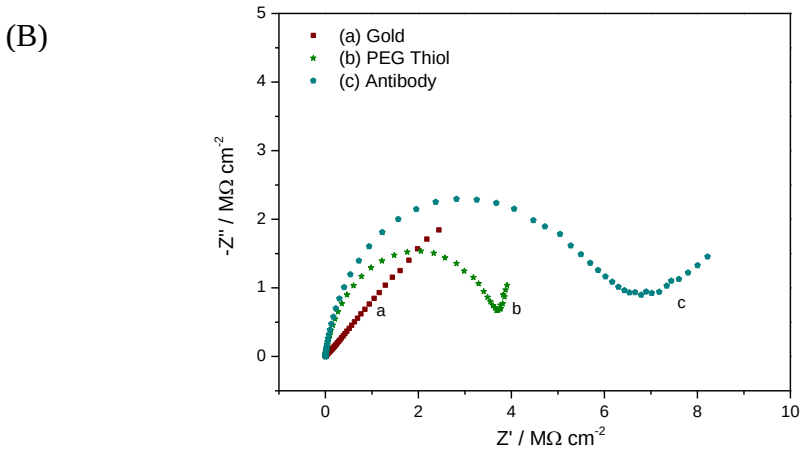


Figure 3.1. (A) Fabrication of the insulin biosensor. (B) Nyquist plots for various films, recorded in PBST (10 mM, pH 7.4) solution (contains 1.0 mM $[Fe(CN)_6]^{3-/4-}$ and 0.1 M KCl). A dramatic increase in R_{ct} was observed after the immobilisation of PEG thiol and insulin antibody onto the gold surface. (a) Bare gold surface (R_{ct} < 160 Ω cm^{-2}); (b) PEG SAM interface (R_{ct} ~ 4 MΩ cm^{-2}); (c) Insulin antibody modified interface (R_{ct} ~ 6 MΩ cm^{-2}).

3.3 The Detection of Insulin in A Buffer Solution

The interaction, between insulin antibody and insulin, can be characterised by measuring R_{ct}, before and after the incubation with solutions of varying insulin concentration. When the biosensor is incubated with a higher concentration of antigen, more antigens will become bound to surface-confined antibodies; similar to the fabrications of PEG thiol and the insulin antibody, an increase in the blocking effect was seen. Accordingly, a series of increases in R_{ct} were observed over the range of concentrations tested (Figure 3.2).

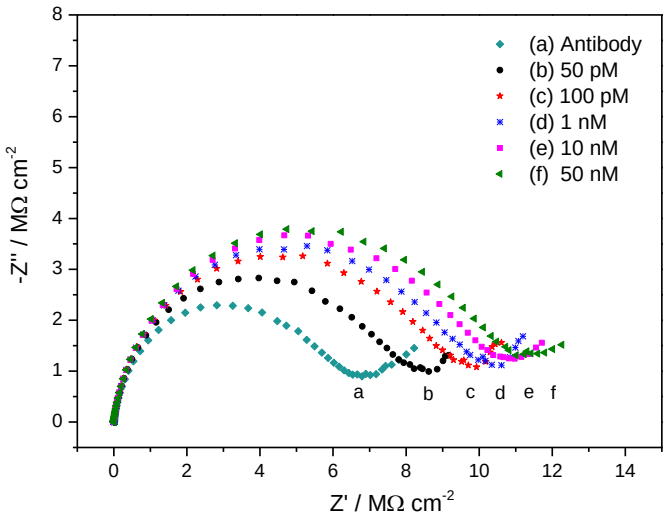


Figure 3.2. Typical Faradaic impedance spectra, corresponding to the response of the biosensor after incubation in PBST solution containing varying concentrations of insulin: curves from (a) to (f) represent 0 pM (Insulin antibody modified interfaces) (a), 50 pM (b), 100 pM (c), 1 nM (d), 10 nM (e), and 50 nM (f) insulin, respectively.

Herein, the detection of insulin was performed, *in situ*, in PBS to determine the sensitivity of the formulated biosensor. Ten different concentrations, ranging from 5 pM to 500 nM, were detected. The representative analytical curve, demonstrates a good

linear correlation (R^2 = 0.99) between R_{ct}' % (Section 2.8) and logarithmic insulin concentrations (Figure 3.3 (A)). A wide linear range, across 4 orders of magnitude, from 5 pM to 50 nM, and a remarkably low detection limit, 1.24 ± 0.01 pM, were observed. The concentration of insulin in a sample of healthy human blood is 57 – 79 pM, between meals[108]; this is within the linear range of this presented insulin biosensor. To explore the selectivity of this biosensor, responses, in R_{ct}' % over the same concentration range of BSA, were recorded (Figure 3.3 (B)). The saturated response for BSA is approximately 3 %; this is regarded to be insignificant. The disassociation constant (K_D), normally used to describe the strength of binding, can be calculated by fitting data into a Langmuir adsorption isotherm (for calculation, see Section 2.8). In this assay, the K_D of insulin and insulin antibody was determined to be 0.85 ± 0.01 nM; this is in good agreement with a previous determination (0.46 ± 0.08 nM).[121]

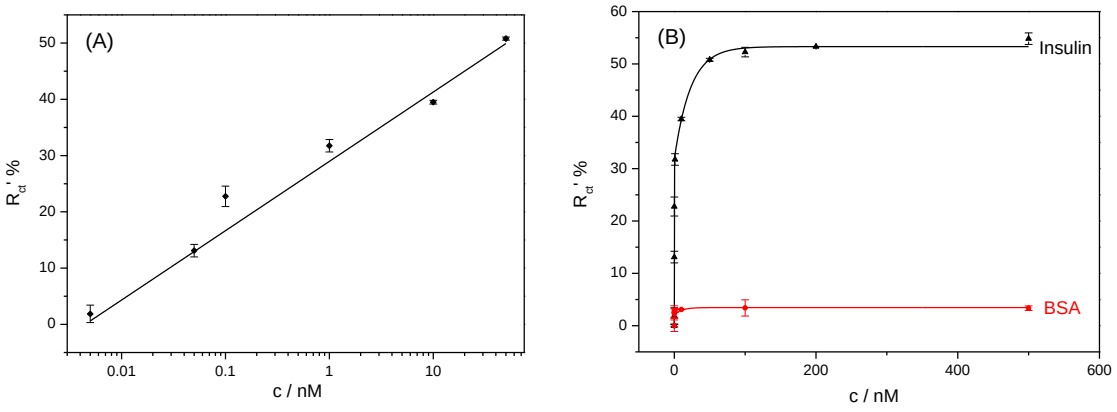


Figure 3.3. Normalised charge transfer resistance (R_{ct}) changes of the biosensor after the incubation with different concentrations of insulin protein in PBST (10 mM, pH 7.4), containing 1.0 mM $[Fe(CN)_6]^{3-/4-}$ and 0.1 M KCl. (A) The corresponding calibration curve for the insulin biosensors. (B) BSA was used as a control protein to show the selectivity of this biosensor. When incubated with 500 nM BSA, the non-specific response of this biosensor is around 3 %.

3.4 The Detection of Insulin in Commercial Blood Serum

Previous assays, performed in buffer, indicate that the use of this biosensor, with a low LOD, a wide linear range across four orders of magnitude, high selectivity, and low K_D (see Section 3.3) is promising in regard of the detection of insulin. However, it is a great challenge to perform detection in complex biological fluid, such as human serum; variation and uncertainty in the components notes its difficulty.[26] To examine the anti-fouling property of this biosensor, a further study was performed in blood serum.

Initially, *in situ* assays were carried out in 10 % serum (Figure 3.4). It is noticeable that this biosensor maintains almost the same sensitivity (~ 9 % per decade concentration) in 10 % serum, as it does in PBS buffer (~ 12 % per decade concentration). The linear range also remains consistent, from 5 pM to 50 nM, and the detection limit (4.70 ± 0.64 pM) is slightly than that in PBS.

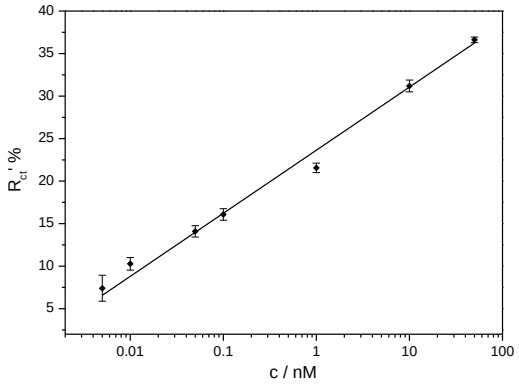


Figure 3.4. Calibration curve for the *in situ* assay of insulin in 10 % blood serum. The biosensor surfaces were incubated in PBST (10 mM, pH 7.4) solution, containing 1.0 mM $[Fe(CN)_6]^{3-/4-}$, 0.1 M KCl and 10 % blood serum, spiked with different concentrations of insulin. EIS measurements were subsequently carried out in the same solution.

Subsequently, *ex situ* incubations were carried out with blood serum, diluted in PBS to differing degrees (1 %, 5 %, 10 %, 50 %, and 80 %). It is worth noting that there is a certain amount of insulin in the serum (~ 60 pM [108]), which will inherently contribute to the measured non-specific responses. Therefore, the original data was corrected; subtraction of the EIS contribution from the insulin in the serum itself was performed. The corrected responses to non-specific adsorption and the response to a 50 pM insulin solution are comparatively shown in Figure 3.5. 50 pM is a very low concentration for clinical applications, since the fasting concentration of insulin in healthy human blood is around 60 pM.[108] Comparing to the response to 50 pM insulin (~ 13 %), the response to 50 % serum is only around 1 %, which suggests that the possibility of performing highly sensitive assays in 50 % blood serum.

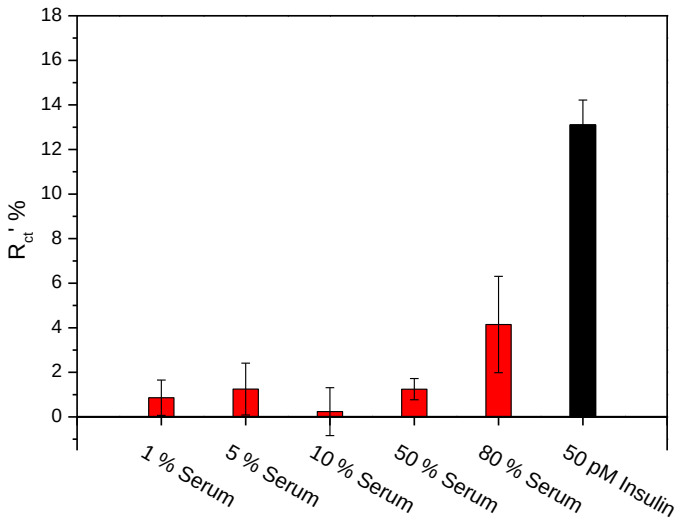


Figure 3.5. The non-specific response (in R_{ct}) of the insulin biosensor after incubation with various dilutions of blood serum in PBS. *Ex situ* EIS measurements were performed to collect the original R_{ct}, then, the measured data were corrected by subtraction of responses that contribution from the insulin in the serum itself as calculated from the calibration curve in PBS. This biosensor is likely to present similarly high sensitivity in up to 50 % serum.

To confirm this, a further *ex situ* assay, in 50 % blood serum, was conducted (Figure 3.6). As previously predicted, a similar sensitivity (around 10 % per decade concentration), four-orders-of-magnitude wide linear range (from 5 pM to 50 nM), and a low LOD (4.77 ± 0.99 pM) was observed. These findings verify that this biosensor is capable of conducting sensitive and specific detection in 50 % human serum. Previous insulin assays only reported detections in up to 20 % serum, through use of SPR.[71, 72] Thus, this Faradaic impedimetric insulin biosensor, based on PEG thiol SAM, has very high resistance to non-specific binding, and can maintain very low LOD at pM level, in 50 % diluted serum.

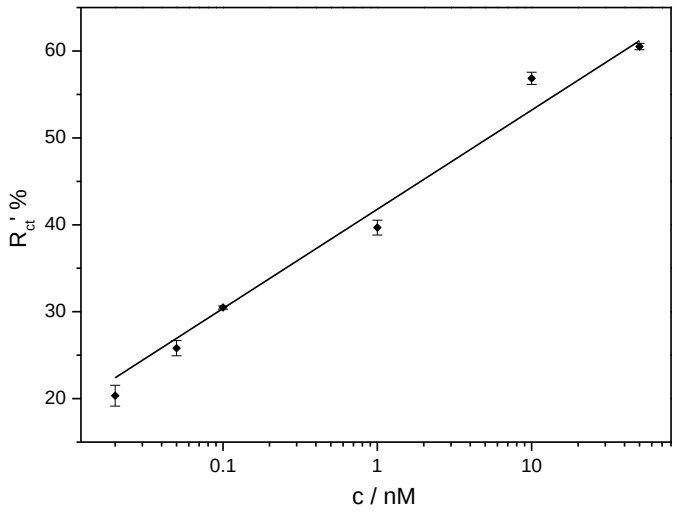


Figure 3.6. Calibration curve for the ex situ assays of insulin in 50 % blood serum. Electrode surfaces were incubated in PBST (10 mM, pH 7.4) solution containing 50 % blood serum, spiked with different concentrations of insulin, and EIS measurements were carried out in PBST (10 mM, pH 7.4) solution containing 1.0 mM $[Fe(CN)_6]^{3-/4-}$ and 0.1 M KCl after rinsing with PBST.

3.5 Regeneration of The Sensor Surface

The concept of breaking the receptor-target bound between insulin and its antibody, and regenerating the receptor interface offers an applicable approach to increase the repeatability across different electrodes and to save the time and effort of associated with the fabrication. The regeneration experiments were performed (Section 2.6.4), and the results are shown in Figure 3.7. It was seen that the process could be repeated three times without a decrease in sensitivity (<4 % deviation). However, the fourth cycle resulted in the loss of materials from the surface, probably arising from damage to the antibody layer. Thus, it suggests that this insulin biosensor is robust and can be reused three times, without significant damage occurring to the surface.

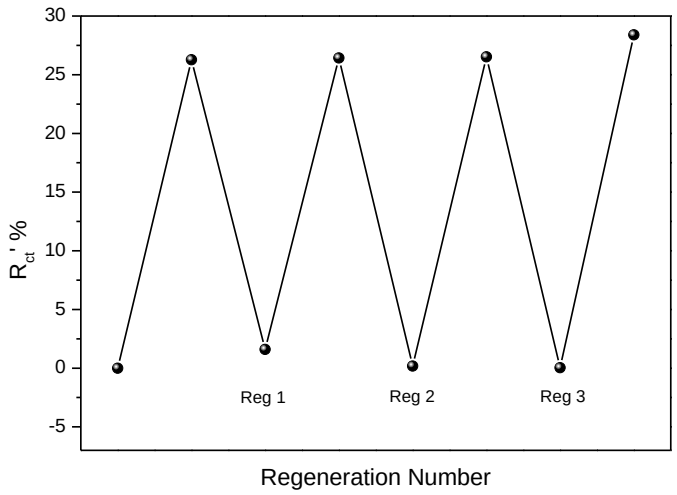


Figure 3.7. Sensory surface regeneration by immersion in 0.2 M Gly–HCl buffer containing 1 % DMSO for 5 min prior to rinsing with PBST, and impedance analysis in PBST (10 mM, pH 7.4) solution containing 1.0 mM $[Fe(CN)_6]^{3-/4-}$ and 0.1 M KCl. 'Reg 1', 'Reg 2', and 'Reg 3' represent the regeneration numbers.

3.6 Conclusions

Insulin, a polypeptide hormone released by the pancreas, plays an essential role in controlling the blood glucose level. The insulin in human subjects can be regarded as a biomarker for Type II diabetes, obesity and some endocrine diseases.[77] To the best of our knowledge, this work is the first example of performing label-free insulin immunoassay, with Faradaic EIS as the measuring method. Comparing with previous insulin assays, this biosensor described here appears to be very promising. Although the SPR insulin assays conducted by Frasconi and co-workers, reported an LOD as low as 0.5 pM, this was achieved by the addition of functionalised Au nanoparticles, which are known to amplify signals. In addition, multi-step performances of modification and detection are time-consuming and labour-intensive, and the reported linear range is particularly narrow (2 – 43 pM). In regard to the anti-fouling ability, previous studies only reported the detection in up to 25 % serum, while this impedimetric biosensor is able to perform assays in up to 50 % serum, without a significant reduction in sensitivity.

In summary, an ultrasensitive (LOD 1.2pM), highly selectivity and reusable insulin biosensor, with a wide linear range across four orders of magnitude, and of high resistance to non-specific adsorption in up to 50 % serum, has been presented in this chapter.

Chapter 4. α-Synuclein Antibody Assay *via* Faradaic EIS

4.1 Objectives

As a result of the increasing incidence of Parkinson's disease,[84] it is of a great desire to discover an accurate method for diagnosis, especially in early stages, where the therapeutic intervention is likely to be most efficient.[95] Recent studies on neurodegenerative disease claim that naturally generated antibodies (auto-antibodies), in response to amyloids, appear to be a promising solution to this problem (in that their presence may be diagnostic).[97, 98]

In 2007, Papachroni *et al.* analysed of the existence of the multi-epitopic auto-antibody against α-synuclein, in healthy controls, familial PD patients, and sporadic PD patients; this work suggests that this auto-antibody is correlated to the incidence of familial PD, since it was found in 90 % of familial PD patients, but only in 30 % of healthy control samples.[99] The work reported afterwards succeeded to produce specific auto-antibodies against monomers of α-synuclein, and proved that it was responsive to the incidence of sporadic PD; the concentration of α-synuclein-monomer auto-antibody increases in the early stages (within 5 years), then declines to the control level after 10 years.[84, 100] More recently, it has been claimed that α-synuclein auto-antibody is likely to be a biomarker, which can differentiate PD from Alzheimer's disease (AD), where contrary results were observed; the concentration of auto-antibody in patient samples is lower than that in controls.[85]

The correlation between α-synuclein auto-antibody and PD has been examined by western blot, SPR,[84] and ELISA.[85] However, a consistent conclusion has not yet been documented. Herein, by utilising the same surface chemistry in Chapter 3, a label-free α-synuclein antibody biosensor was fabricated and characterised by employing Faradaic EIS. With the aim of developing a reliable method for the diagnosis of early-onset PD, this biosensor was also applied to detect the concentration levels of α-synuclein auto-antibody in early stage PD patients and healthy controls.

4.2 Biosensor Fabrication

The label-free α-synuclein antibody biosensor was fabricated by using the same surface chemistry (PEG thiol SAM) as for the previous label-free insulin biosensor, however replacing the insulin antibody with α-synuclein, in Figure 4.1 (A). Nyquist plots of various interfaces illustrate the increase in R_{ct}, induced by the formation of PEG thiol SAM and insulin antibody interface, in Figure 4.1 (B). As expected, the formation of PEG thiol SAM and the subsequent immobilisation of α-synuclein induced successively tremendous increases in R_{ct}, in regard to the response seen at bare gold surface. These observations are consistent with reported studies on Faradaic EIS.[117-120]

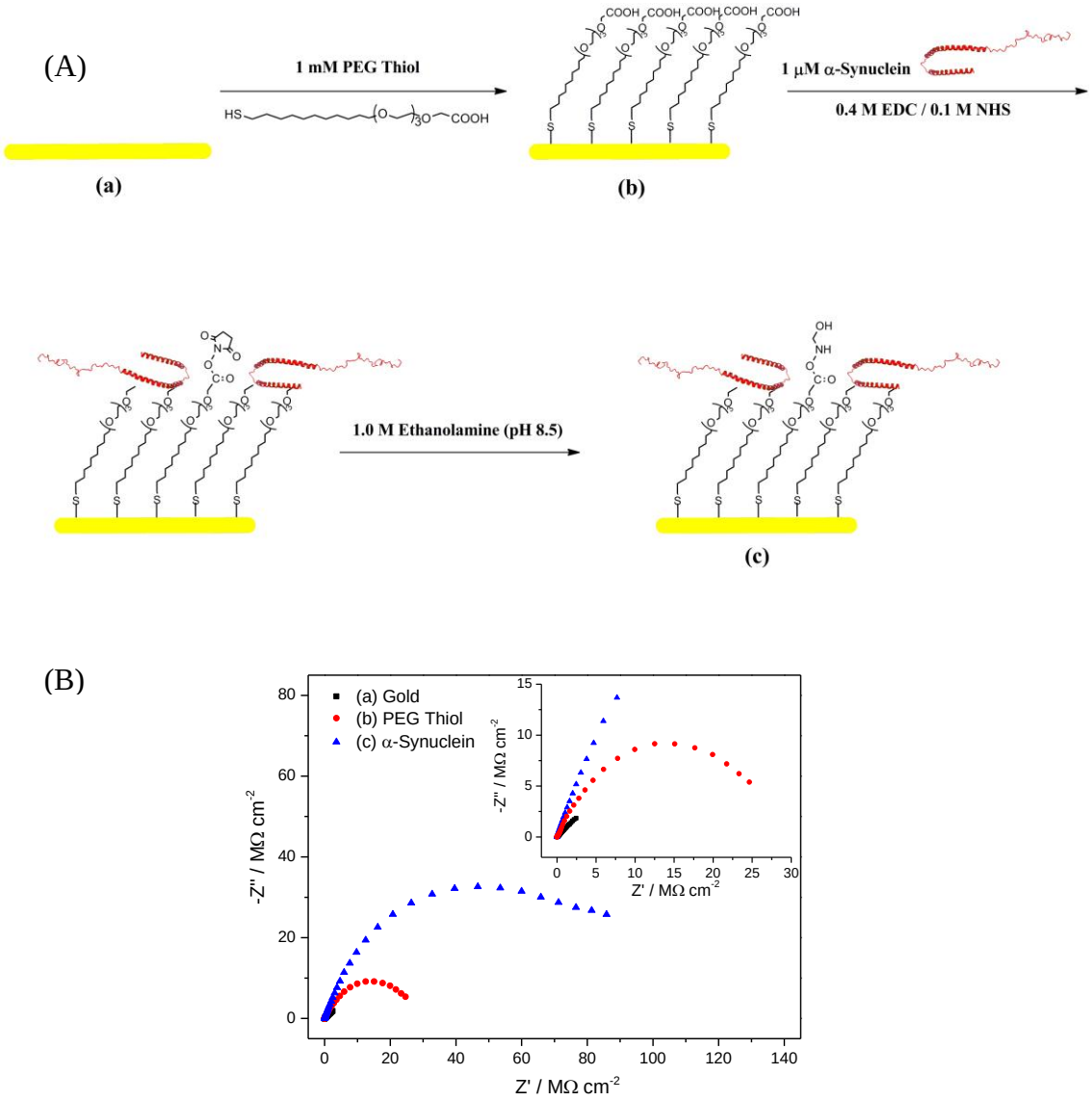


Figure 4.1. (A) Fabrication of α-synuclein antibody biosensor. (B) Nyquist plots of different films, recorded in PBST (10 mM, pH 7.4) solution containing 1.0 mM $[Fe(CN)_6]^{3-/4-}$ and 0.1 M KCl. Dramatic increases in R_{ct} have been observed after the immobilisations of PEG thiol and α-synuclein. (a) Bare gold surface (R_{ct} < 160 Ω cm^{-2}), (b) PEG SAM interface (R_{ct} ~ 4 MΩ cm^{-2}), (c) α-synuclein modified interface (R_{ct} ~ 6 MΩ cm^{-2}).

4.3 Detection of Commercial α-Synuclein Antibody in A Buffer Solution

The sensitivity and linear range of this α-synuclein biosensor were determined in buffer solution (PBS, pH 7.4), by incubating the biosensor in different concentrations of

commercial α-synuclein antibody solutions, 50 pM to 10 nM. The detection of α-synuclein antibody, in PBS, was performed *ex situ* (Section 2.5), and the response in R_{ct} was recorded before and after each incubation. As expected, the value of R_{ct} increases as the concentration of α-synuclein antibody raise (Figure 4.2).

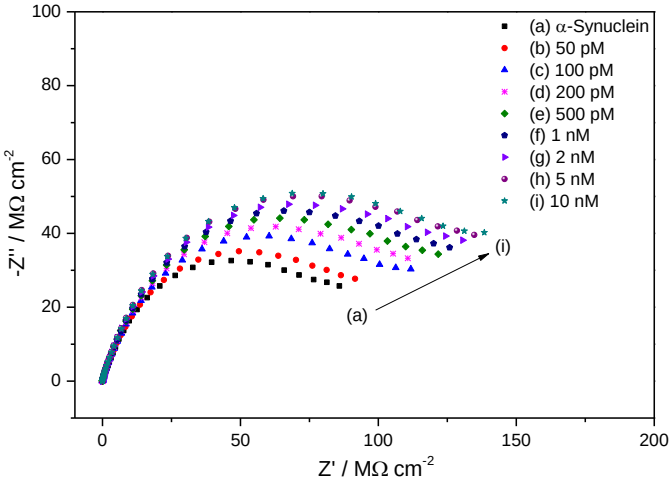


Figure 4.2. Faradaic impedance spectra responsive to the incubation in PBS solution with different concentrations of α-synuclein antibody: curves represent 0 pM (α-synuclein modified interfaces) (a), 50 pM (b), 100 pM (c), 200 pM (d), 500 pM (e), 1 nM (f), 2 nM (g), 5 nM (h), and 10 nM (i), respectively.

The representative analytical curve (Figure 4.3), demonstrates a good linear correlation (R^2 = 0.99) between the normalised R_{ct} (R_{ct}' *%*, normalisation see Section 2.8) and the logarithmic concentrations of α-synuclein antibody. Error bars were obtained by carrying out duplicate tests on the same biosensor, and this assay was repeated across three different electrodes. A wide linear range, across around 3 orders of magnitude, from 50 pM to 10 nM, and an LOD of 31.2 ± 2.1 pM were obtained. In this assay, K_D of α-synuclein and α-synuclein antibody was determined to be 0.34 ± 0.23 nM.

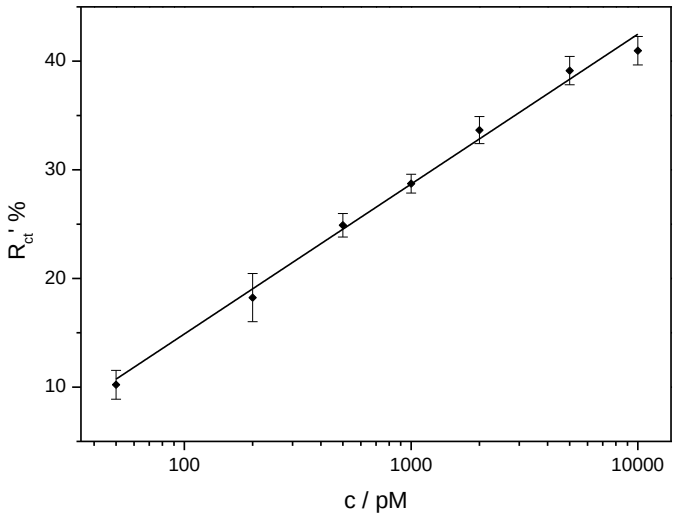


Figure 4.3. Normalised charge transfer resistance (R_{ct}) changes of the biosensor after the incubation with different concentrations of α-synuclein antibody in PBST (10 mM, pH 7.4). The measurements of original R_{ct} were conducted in 10 mM PBS containing 1.0 mM $[Fe(CN)_6]^{3-/4-}$ and 0.1 M KCl. This representative analytical curve has good linearity (R^2 = 0.99, n = 3 for each concentration) and a sensitivity of 13.80 % per decade concentration.

4.4 Detection of Commercial α-Synuclein Antibody in Human Serum

The selectivity of this α-synuclein biosensor was determined by performing *ex situ* EIS measurements, before and after the incubations in diluted human serum (Figure 4.4); the serum was diluted in PBS to differing degrees (10 %, 20 %, and 50 % serum). The non-specific response remains insignificant up to 50 %, which suggests the possibility of performing highly sensitive assays in 50 % blood serum.

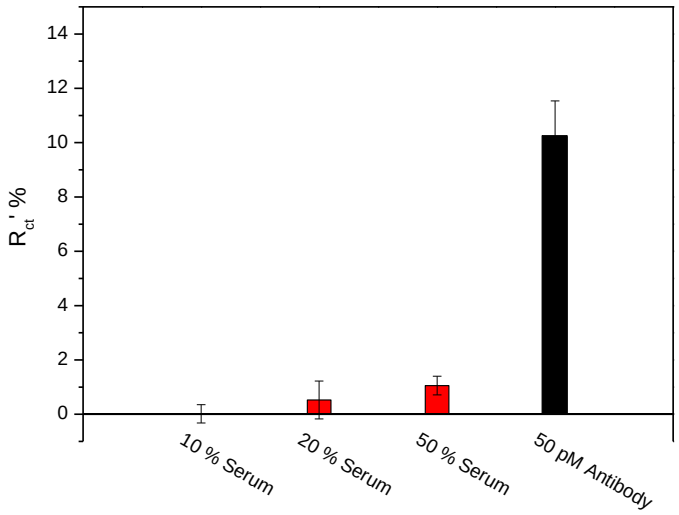


Figure 4.4. *Ex situ* EIS measurements were performed to determine the non-specific response of the α-synuclein antibody sensing interface. This biosensor is likely to present similarly high sensitivity in 50 % diluted serum.

To confirm that 50 % human serum would not cause severe reduction in the sensitivity of this α-synuclein antibody biosensor, a further *ex situ* assay in 50 % blood serum, spiked with various concentrations of commercial α-synuclein antibody, was conducted (Figure 4.5). In comparison to the assays performed in PBS (Section 4.3), a similar sensitivity (12.90 % per decade concentration) and linear range (50 pM – 10 nM) were observed. The LOD for the detection in 50 % serum (38.9 ± 3.2 pM) is slightly higher than that calculated in buffer solution (31.2 ± 2.1 pM).

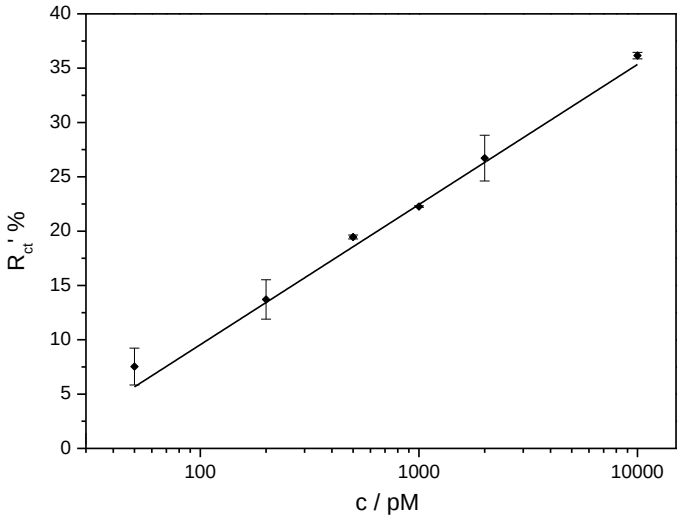


Figure 4.5. The calibration curve for the insulin assays, performed *ex situ* in 50 % blood serum (R^2 = 0.97). Electrode surfaces were incubated in PBST (10 mM, pH 7.4) containing 50 % human serum, spiked with different concentrations of α-synuclein antibody, and EIS measurements were carried out in PBST (10 mM, pH 7.4) solution containing 1.0 mM $[Fe(CN)_6]^{3-/4-}$ and 0.1 M KCl after rinsing with PBST.

4.5 Determining The Accuracy of This Methodology

Previous assays in PBS (Section 4.3) and in 50 % human serum (Section 4.4), indicate that this α-synuclein antibody biosensor is capable of sensitively detecting α-synuclein antibody in up to 50 % serum; the linear range is across three orders of magnitude from pM to nM. Accordingly, the experiments of self-calibration and standard addition were designed to perform the detection of α-synuclein auto-antibody in patient samples with 2-fold dilution. However, there is a challenge in adapting this methodology; though each electrode was self-calibrated for each performance of detection, the experimental error, due to the variability in the sensitivity of each electrode, can still be of notice. Therefore, prior to the detection in patient samples, the detection of commercial α-synuclein antibodies in standard solutions (spiked 50 %

commercial serum with known concentrations of α-synuclein antibody) was performed to examine the accuracy of this methodology. Two concentrations, 350 pM and 500 pM, were detected by self-calibration and standard addition methods (Section 2.9.2 and 2.9.3 respectively). The results are shown in Figure 4.6, where the black bars illustrate the concentrations calculated by self-calibration, and red bars are by standard addition. The difference, between the determined concentrations and the given values (350 pM or 500 pM), varies from 0.08 % to 9 %. Thus, the error, induced by the methodology, is generally lower than 10 %.

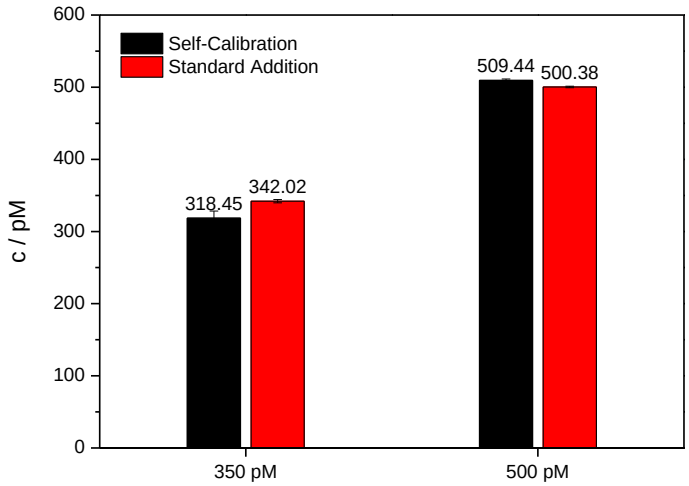


Figure 4.6. The accuracy of these two methods, self-calibration and standard addition, was determined by performing the detection of α-synuclein antibody in standard solutions, containing 350 or 500 pM commercial α-synuclein antibody and 50 % human serum in PBS. In regard to the given values, the highest error of experimental values is determined to be less than 10 % (318.45 pM comparing to 350 pM), *via* self-calibration.

The accuracy of this methodology was further estimated by determining the variation of the detection across different electrodes; the variation was examined by using two individual controllably-fabricated biosensors to detect the same sample. One

control sample (# 7530) and one H-Y 2 patient sample (# 8556) from *Umeå University* patient cohort (description, see Section 2.9.1) were selected. The concentrations of the same samples, determined on two individual electrodes, were seen to be consistent for both the control and patient samples; the coefficients of variation for the control and the patient samples are 3 % and 8 %, respectively (Figure 4.7). Thus, this experiment further confirms that this methodology is reliable for the determination of the concentration levels of α-synuclein auto-antibody, in control and patient samples diluted to 50 %.

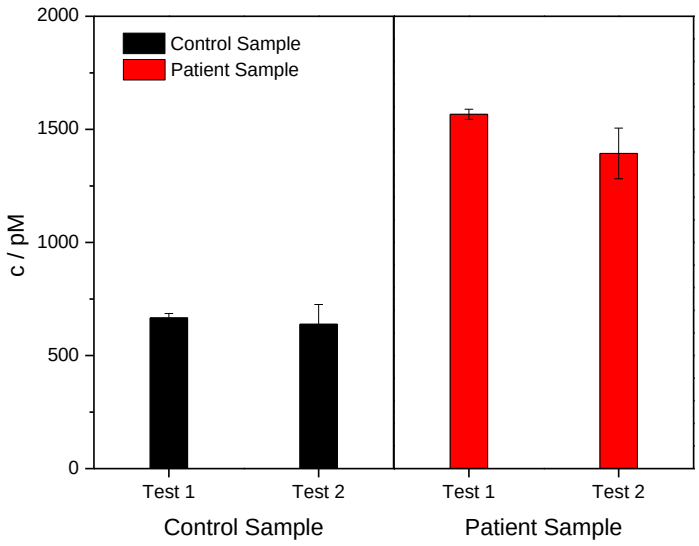


Figure 4.7. The variation of the detection between various electrodes was determined by detecting the same samples, one control (# 7530, black bars) and one patient sample (# 8556, red bars), on two individual electrodes (n = 3 for each test). The coefficient of variations for the control and the patient sample are 3 % and 8 %, respectively.

4.6 Detection of α-Synuclein Auto-Antibody in Patient Samples

Herein, two cohorts of patient samples were studied: one was supplied by *Professor Ludmilla Morozova-Roche's group at the Department of Medical*

Biochemistry and Biophysics, Umeå University, Sweden; the other was from *Dr Richard Wade-Martins' group at the Department of Physiology, Anatomy and Genetics, University of Oxford, United Kingdom*.

Fourteen control samples and fourteen H-Y 2 patient samples from the *Umeå University* patient cohort were initially tested *via* self-calibration method (Section 2.9.2), and the results are shown in Figure 4.8 and Table 4.1. The concentration range of α-synuclein auto-antibody in control samples was determined to be from 0.25 nM to 1.0 nM (mean ca. 0.73 pM), while the range in H-Y 2 patient samples was determined to be slightly wider, that is from 0.43 nM to 2.1 nM (mean ca. 1.2 pM). Both the control and the H-Y 2 samples have outliers, which are 1.8 nM and 3.4 nM respectively. A Student's *t*-test was conducted with the exclusion of the outliers; a two-tail *p* value of 0.037 was calculated. This result indicates that there is significant difference between the control and patient samples in the concentration level of α-synuclein auto-antibody; these primary results strongly suggest that the α-synuclein auto-antibody is potentially a sensitive biomarker for the diagnosis of PD in the early stage (H-Y 2).

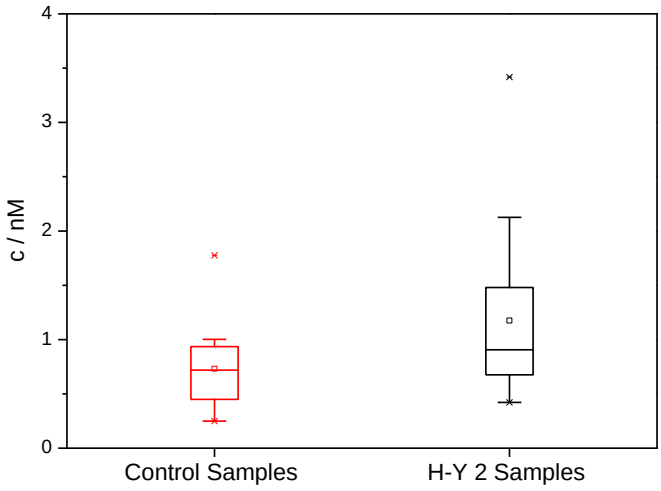


Figure 4.8. A Box-and-whisker plot of the detection of the α-synuclein auto-antibody concentrations in the control and H-Y 2 patient samples.

Table 4.1. The data of analysed control and H-Y 2 patient samples (n = 3 for each sample).

Control		**H-Y 2**	
Subject Code	Concentration (nM)	Subject Code	Concentration (nM)
8509	0.26 ± 0.01	8712	0.47 ± 0.05
8700	0.27 ± 0.01	8610	0.47 ± 0.09
8518	0.45 ± 0.03	8569	0.66 ± 0.07
8508	0.45 ± 0.01	6236	0.68 ± 0.03
8914	0.49 ± 0.02	8733	0.83 ± 0.06
8521	0.60 ± 0.05	8550	0.83 ± 0.12
7530	0.67 ± 0.09	8512	0.84 ± 0.10
8877	0.77 ± 0.05	8563	0.97 ± 0.15
8738	0.79 ± 0.10	8738	0.97 ± 0.17
8573	0.84 ± 0.05	7820	1.19 ± 0.13
8550	0.94 ± 0.02	8500	1.48 ± 0.09
8749	0.95 ± 0.11	8556	1.57 ± 0.11
8714	1.00 ± 0.09	8950	2.13 ± 0.18
8516	1.60 ± 0.18	8577	3.42 ± 0.24

To verify the observation based on the *Umeå University* patient cohort, the detection of concentration levels of the α-synuclein auto-antibody, using the samples provided by the *University of Oxford*, were carried out, *via* the previously detailed standard addition method (Section 2.9.3). Five unknown samples were initially tested blindly; the details of these five samples were revealed after the determination, as four of them are in the H-Y 2 stage (Table 4.2).

Table 4.2. Determined concentrations of five unknown samples.

Subject Code	Concentration (nM)	H-Y
RH / 101	1.4 ± 0.2	2
RH / 103	1.5 ± 0.3	2
RH / 104	1.8 ± 0.1	2
RH / 105	2.1 ± 0.1	2

The concentration range of the α-synuclein auto-antibody in the H-Y 2 patient samples, which was determined by performing assays of the samples in the *Umeå University* patient cohort, was found to be between 0.43 and 2.13 nM. The concentration levels in these four H-Y 2 patient samples, which provided by the *University of Oxford*, are completely within this range (Figure 4.9). The consistency of these results, demonstrates that this methodology, for determining the concentration of α-synuclein auto-antibody in a bid to distinguish H-Y 2 stage patients from healthy controls, can be applied to various sample cohorts. In addition, it suggests that α-synuclein auto-antibody is a promising biomarker for the diagnosis of Parkinson's disease at the H-Y 2 stage.

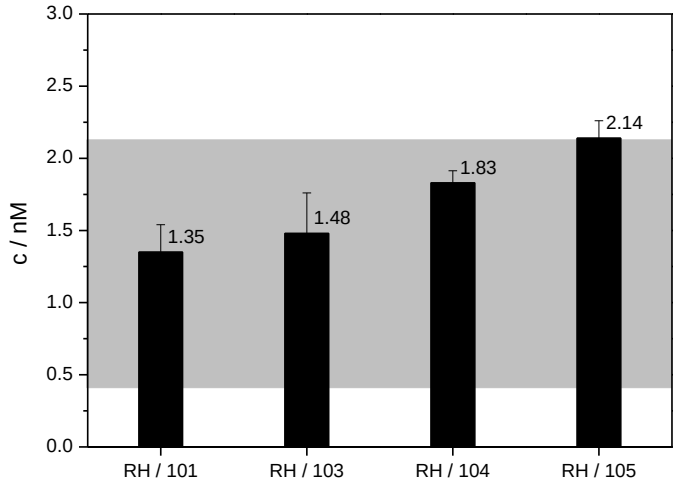


Figure 4.9. The concentrations of α-synuclein auto-antibody in four H-Y 2 patient samples, supplied by the *University of Oxford,* RH / 101, RH / 103, RH / 104, and RH / 105. The grey square highlights the concentration range of H-Y 2 patient samples, in *Umeå University* patient cohort. These four concentrations are completely in the range.

4.7 Conclusions

With a great desire on developing sensitive method for the early onset diagnosis of Parkinson's disease (PD), a variety of attempts to discover the most reliable biomarker have been described. Recently, naturally generated antibodies (auto-antibody), in response to α-synuclein have attracted enormous attention, and a number of relevant studies have been reported.[84, 85, 99, 100] However, there is still no agreement on whether the concentration level of α-synuclein auto-antibody in patient samples is higher than that in controls, or lower.

Herein, a label-free impedimetric biosensor, capable of reliably detecting α-synuclein auto-antibody in 50 % diluted PD samples, has been described. Consistent results have been observed across two different patient cohorts; that is the concentration

range of α-synuclein auto-antibody for healthy controls is from 0.25 nM to 1.0 nM, while that for H-Y 2 patient samples is higher, from 0.43 nM to 2.1 nM. A Student's *t*-test indicates that there is a significant difference between the control and H-Y 2 patient samples ($p \sim 0.037$). Thus, α-synuclein auto-antibody is likely to be a robust and promising biomarker for the diagnosis of PD in the H-Y 2 stage, and an increase in concentration was observed in patients.

Chapter 5. Insulin Assay *via* Non-Faradaic EIS

5.1 Objectives

Non-Faradaic EIS is a more transferrable technique for the point-of care devices than Faradaic EIS, due to the absence of redox probes.[27] Thus, it is of great interest to develop an insulin assay based on non-Faradaic EIS measurements. Although non-Faradaic EIS have been employed on various immunoassays (of virus, bacterial, *etc*),[49, 122-124] the insufficient selectivity remains challenge in its applications on assays of small targets like insulin. The most promising solution to this insufficiency of selectivity is to form an anti-fouling interface. For example, constructing an OEGylated or a PEGylated monolayer has been well established and achieved noticeable improvement on selectivity.[125-128] The PEG thiol SAM, previously used to fabricate insulin and α-synuclein antibody biosensors, also succeeded in significantly resisting non-specific adsorption in 50 % serum (Chapter 3 & Chapter 4).

In addition to traditional PEGylated materials, the neutrally-charged, biocompatible zwitterionic polymers (PCBMA) have been used as the anti-fouling reagent. Not only can it improve the surface resistance to non-specific components' association, but also its abundant carboxyl groups can act as coupling sites for stable receptor immobilisation.[32] For example, a SPR, cancer biosensor, using the 3,4-dihydroxy-(*L*)-phenylalanine-conjugated PCBMA to form an anti-fouling interface, presented a low LOD (0.64 nM) even in neat human serum.[33] With the great advantage of reducing non-specific background, it is interesting to apply this polymer in the assays

via non-Faradaic EIS (the preferred label-free measurement method), which has not been reported in literature.

In addition, though both of these two anti-fouling materials, PEG and PCBMA, have been reported to be promising, there is no detailed comparative study to investigate which one is preferred for the fabrication of label-free biosensors. Furthermore, it is also interesting to apply this non-fouling polymer, PCBMA, on fabricating impedimetric label-free biosensor, to hopefully further improve the sensitivity and selectivity of biosensors characterised by non-Faradaic EIS. Therefore, two types of label-free insulin biosensors: one based on PEG thiol SAM and the other on PCBMA film, were characterised by using non-Faradaic EIS. Real impedance (Z'), as one of the most common parameters for non-Faradaic EIS, was used throughout this chapter. Comparisons of sensitivity, linearity and anti-fouling ability in serum, between these two types of biosensors, were conducted.

5.2 Zwitterionic Polymer Interfaces

5.2.1 Stability Test

As mentioned in Section 2.7.2, comparing to chemical immobilisation, physical attachment of this polymer film, though faster, can result in possible dissociation during measurement. Therefore, the stability of this polymer interface was investigated by performing non-Faradic EIS measurements regularly over 24 days.

Repeatable results were obtained, in Figure 5.1. An obvious change in relative response (*RZ′*, the ratio of responses measured on different days to those of the freshly-prepared biosensor) was observed on the second day; this fluctuation probably results from the dissolution of extra reactants and small oligomers into solution. After that, considerably stable responses were seen in the following days, with the variation < 3 %. Therefore, this polymer interface was stable up to 23 days, which dramatically exceeds the typical experimental period, 2 – 3 days. However, due to the fluctuation observed on the second day, freshly prepared polymer films should be immersed in PBS for at least 24 hours to stabilise the surface, before further experiments.

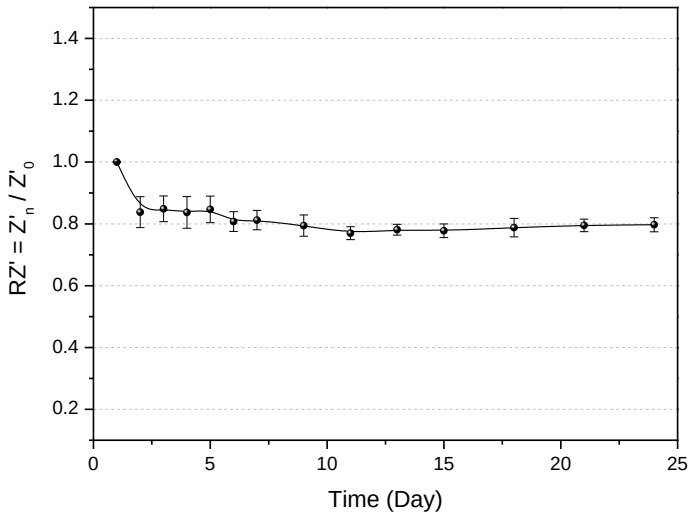


Figure 5.1. Assessing the stability of zwitterionic polymer interfaces over the course of 24 days. Relative response (*RZ′*) is the ratio of responses in real impedance, measured on different days (Z'_n), to those of the freshly-prepared biosensor (Z'_0). Error bars are the standard deviation of *RZ′* at four frequencies (0.85, 0.53, 0.11 and 0.01 Hz), tested on the same day. The polymer film appears to be stable for at least 23 days, with the variation of 3 %.

5.2.2 Biosensor Fabrication

The insulin biosensor was fabricated by firstly depositing the polymer film onto the gold surface (254 nm UV-initiated polymerisation), loading insulin antibodies by the use of EDC / NHS activation (Figure 5.2 (A)). The entire fabrication process was monitored by non-Faradaic EIS. The responses in Z' upon the modification of each interface were recorded, in Figure 5.2 (B). As mentioned previously, the impedance describes the one-dimensional diffusion process of cations or anions, from the bulk solution to the working electrode (Section 1.2.2).[47] There are many factors, such as the steric hindrance and the surface charge, leading to the changes in this diffusion process, hence, demonstrating increases or decreases in impedance.[109, 110] The constructions of both the polymer film (thickness ~ 13 nm)[32] and the insulin antibody (MW ~ 160 kDa)[129] interface induced considerable increases in the steric hindrance on the working electrode surface (more effective than changes in the surface charge); this huge steric hindrance severely impeded this diffusion process from solution to the working electrode, thus, dramatic increases in Z' were observed as expected, in comparison to the response on a bare gold surface. In addition, it can be seen from the Bode plots that signals at lower frequencies are more responsive to the changes of interfaces. Therefore, in the later experiments, the frequency range was moved down towards the lower frequencies, from 1 to 0.01 Hz (30 evenly-selected data points).

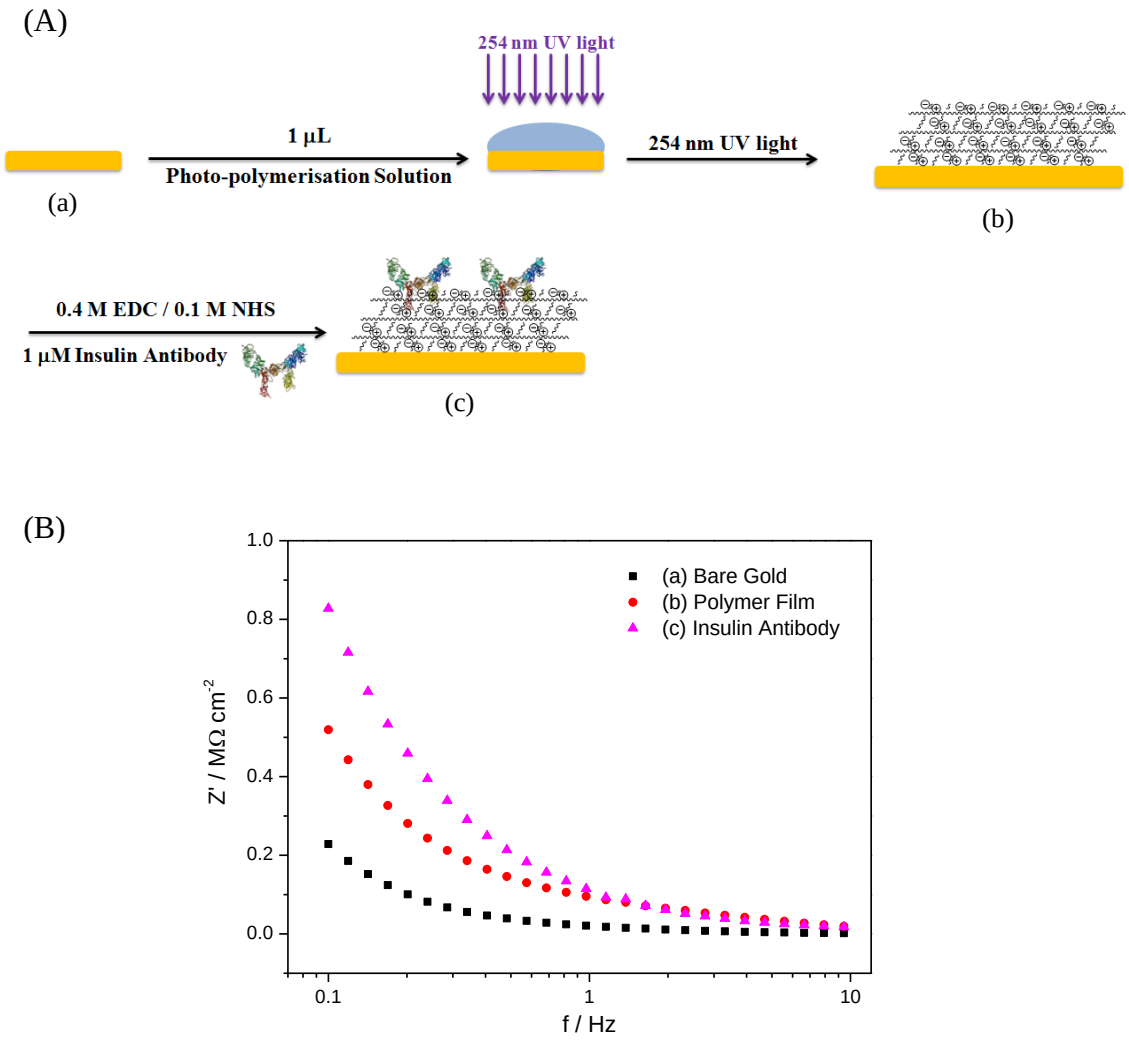


Figure 5.2. (A) The scheme of fabrication process, demonstrating the structure and formation of each interface. The photo-polymerisation solution is an aqua solution, which consists of 172 g/L CBMA, 2 g/L ethylene glycol dimethacrylate and 11.7 g/L 2-hydroxyl-2-methylpropiophenone. (B) Bode plots of various interfaces recorded by non-Faradaic EIS technique in 10 mM PBS (pH 7.4) solution. The effective area of the electrode is about 0.038 cm^2. (a) Bare gold surface, (b) polymer film (*hv* time 30 min), and (c) insulin antibody interface.

5.2.3 Frequency-Dependent Response

The non-Faradaic detection of insulin, based on the use of polymer film, was carried out *ex situ* by performing non-Faradaic EIS, in 10 mM PBS, within the frequency range from 1 to 0.01 Hz (30 analysing points) (experimental details see Section 2.7). A series of responses in Z' were recorded by applying various frequencies.

Prior to the investigation on concentration-dependent responses, the frequency dependence of responses to the variation of the concentration of insulin were analysed to find the most responsive frequencies. Different from the increasing responses observed in the fabrication process (Section 5.2.2), where the entire response was dominated by the considerable increase in the steric hindrance, the response to the binding of insulin decreased, in regard of the increase in concentration (Figure 5.3); the possible reason is that the changes in the surface charge dominate the entire response, and at pH 7.4, insulin is negatively charged (pI ~ 5.3),[62] which is opposite to the surface charge of insulin antibody interface (pI ~ 8).[130] In the following concentration-dependent analysis, responses at the four lowest frequencies, 0.010, 0.012, 0.014 and 0.016 Hz, which display relatively more responsive signals, were selected.

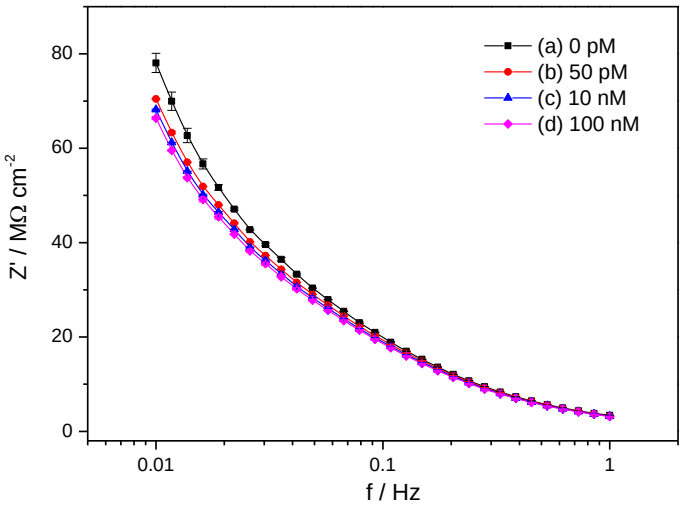


Figure 5.3. The frequency-dependent responses in *Z'*, recorded on antibody film incubating with different concentrations of antigen: (a) 0 pM, the antibody interface, (b) 50 pM, (c) 10 nM, and (d) 100 nM.

5.2.4 Concentration-Dependent Response

Based on previous frequency-dependent analysis, responses at the four lowest frequencies, 0.010, 0.012, 0.014 and 0.016 Hz, were selected to study the concentration-dependent responses; the analysis was carried out by performing a series of *ex situ* insulin detections from 5 pM to 500 nM in a 10 mM PBS solution (Section 2.7). Critical pieces of information for the four different frequencies, such as sensitivity, R^2, LOD, and linear range, determined based on the analytical curves, are all listed in Figure 5.4. Responses at all four frequencies presented the same linear range (5 – 100 pM) and similar sensitivity (~ 3 % per decade concentration). In regard to the values of LOD, 0.010 Hz is the frequency, where the lowest LOD was seen (0.73 ± 0.06 pM). In addition, the analytical curve at 0.010 Hz displays the best linearity, with the R^2 determined to be 0.99. Therefore, the best responses for label-free insulin biosensor, based on PCBMA polymer film, demonstrated the sensitivity of approximately 3 % per decade concentration, the linear range from 5 – 100 pM, and an LOD ~ 0.73 pM. The K_D for the binding between insulin antibody and insulin, was determined to be 4.2 ± 0.2 pM.

Frequency (Hz)	Sensitivity (% per decade concentration)	R^2	LOD (pM)	Linear range (pM)
0.010	3.4 ± 0.2	0.99	0.73 ± 0.06	5 – 100
0.012	3.4 ± 0.1	0.99	1.86 ± 0.60	5 – 100
0.014	2.9 ± 0.3	0.97	3.84 ± 0.85	5 – 100
0.016	3.3 ± 0.2	0.98	6.48 ± 0.68	5 – 100

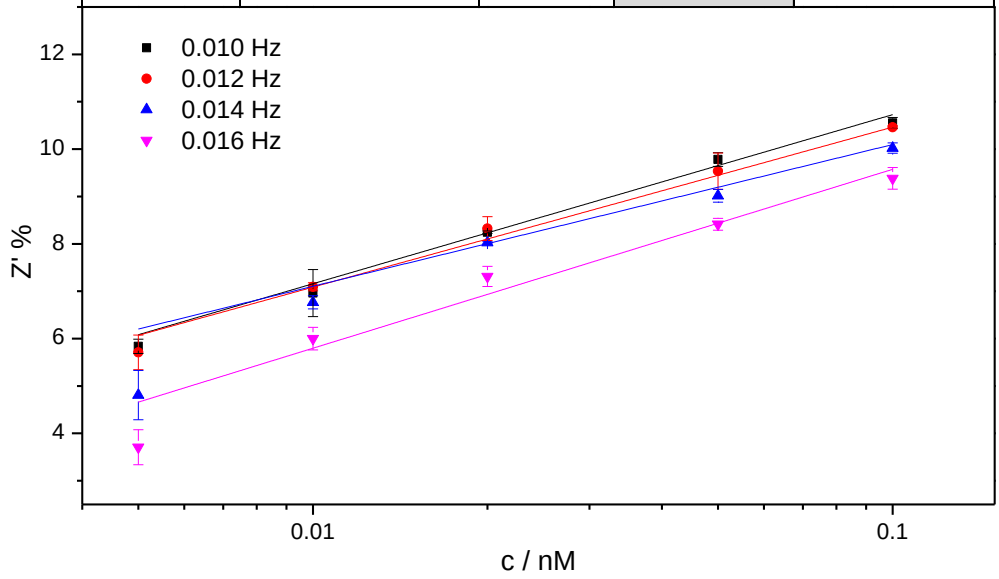


Figure 5.4. Comparing the concentration-dependent response in *Z′* at four selected frequencies (0.010, 0.012, 0.014 and 0.016). Critical information is shown in the table (top), such as sensitivity (the slope), R^2, LOD and linear range. LOD, showing the most significant variation among frequencies, is highlighted. All the information was determined based on the analytical curves (bottom).

The Langmuir isotherm plots of the responses at 0.010 Hz, induced by the binding of the specific target (insulin), and the control protein (BSA), are shown in Figure 5.5. The insert is the calibration curve of the responses at 0.010 Hz, within the linear range. It is clear that the binding of the insulin reaches saturation after roughly 200 nM. To investigate the selectivity of this interface, the detection of various concentrations of BSA, using the same insulin antibody-modified polymer interface, were performed as a

control experiment. The saturated non-specific response (to 500 nM BSA) is about 1.3 %, which is considerably lower than the specific response to only 5 pM insulin (~ 6 %); it indicates that the selectivity of this insulin biosensor is potentially good.

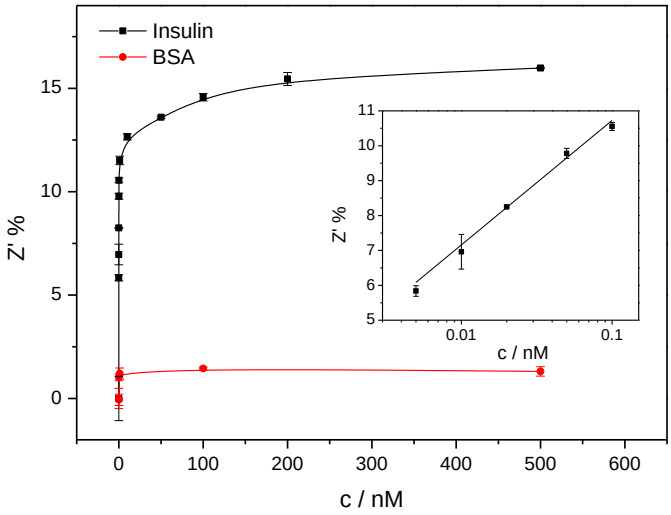


Figure 5.5. The Langmuir isotherm plots of the responses to the target, insulin, and the control protein, BSA, at 0.010 Hz. The insert is the calibration curve for 0.010 Hz. The value of R^2 is 0.99. The K_D was determined to be 4.2 ± 0.2 nM.

5.2.5 Characterisation of Anti-Fouling Property

Zwitterionic polymers, which have a neutral surface charge and are hydrophilic, are claimed to be promising non-fouling materials (structure in Figure 2.4).[32, 131, 132] The anti-fouling property of this zwitterionic polymer was characterised by performing *ex situ* incubations with various diluted blood serum samples (varying from 1 % to 100 %) in 10 mM PBS. Responses in *Z′ %* at 0.010 Hz, where the optimum analytical curve was obtained, were corrected by subtracting the responses contributed from the serum insulin (~ 60 pM [108]) and presented in Figure 5.6. The black bar represents the specific

response to 50 pM insulin; 50 pM is a very low concentration for clinical applications, since the fasting concentration of insulin in healthy human blood is around 60 pM.[108] In comparison to the response to 50 pM (~ 10 %), the non-specific binding in up to 80 % serum is insignificant (~ 0.5 %). Thus, this zwitterionic polymer film is highly anti-fouling, in up to 80 % human serum.

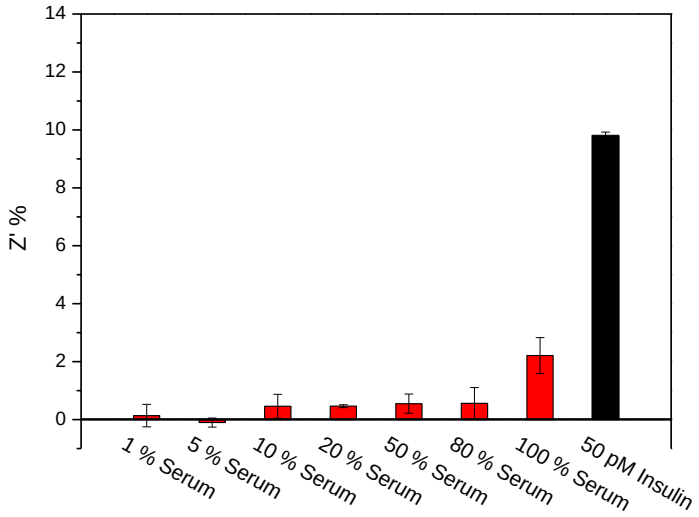


Figure 5.6. Response in *Z' %* to various serum concentrations (1 %, 5 %, 10 %, 20 %, 50 %, 80 %, and 100 %) is displayed. The black bar illustrates the specific response to 50 pM insulin. Comparing to the response to 50 pM insulin (~ 10 %), the non-specific response in 80 % is still tiny (~ 0.5 %); it suggests that this biosensor is therefore, likely to demonstrate high resistance to irrelevant components, even in 80 % serum.

5.3 PEG Thiol SAM Interfaces

5.3.1 Biosensor Fabrication

By using the same surface chemistry in Chapter 3, insulin biosensor based on PEG thiol SAM was fabricated, and the formation of each interface was characterised *via* non-Faradaic EIS (Figure 5.7). Similarly to the polymer film, the construction of

PEG thiol SAM (thickness ~ 2.5 nm)[133] also resulted in significant increase in steric hindrance on the gold surface. Thus, as expected, the fabrications of PEG thiol SAM and subsequent insulin antibody interface induced successive increases in *Z′*.

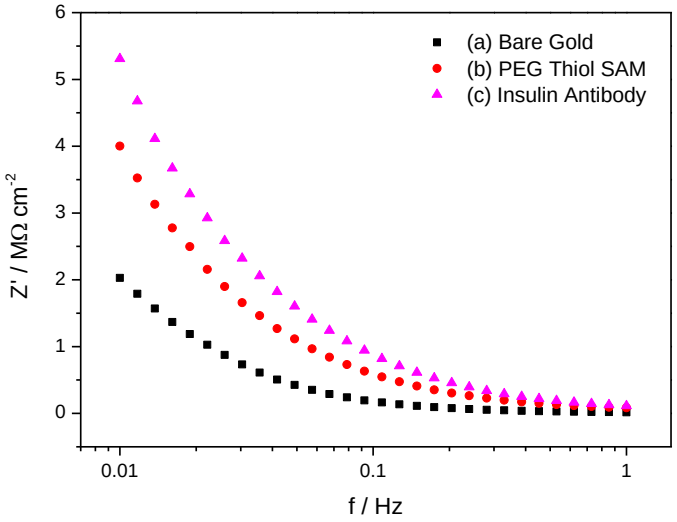


Figure 5.7. The Bode plots observed of various films in 10 mM PBS (pH 7.4) solution, under non-Faradaic EIS technique: (a) bare gold surface, (b) PEG thiol SAM, (c) insulin antibody interface.

5.3.2 Frequency-Dependent Response

The non-Faradaic detection of insulin using a PEG thiol SAM-based film was carried out *ex situ* under non-Faradaic EIS conditions, in 10 mM PBS. The same 30 measured points were selected in the same frequency range (0.01 – 1 Hz). Similar to the zwitterionic polymer film (Section 5.2.3), the decreasing responses to various concentrations of insulin are relatively more responsive at low frequencies (Figure 5.8). Therefore, the responses at the four lowest frequencies, 0.010, 0.012, 0.014 and 0.016 Hz, were further studied for observing the response variability induced by varying the concentration of insulin.

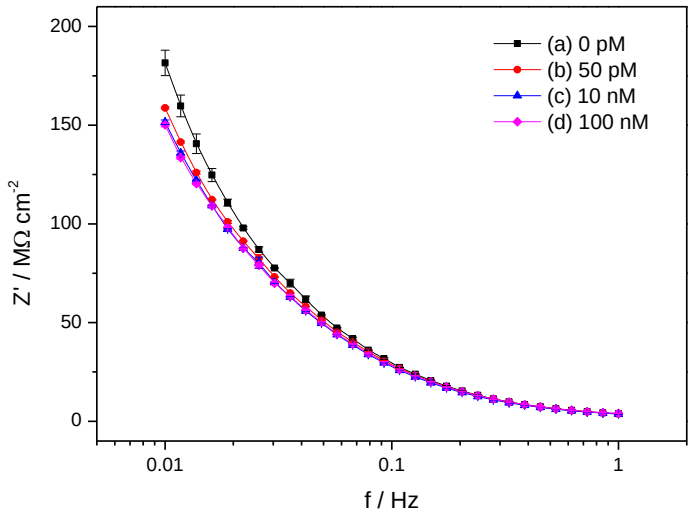


Figure 5.8. The frequency-dependent responses in *Z′* recorded on an antibody film, incubated with four different concentrations of antigen: (a) 0 pM, the antibody interface, (b) 50 pM, (c) 10 nM, and (d) 100 nM.

5.3.3 Concentration-Dependent Response

Similar to the concentration-dependent analysis for polymer-based insulin biosensor in Section 5.2.4, detailed information of the comparative studies on the four selected frequencies, 0.010, 0.012, 0.014, and 0.016 Hz, is shown in Figure 5.9. Again, responses at all four frequencies demonstrate the same linear range, from 5 to 100 pM. In terms of the values of LOD, the responses obtained at 0.010 and 0.012 Hz (LOD ~ 1 pM) are better than those at the other two frequencies (LOD > 4 pM). Furthermore, considering the linearity of the analytical curve at 0.010 Hz (R^2 = 0.96) is slightly better than 0.012 Hz (R^2 = 0.92), the best frequency for the non-Faradaic EIS measurements of PEG thiol SAM-based insulin assays appears to be 0.010 Hz, where a sensitivity of ~ 3 % per decade concentration, the linear range from 5 – 100 pM (R^2 = 0.96) and an

LOD of 1.08 (± 0.62) pM were determined. The K_D of binding between insulin antibody and insulin based on PEG thiol SAM was calculated to be 0.69 ± 0.10 nM.

Frequency (Hz)	Sensitivity (% per decade concentration)	R^2	LOD (pM)	Linear range (pM)
0.010	3.3 ± 0.3	0.96	1.08 ± 0.62	5 – 100
0.012	3.4 ± 0.5	0.92	1.07 ± 0.58	5 – 100
0.014	2.6 ± 0.2	0.96	4.05 ± 0.75	5 – 100
0.016	2.4 ± 0.1	0.92	5.98 ± 0.60	5 – 100

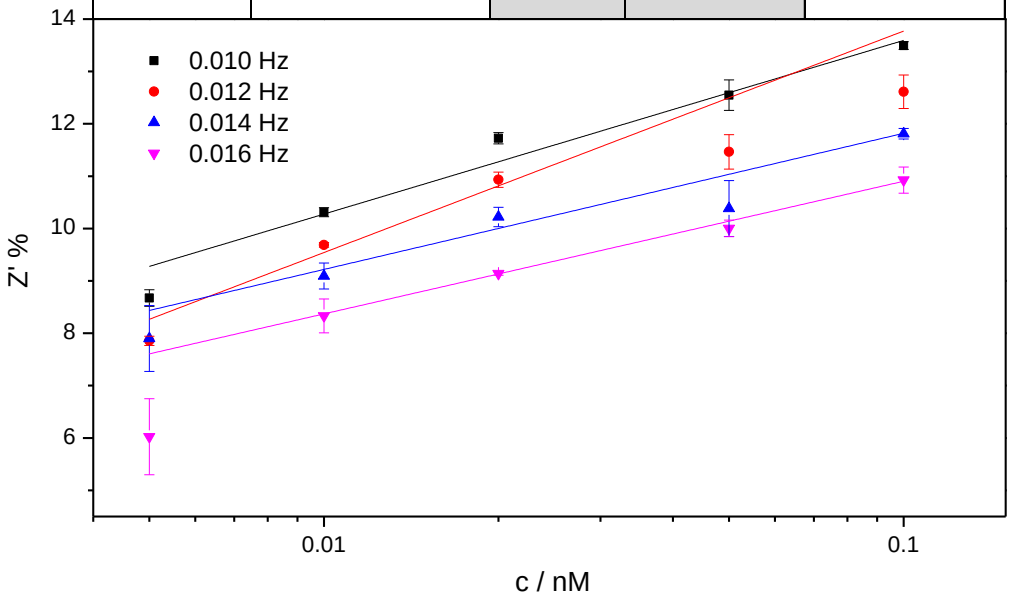


Figure 5.9. Comparing the concentration-dependent response in *Z′* at four selected frequencies (0.010, 0.012, 0.014 and 0.016). Critical information is shown in the table (top), such as sensitivity (the slope), R^2, LOD and linear range. LOD and R^2, presenting the most significant variation among frequencies, are highlighted. All the information was determined from the analytical curves (bottom).

The Langmuir isotherm plots of the detection of the specific target (insulin) and control (BSA) were comparatively demonstrated in Figure 5.10. The insert is the calibration curve of the responses at 0.010 Hz. The signal induced by the binding of 500

nM BSA PBS solution was observed to be ~ 1.7 %, which is significantly lower than the specific response to the binding of 5 pM insulin (~ 8 %). Thus, the selectivity of this biosensor is likely to be high.

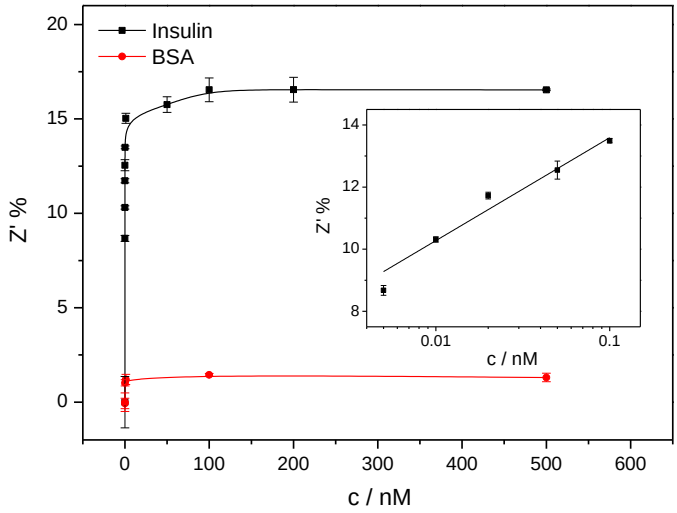


Figure 5.10. The Langmuir isotherm plots of the responses to the target, insulin, and the control protein, BSA, at 0.010 Hz. The insert is the calibration curve for 0.010 Hz. The value of R^2 is 0.96. The K_D was determined to be 0.69 ± 0.10 nM.

5.3.4 Characterisation of Anti-Fouling Property

In the previous chapter, the anti-fouling property of this insulin antibody-modified PEG thiol SAM was determined to be capable of remaining high sensitivity in 50 % serum (Section 3.4). Similar characterisation was performed upon the same surface by the use of non-Faradaic EIS, in Figure 5.11. Comparing to the response to 50 pM insulin (~ 12.5 %), the non-specific adsorption in 50 % serum merely brings about an increase of 0.5 % in Z' %. However, noticeable response in 80 % serum (~ 5.7 %) indicates the occurrence of significant non-specific attachment onto the gold surface.

Thus, the limit of the concentration of serum is 50 %, which is consistent to the results observed in Faradaic insulin assays (Section 3.4).

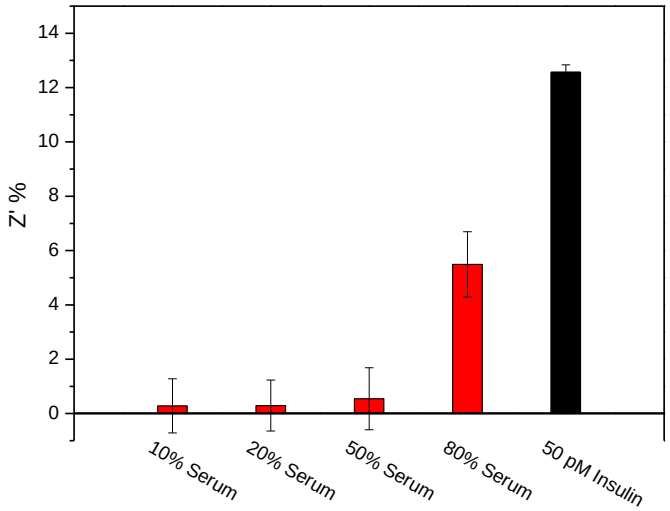


Figure 5.11. The response in *Z′ %* to various serum concentrations (10 %, 20 %, 50 %, and 80 %) in 10 mM PBS solutions is displayed. The black bar illustrates the specific response to 50 pM insulin. Comparing to the response to 50 pM insulin (~ 12.5 %), the non-specific response in 80 % is still tiny (~ 0.5 %); it suggests that this biosensor is capable of resisting non-specific adsorption in 50 % serum.

5.4 Conclusions

Both the zwitterionic polymer and the PEG thiol have been reported to be promising anti-fouling materials of excellent biocompatibility. However, there is still no literature stating the comparison between them, in terms of the achievement of efficient anti-fouling interfaces. Herein, parallel experiments were carried out to compare the sensitivity and selectivity of insulin biosensors based on a zwitterionic polymer (PCBMA) and PEG thiol SAM, *via* non-Faradaic EIS. The results collected herein, as well as those of Faradaic EIS measurements (Chapter 3), are listed in Table 5.1.

Non-Faradaic EIS was performed to characterise the insulin biosensors, fabricated on two different interfaces, PEG thiol SAM and PCBMA film. The latter one seems to be the better option, in terms of LOD, linearity and affinity between insulin and its antibody (K_D). However, it is noticeable that the K_D for the polymer interface is significantly lower than that presented in the literature (two-decade difference).[121] The possible reason for this specially low K_D is likely to be the excellent hydrophilicity of this zwitterionic polymer; this could contribute to the exposure of the epitopes of antibodies by forming a hydrophobic environment on the receptor surface, and thus increase the antibody-antigen binding affinity.[134]

In addition, this polymer has been reported to be a non-fouling material, which can resist non-specific adsorption, even in pure human serum.[33] However, herein, the limit for resisting significant non-specific adsorption was observed to be 80 % serum. This reduction in anti-fouling ability could result from the fact that this polymer film is physically adsorbed onto the gold surface, and might not be able to well cover the edges of the gold surface.

Previous studies on Faradaic EIS insulin assays (Chapter 3) report the ability of sensing pico-molar concentrations of insulin, with a linear range spanning from 5 pM to 50 nM; maintains high sensitivity in 50 % human serum. Non-Faradaic insulin biosensors present slightly better antibody-antigen affinity (K_D), similar LOD and equally good anti-fouling ability, in comparison to those performed under Faradaic conditions. However, the advantage of Faradaic EIS measurements lies with the wide linear range (~ four orders of magnitude).

Table 5.1. Comparison of the three different assays.

	Polymer Film (Non-Faradaic)	**PEG Thiol SAM (Non-Faradaic)**	**PEG Thiol SAM (Faradaic Chapter 3)**
Sensitivity (% per decade concentration)	3.4	3.3	12
R^2	0.99	0.96	0.99
LOD (pM)	0.73 ± 0.06	1.08 ± 0.62	1.24 ± 0.01
Linear range (pM)	5 – 100	5 – 100	5 – 50000
K_D **(pM)**	4.2 ± 0.2	690 ± 100	850 ± 10
Test in Serum	80 %	50 %	50 %

Chapter 6. Electrochemical Immittance Analysis

6.1 Objectives

There have been various studies and applications on biosensors, by the use of Faradaic and non-Faradaic EIS.[101] For Faradaic EIS, charge transfer resistance (R_{ct}) obtained by fitting the signal with Randles equivalent circuit is the most widely used analysing parameter, while most non-Faradaic EIS studies presented data in impedance (Z) or capacitance (C).[27] Since the biosensor performances, such as measuring time, LOD and linearity, are variable, depending on different applied frequencies (see examples in Chapter 5), it suggests the importance of finding the optimum frequencies and parameters, with the aim of achieving high efficiency assays for protein biomarker screening. However, in the literature, there is no systematic analysis of the sensing performances at various frequencies, as well as in different parameters. Furthermore, there is also a lack of the discussion about the selection of these two EIS techniques, with the aim of improving assay performances.

Herein, responses of insulin assays in various parameters based on four mathematically derived immittance functions (the complex impedance (Z^*), the complex capacitance (C^*), the complex modulus (M^*) and the complex admittance (Y^*)) were thoroughly analysed across the frequency range of eight orders of magnitude (from 0.01 Hz to 1 M Hz). The objective is to find the optimum parameters and frequencies, presenting the most sensitive responses and relatively low noise. In addition, a parallel analysis was performed on the data obtained by the use of both

Faradaic and non-Faradaic EIS, it was hoped that suggestions on how to select the appropriate parameters for the right EIS techniques could be elucidated.

6.2 Frequency Spectra (FS)

As presented in Section 2.10.3, the raw data was converted to the values of relative sensitivity (*RS*) in different parameters, which a normalised response that accounts for spectral noise, taking the ratio of the binding-induced response (R_n *%*) to the noise (*CV*). Since the response varies depending on different frequencies the selection of the most responsive frequency (the frequency of RS_{MAX}) was aided by plotting the response across forty evenly selected frequencies, in the range from 0.01 Hz to 1 M Hz, this plot named as frequency spectra (FS). These spectra are widely used in the work to investigate the frequency-dependent responsivity of all twelve parameters in Table 2.3.

FS for responses of Faradaic insulin assays in Z'' are taken as an example (Figure 6.1). R_n *%* changed gradually along with the frequency, and the maximum response is observed at 0.04 Hz. However, the FS for *CV* and *RS* display several sharp peaks, such as at 1 Hz in the FS of noise and at 0.04 Hz in the FS of *RS*, which can confuse the selection of the maximum values. Therefore, a fast Fourier transform (FFT) smoothing process was applied to eliminate those irregular data points. As shown in the Figure 6.1 (c), the optimum response shifts to the higher frequency (from 0.04 Hz to 0.06 Hz), when the noise is taken into account. The FSs for other parameters are shown in Appendix A.

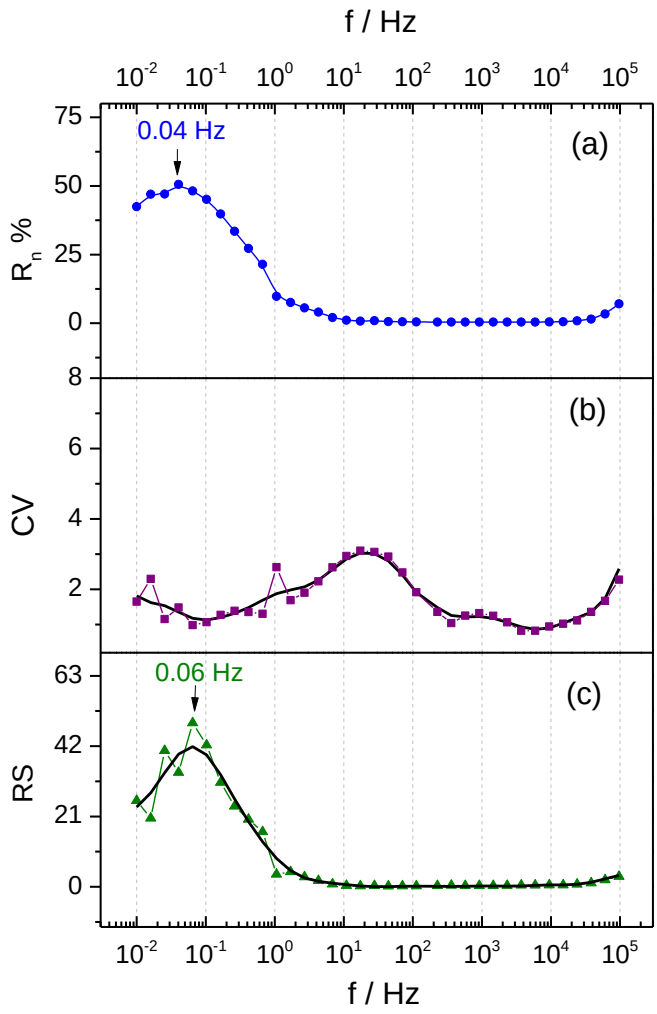


Figure 6.1. One example of frequency-dependent responses in normalised *Z″* (*R_n %*) (a), noise (*CV*) (b) and the relative sensitivity (*RS*) (c). An FFT smoothed analysis was applied to find the maximum. According to (a), 0.04 Hz seems to be the best frequency where demonstrates the most sensitive response. However, if taking noise into account, 0.06 Hz should be the best frequency (c).

6.3 Frequency-Dependent Analysis

Comparative insulin assays *via* Faradaic EIS and non-Faradic EIS were performed in parallel. To investigate the frequency-dependent responses of investigated parameters based on immittance functions (Z^*, C^*, M^* and Y^* for both Faradaic and non-Faradaic EIS) and R_{ct} (for Faradic EIS), the relative sensitivity (*RS*) of 1 nM insulin

were selected; at this concentration, the optimum responses (RS_{MAX}) of R_{ct} and all investigated parameters, and the optimum frequency ranges were calculated and shown in Figure 6.2.

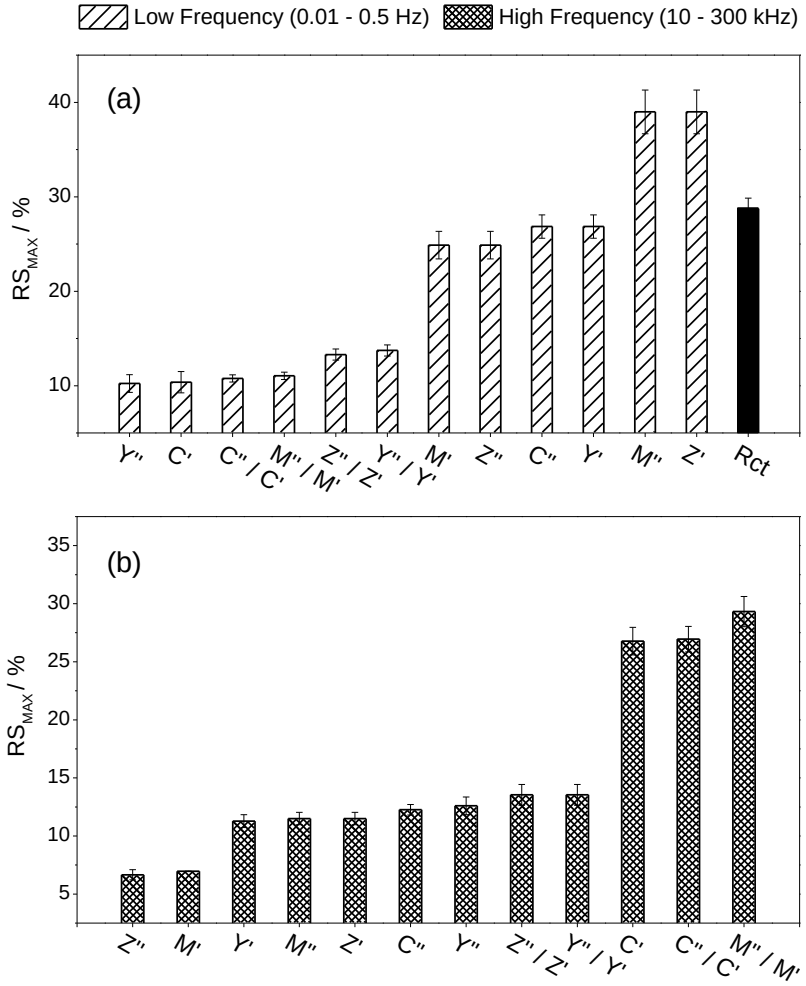


Figure 6.2. The optimum responses (RS_{MAX}), for 1 nM insulin, of R_{ct} and all investigated parameters based on immittance functions, and the optimum frequency ranges, were demonstrated ((a) Faradaic EIS, (b) non-Faradaic EIS). The response for R_{ct} is not frequency dependent, in the black bar. Error bars were obtained by three repetitions on the same electrode. Corresponding results have been observed on three individual detections. The optimum parameters for Faradaic EIS were observed to be Z' and M″ at low frequency (0.01 – 0.5 Hz), both of which are significantly more responsive than R_{ct}, while those for non-Faradaic EIS are C', C'' / C', and M'' / M' at high frequency (10 – 300 kHz).

For Faradaic EIS, the analyses of frequency-dependent responses in parameters, obtained based on immittance functions, suggest that low frequency (from 0.01 to 0.5 Hz) is the optimum frequency range; in this optimum frequency range, the optimum parameters were observed to be Z' and M'' (RS_{MAX} = 39 ± 2 %) (Figure 6.2, (a)). Across the twelve investigated parameters, the values of RS_{MAX} vary from ~ 10 % (Y'') to ~ 39 % (Z' and M''); this difference is almost 4 fold. To date, in assays *via* Faradaic EIS, R_{ct} is the most commonly used parameter, determined by fitting response with Randles equivalent circuit.[27] Herein, the relative sensitivity of R_{ct} ($RS(R_{ct})$), which is not a frequency-dependent parameter, was calculated to be 29 ± 1 %. Comparing to the optimum parameter (Z' and M''), R_{ct} appears to be 25 % less responsive. This result suggests that, for insulin assay via Faradaic EIS, Z' and M'' can be the better parameters than R_{ct}, which is the most commonly used parameter in literature.

For non-Faradaic EIS, the great advantages lie with the absence of a redox probe and zero initial bias voltage, but, in the meantime, there are concerns about the possible low sensitivity to perform label-free assays due to the lack of signal amplification resulting from the added redox probe or labels. Therefore, it is of considerable importance to find the optimum parameters and frequency ranges, in order to achieve higher sensitivity. To date, impedance (Z) and capacitance (C) are the most widely used parameters,[27] but there is no detailed analysis of other parameters and reported optimum frequency range. Detailed results of the analysis of insulin assays *via* non-Faradaic EIS are shown in (Figure 6.2, (b)). The optimum response (RS_{MAX}) for each investigated parameter was observed at higher frequency, from 10 to 300 kHz, and in this frequency range, the best parameters are resolved as C', C'' / C', and M'' / M', exhibiting the RS of

~ 28 %, which is about 3-fold higher than the least responsive parameter (Z''). However, the optimum parameters for non-Faradaic EIS appear to be less responsive than those for Faradaic EIS.

6.4 Concentration-Dependent Analysis

Based on the results of the frequency-dependent analysis above (Section 6.3), the analytical curves of the least, the moderate, and the most responsive parameters were selected to investigate the variation of responses, depending on the concentration of insulin (Figure 6.3). For Faradaic EIS (Figure 6.3 (A)), all analytical curves of the selected parameters demonstrate the same linear range, across four orders of magnitude. The slope of the optimum parameters (Z' and M'') is 6-fold larger than that of the least responsive parameter (Y''), and the slope of R_{ct} is equal to that of the moderate responsive parameter (M'); this, again, suggests that the optimum parameters (Z' and M'') presented here are potentially to be better than R_{ct}. For non-Faradaic EIS (Figure 6.3 (B)), the linear range is from 5 pM to 1 nM, and there is less significant difference in slope of various parameters. However, it is still clear that the slope of optimum parameters (C'' / C', and M'' / M') is 2 fold of those of the moderate and least responsive ones (C'' and Z'' respectively).

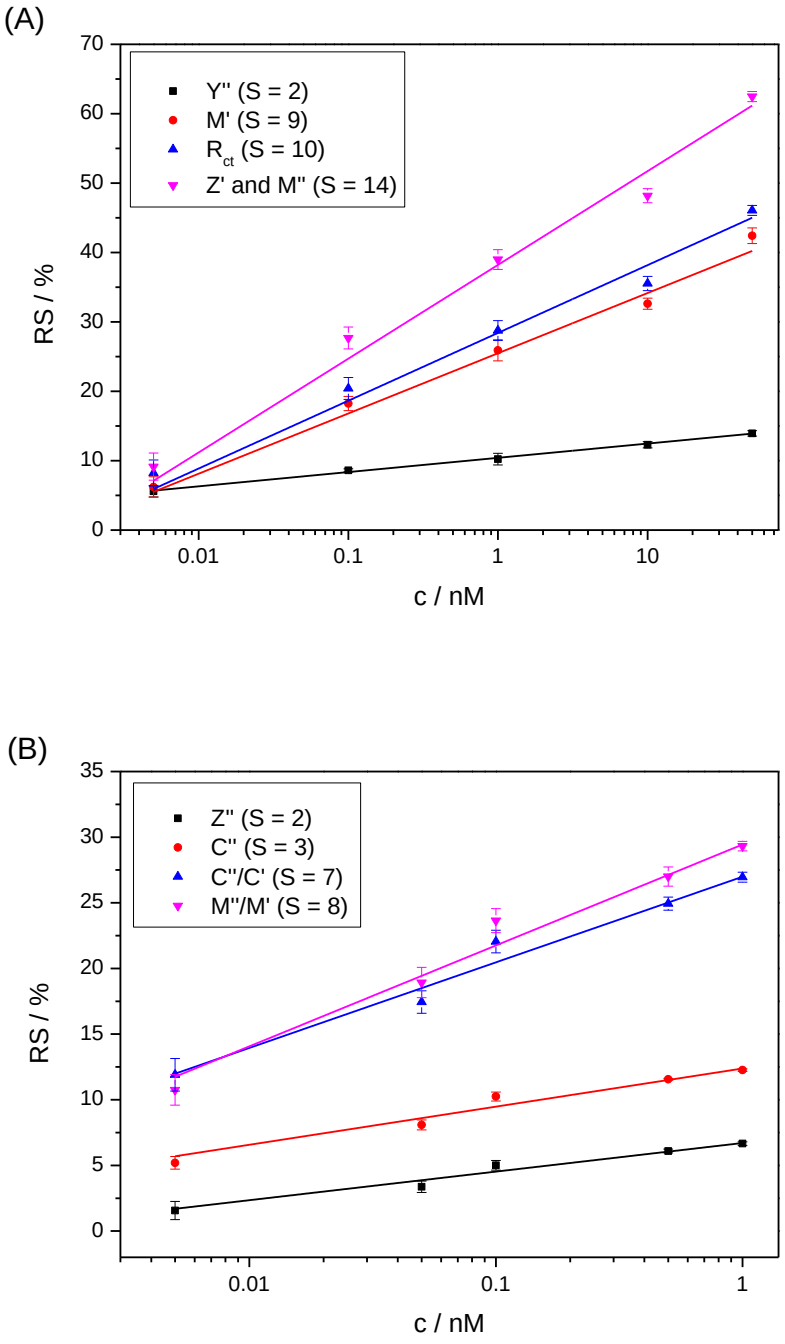


Figure 6.3. Analytical curves of the insulin assays, in the selected parameters. The numbers in the brackets are the values of the slope of each analytical curve, which represents the sensitivity. The values of slope are shown in the brackets, expressed in % per decade concentration. (A) Faradaic EIS, (B) non-Faradaic EIS. Error bars were obtained by three repetitions on the same electrode. Corresponding results have been observed on three individual detections.

6.5 Conclusions

EIS is a very powerful technique for the characterisation of biosensors because of its high sensitivity and non-destructive effect on analytes. However, the disadvantages, recording signals across a wide range of frequencies and processing data in a large library of parameters, have significantly constrained the applications of this technique. Herein, parameters, obtained based on four functions, complex impedance function (Z^*), complex capacitance function (C^*), complex modulus function (M^*) and complex admittance function (Y^*), are picked from the library and systematically analysed from 0.01 Hz to 1 MHz for both Faradaic and non-Faradaic EIS assays, by using insulin as targets, with the aim of selecting optimum parameters and small range of optimum frequencies.

The frequency-dependent analysis suggests that Faradaic EIS appears to be more responsive at lower frequency (0.01 – 0.5 Hz), while non-Faradaic EIS is more responsive at higher frequency (10 – 300 kHz). Thus, non-Faradaic EIS is likely to be a more efficient method, due to the observation that the optimum response for each parameter arise at higher frequency (10 – 300 kHz), where the measuring time for each data point is much shorter (above 10 fold) than performing measurements at low frequencies. However, assays performed by Faradaic EIS are overall more sensitive and demonstrate wider linear range, when compared with non-Faradaic EIS. In addition, the concentration-dependent analysis proposed that, although R_{ct} is the most widely used parameter for assays using Faradaic EIS, the optimum parameters reported here (Z' and M'') presented significantly higher sensitivity than R_{ct} (75 % higher), when both signal and noise were taken into account. For non-Faradaic EIS, not only did the traditional

parameter C' demonstrate high sensitivity, but the ratio parameters C'' / C', and M'' / M' seemed to be promising.

In summary, the main advantages of Faradaic EIS are considerably higher signal-to-noise responses and a remarkably wide linear range (across four orders of magnitude), while the outstanding advantage of non-Faradaic EIS is that it enables performing highly sensitive assays at higher frequencies, which could dramatically reduce the measuring time. It is expected that this work may lead researchers to consider about, when developing EIS biomarker sensing systems, the selection of right EIS technique and proper parameters, so as to achieve more efficient assays with higher sensitivity and shorter time.

Chapter 7. Conclusions & Future Work

In this thesis, EIS, a potent electrochemical technique, has been employed to assess the performances of label-free assays of various biomarkers. An assembly protocol, including the formation of PEG thiol SAM and the subsequent immobilisation of receptors *via* EDC / NHS activation, was firstly applied to generate a label-free insulin biosensor. The sensitivity and selectivity were characterised by Faradaic EIS, and an outstanding LOD (1.2 pM), a wide linear range (across four orders of magnitude) and successful anti-fouling in up to 50 % serum were obtained, while previous insulin immunoassays *via* SPR only reported in 25 % serum[71].

The results observed for label-free insulin assays *via* Faradaic EIS suggest strong potential for performing detection of biomarkers in real patient samples, with the aim of developing novel and highly sensitive diagnostic methods. Therefore, employing the same assembly protocol, an α-synuclein antibody biosensor was generated, allowing detection of the α-synuclein auto-antibody in early stage (H-Y 2) Parkinson's disease (PD) patients and healthy controls. The concentration levels of α-synuclein auto-antibody in patient samples and control samples were determined to be statistically significantly different ($p \sim 0.037$). Furthermore, consistency in the measurement of the α-synuclein auto-antibody concentration was observed in the H-Y 2 patient samples from a second PD cohort. Thus, this label-free, impedimetric α-synuclein antibody biosensor appears to be robust and promising for the diagnosis of early-onset PD.

Both Faradaic and non-Faradaic EIS are powerful techniques, with the potential of being applied in the development of highly efficient point-of-care devices. However, in comparison to Faradaic EIS, non-Faradaic EIS, performed in the absence of redox probes, is a more transferable approach in this respect. Therefore, it is of great interest to utilise non-Faradaic EIS in the label-free detection of insulin. Herein, in addition to the insulin biosensor based on PEG thiol SAM, another insulin biosensor, fabricated based on a zwitterionic polymer (PCBMA) film, was also examined. This polymer-based biosensor, presenting a sub-pico-molar LOD succeeded in effectively resisting non-specific adsorption in up to 80 % serum. Hence, by employing this zwitterionic polymer, the anti-fouling ability of the sensing interfaces was highly improved.

The application of non-Faradaic EIS suggests that sensing performance (*e.g.* sensitivity, LOD, linearity) varies at different applied frequencies. However, to date, impedance assays typically operate by recording responses in one of the available parameters (mostly, R_{ct} for Faradaic EIS, C or Z for non-Faradaic EIS), at a certain number of applied frequencies without optimisation. Thus, herein, a thorough analysis of the responsivity of various parameters derived from four mathematically defined immittance functions, across the frequency range from 0.01 Hz to 1000 kHz, was conducted, based on the data obtained from insulin assays in both EIS techniques. The results demonstrate that Faradaic EIS is generally more sensitive, presenting a wider linear range, while non-Faradaic EIS is more rapid, performing highly sensitive assays at higher frequencies (10 – 300 kHz).

The assembly protocol and EIS techniques described in this thesis presented excellent applicability in the assays of various biomarkers and have been demonstrated

using insulin and α-synuclein auto-antibodies. However, the fabrication and detection was performed on planar gold electrodes (area ~ 0.02 cm^2), which require larger sample volumes (> 200 μL). This can be avoided by utilising microelectrode (area ~ 0.2 mm^2) arrays, which are able to perform multi-detection by constructing various sensing interfaces on one plate. Thus, it can not only reduce the volume, but also improve the assay throughput. In addition, the electrochemical immittance analysis provides highly sensitive frequency ranges for EIS. If these frequency ranges can be confirmed by analysing a larger dataset, real-time EIS measurements could potentially be developed by monitoring the signals at a single frequency, selected from the sensitive frequency range. This will allow further improvements of the efficiency of EIS.

Chapter 8. References:

1. R. S. Yalow and S. A. Berson, *Nature*, 1959, **184**, 1648-1649.
2. M. J. Schmerr and A. Jenny, *Electrophoresis*, 1998, **19**, 409-414.
3. J. J. Pratt, M. G. Woldring and L. Villerius, *J. Immunol. Methods*, 1978, **21**, 179-184.
4. G. Kohler and C. Milstein, *Nature*, 1975, **256**, 495-497.
5. M. Herrmann, T. Veres and M. Tabrizian, *Anal. Chem.*, 2008, **80**, 5160-5167.
6. M. H. V. Van Regenmortel and J. Burckard, *Virology*, 1980, **106**, 327-334.
7. R. A. Respess, M. A. Rayfield and T. J. Dondero, *AIDS*, 2001, **15**, S49-S59.
8. H.-T. Kuo, J. Z. Yeh, C.-M. Jiang and M.-C. Wu, *J. Immunol. Methods*, 2012, **381**, 32-40.
9. J. D. Thacker, E. S. Casale and C. M. Tucker, *J. Agric. Food Chem.*, 1996, **44**, 2680-2685.
10. P. Hornbeck, in *Current Protocols in Immunology*, John Wiley & Sons, Inc., 2001.
11. J. G. Erhardt, J. E. Estes, C. M. Pfeiffer, H. K. Biesalski and N. E. Craft, *J. Nutr.*, 2004, **134**, 3127-3132.
12. X. Fan, I. M. White, S. I. Shopova, H. Zhu, J. D. Suter and Y. Sun, *Anal. Chim. Acta*, 2008, **620**, 8-26.
13. A. S. Afonso, B. F. Zanetti, A. C. Santiago, F. Henrique-Silva, L. H. C. Mattoso and R. C. Faria, *Talanta*, 2013, **104**, 193-197.
14. B. Li, Y. Du, H. Wei and S. Dong, *Chem. Commun.*, 2007, **0**, 3780-3782.
15. A. Shons, F. Dorman and J. Najarian, *J. Biomed. Mater. Res.*, 1972, **6**, 565-570.
16. R. L. Bunde, E. J. Jarvi and J. J. Rosentreter, *Talanta*, 1998, **46**, 1223-1236.
17. Y.-C. Liu, C.-M. Wang and K.-P. Hsiung, *Anal. Biochem.*, 2001, **299**, 130-135.
18. E. Wijaya, C. Lenaerts, S. Maricot, J. Hastanin, S. Habraken, J.-P. Vilcot, R. Boukherroub and S. Szunerits, *Curr. Opin. Solid State Mater. Sci.*, 2011, **15**, 208-224.
19. C. Boozer, G. Kim, S. Cong, H. Guan and T. Londergan, *Curr. Opin. Biotechnol.*, 2006, **17**, 400-405.
20. A. W. Wark, H. J. Lee and R. M. Corn, *Anal. Chem.*, 2005, **77**, 3904-3907.
21. S. Yan, N. He, Y. Song, Z. Zhang, J. Qian and Z. Xiao, *J. Electroanal. Chem.*, 2010, **641**, 136-140.
22. M. H. Pournaghi-Azar, F. Ahour and M. S. Hejazi, *Electroanalysis*, 2009, **21**, 1822-1828.
23. L. Li, H. Zhao, Z. Chen, X. Mu and L. Guo, *Biosensors Bioelectron.*, 2011, **30**, 261-266.
24. D. Telsnig, V. Kassarnig, C. Zapf, G. Leitinger, K. Kalcher and A. Ortner, *Int. J. Electrochem. Sci.*, 2012, **7**, 10476-10486

25. G. Zheng, F. Patolsky, Y. Cui, W. U. Wang and C. M. Lieber, *Nat Biotech*, 2005, **23**, 1294-1301.
26. X. Luo and J. J. Davis, *Chem. Soc. Rev.*, 2013.
27. J. S. Daniels and N. Pourmand, *Electroanalysis*, 2007, **19**, 1239-1257.
28. E. Herczenik and M. F. B. G. Gebbink, *The FASEB Journal*, 2008, **22**, 2115-2133.
29. H. Otsuka, Y. Nagasaki and K. Kataoka, *Current Opinion in Colloid & Interface Science*, 2001, **6**, 3-10.
30. S. Sharma, R. W. Johnson and T. A. Desai, *Biosensors Bioelectron.*, 2004, **20**, 227-239.
31. J. Piehler, A. Brecht, R. Valiokas, B. Liedberg and G. Gauglitz, *Biosensors Bioelectron.*, 2000, **15**, 473-481.
32. Z. Zhang, S. Chen and S. Jiang, *Biomacromolecules*, 2006, **7**, 3311-3315.
33. N. D. Brault, C. Gao, H. Xue, M. Piliarik, J. Homola, S. Jiang and Q. Yu, *Biosensors Bioelectron.*, 2010, **25**, 2276-2282.
34. A. B. Kharitonov, L. Alfonta, E. Katz and I. Willner, *J. Electroanal. Chem.*, 2000, **487**, 133-141.
35. A. Bardea, F. Patolsky, A. Dagan and I. Willner, *Chem. Commun.*, 1999, 21.
36. S. Liu, J. Liu, X. Han, Y. Cui and W. Wang, *Biosensors Bioelectron.*, 2010, **25**, 1640-1645.
37. X. Li, J. Xia, W. Li and S. Zhang, *Chemistry – An Asian Journal*, 2010, **5**, 294-300.
38. S. Bayoudh, A. Othmane, L. Ponsonnet and H. Ben Ouada, *Colloids Surf. Physicochem. Eng. Aspects*, 2008, **318**, 291-300.
39. A.-E. Radi, J. L. Acero Sánchez, E. Baldrich and C. K. O'Sullivan, *J. Am. Chem. Soc.*, 2005, **128**, 117-124.
40. R. Elshafey, C. Tlili, A. Abulrob, A. C. Tavares and M. Zourob, *Biosensors Bioelectron.*, 2013, **39**, 220-225.
41. J. Rickert, W. Göpel, W. Beck, G. Jung and P. Heiduschka, *Biosens. Bioelectron.*, 1996, **11**, 757-768.
42. X. Fang, O. K. Tan, M. S. Tse and E. E. Ooi, *Biosensors Bioelectron.*, 2010, **25**, 1137-1142.
43. C. Gautier, C. Esnault, C. Cougnon, J.-F. Pilard, N. Casse and B. Chénais, *J. Electroanal. Chem.*, 2007, **610**, 227-233.
44. I. V. Benilova, A. P. Soldatkin, C. Martelet and N. Jaffrezic-Renault, *Electroanalysis*, 2006, **18**, 1950-1956.
45. E. A. de Vasconcelos, N. G. Peres, C. O. Pereira, V. L. da Silva, E. F. da Silva Jr and R. F. Dutra, *Biosensors Bioelectron.*, 2009, **25**, 870-876.
46. K.-C. Lin, V. Kunduru, M. Bothara, K. Rege, S. Prasad and B. L. Ramakrishna, *Biosensors Bioelectron.*, 2010, **25**, 2336-2342.
47. B.-Y. Chang and S.-M. Park, *Annual Review of Analytical Chemistry*, 2010, **3**, 207-229.
48. C. M. Pettit, P. C. Goonetilleke, C. M. Sulyma and D. Roy, *Anal. Chem.*, 2006, **78**, 3723-3729.

49. T. L. Lasseter, W. Cai and R. J. Hamers, *Analyst*, 2004, **129**, 3-8.

50. H. N. Tsao, J. Burschka, C. Yi, F. Kessler, M. K. Nazeeruddin and M. Gratzel, *Energy & Environmental Science*, 2011, **4**, 4921-4924.

51. E. R. Larios-Durán and R. Antaño-López, *J. Electroanal. Chem.*, 2011, **658**, 10-17.

52. N. Xu and D. J. Riley, *Electrochim. Acta*, 2013, **94**, 206-213.

53. M. Bart, E. C. A. Stigter, H. R. Stapert, G. J. de Jong and W. P. van Bennekom, *Biosensors Bioelectron.*, 2005, **21**, 49-59.

54. A. J. Atkinson, W. A. Colburn, V. G. DeGruttola, D. L. DeMets, G. J. Downing, D. F. Hoth, J. A. Oates, C. C. Peck, R. T. Schooley, B. A. Spilker, J. Woodcock and S. L. Zeger, *Clin. Pharmacol. Ther.*, 2001, **69**, 89-95.

55. H. M. Heneghan, N. Miller, A. J. Lowery, K. J. Sweeney, J. Newell and M. J. Kerin, *Ann. Surg.*, 2010, **251**, 499-505.

56. V. S. Vaidya, M. A. Niewczas, L. H. Ficociello, A. C. Johnson, F. B. Collings, J. H. Warram, A. S. Krolewski and J. V. Bonventre, *Kidney Int.*, 2011, **79**, 464-470.

57. W. Hu, A. Chen-Plotkin, S. Arnold, M. Grossman, C. Clark, L. Shaw, L. McCluskey, L. Elman, J. Karlawish, H. Hurtig, A. Siderowf, V. Y. Lee, H. Soares and J. Trojanowski, *Acta Neuropathol. (Berl).* 2010, **120**, 385-399.

58. K. Blennow, H. Hampel, M. Weiner and H. Zetterberg, *Nat Rev Neurol*, 2010, **6**, 131-144.

59. D. S. H. W. Nicol and L. F. Smith, *Nature*, 1960, **187**, 483-485.

60. A. C. Welinder, J. Zhang, D. B. Steensgaard and J. Ulstrup, *PCCP*, 2010, **12**, 9999-10011.

61. A. R. Colwell, *Arch. Intern. Med.*, 1944, **74**, 331-345.

62. L. Bromberg, J. Rashba-Step and T. Scott, *Biophys. J.*, 2005, **89**, 3424-3433.

63. R. I. G. Holt and P. H. Sönksen, *Br. J. Pharmacol.*, 2008, **154**, 542-556.

64. C. E. Mathews, *Pediatric Diabetes*, 2002, **3**, 163-173.

65. D. M. Carneiro, J. U. Levi and G. L. Irvin Iii, *Surgery*, 2002, **132**, 937-943.

66. D. R. Whiting, L. Guariguata, C. Weil and J. Shaw, *Diabetes Res. Clin. Pract.*, 2011, **94**, 311-321.

67. A. Arvinte, A. C. Westermann, A. M. Sesay and V. Virtanen, *Sensors Actuators B: Chem.*, 2010, **150**, 756-763.

68. M. Jaafariasl, E. Shams and M. K. Amini, *Electrochim. Acta*, 2011, **56**, 4390-4395.

69. M. Zhang, C. Mullens and W. Gorski, *Anal. Chem.*, 2005, **77**, 6396-6401.

70. A. Salimi, M. Roushani, S. Soltanian and R. Hallaj, *Anal. Chem.*, 2007, **79**, 7431-7438.

71. K. V. Gobi, H. Iwasaka and N. Miura, *Biosensors Bioelectron.*, 2007, **22**, 1382-1389.

72. M. Frasconi, C. Tortolini, F. Botrè and F. Mazzei, *Anal. Chem.*, 2010, **82**, 7335-7342.

73. J. A. Cox and T. J. Gray, *Anal. Chem.*, 1989, **61**, 2462-2464.

74. J. Wang, J.-W. Mo and A. Erdem, *Electroanalysis*, 2002, **14**, 1365-1368.

75. J. Wang and M. Musameh, *Anal. Chim. Acta*, 2004, **511**, 33-36.

76. A. Salimi, M. Roushani, B. Haghighi and S. Soltanian, *Biosensors Bioelectron.*, 2006, **22**, 220-226.

77. A. Salimi, A. Noorbakhash, E. Sharifi and A. Semnani, *Biosens. Bioelectron.*, 2008, **24**, 798-804.

78. R. M. Snider, M. Ciobanu, A. E. Rue and D. E. Cliffel, *Anal. Chim. Acta*, 2008, **609**, 44-52.

79. Y. Wang and J. Li, *Anal. Chim. Acta*, 2009, **650**, 49-53.

80. A. Salimi, L. Mohamadi, R. Hallaj and S. Soltanian, *Electrochem. Commun.*, 2009, **11**, 1116-1119.

81. B. Rafiee and A. R. Fakhari, *Biosensors Bioelectron.*, 2013, **46**, 130-135.

82. H. Zhang, L.-Q. Xu and S. Perrett, *Methods*, 2011, **53**, 285-294.

83. M. R. Sierks, G. Chatterjee, C. McGraw, S. Kasturirangan, P. Schulz and S. Prasad, *Integrative Biology*, 2011, **3**, 1188-1196.

84. K. Yanamandra, M. A. Gruden, V. Casaite, R. Meskys, L. Forsgren and L. A. Morozova-Roche, *PLoS One*, 2011, **6**, e18513.

85. D. Besong-Agbo, E. Wolf, F. Jessen, M. Oechsner, E. Hametner, W. Poewe, M. Reindl, W. H. Oertel, C. Noelker, M. Bacher and R. Dodel, *Neurology*, 2013, **80**, 169-175.

86. L. M. Patrias, A. C. Klaver, M. P. Coffey and D. A. Loeffler, *Clin. Exp. Immunol.*, 2010, **161**, 527-535.

87. M. Periquet, T. Fulga, L. Myllykangas, M. G. Schlossmacher and M. B. Feany, *The Journal of Neuroscience*, 2007, **27**, 3338-3346.

88. A. J. Lees, J. Hardy and T. Revesz, *The Lancet*, **373**, 2055-2066.

89. C. Li, E. A. Lutz, K. M. Slade, R. A. S. Ruf, G.-F. Wang and G. J. Pielak, *Biochemistry (Mosc).* 2009, **48**, 8578-8584.

90. K. Volkova, V. Kovalska, G. Segers-Nolten, G. Veldhuis, V. Subramaniam and S. Yarmoluk, *Biotech. Histochem.*, 2009, **84**, 55-61.

91. J. Liu, Y. Zhou, Y. Wang, H. Fong, T. M. Murray and J. Zhang, *J. Proteome. Res.*, 2007, **6**, 3614-3627.

92. B. Mollenhauer, V. Cullen, I. Kahn, B. Krastins, T. F. Outeiro, I. Pepivani, J. Ng, W. Schulz-Schaeffer, H. A. Kretzschmar, P. J. McLean, C. Trenkwalder, D. A. Sarracino, J.-P. VonSattel, J. J. Locascio, O. M. A. El-Agnaf and M. G. Schlossmacher, *Exp. Neurol.*, 2008, **213**, 315-325.

93. A. Rekas, C. G. Adda, J. Andrew Aquilina, K. J. Barnham, M. Sunde, D. Galatis, N. A. Williamson, C. L. Masters, R. F. Anders, C. V. Robinson, R. Cappai and J. A. Carver, *J. Mol. Biol.*, 2004, **340**, 1167-1183.

94. Y. An, L. Tang, X. Jiang, H. Chen, M. Yang, L. Jin, S. Zhang, C. Wang and W. Zhang, *Chem-Eur. J.*, 2010, **16**, 14439-14446.

95. S. Fahn, D. Oakes, I. Shoulson, K. Kieburtz, A. Rudolph, A. Lang, C. W. Olanow, C. Tanner, K. Marek and null, *The New England journal of medicine*, 2004, **351**, 2498-2508.

96. E. Tolosa, C. Gaig, J. Santamaría and Y. Compta, *Neurology*, 2009, **72**, S12-S20.

97. M. A. Gruden, T. B. Davudova, M. Mališauskas, V. V. Zamotin, R. D. E. Sewell, N. I. Voskresenskaya, I. A. Kostanyan, V. V. Sherstnev and L. A. Morozova-Roche, *Dement. Geriatr. Cogn. Disord.*, 2004, **18**, 165-171.

98. M. A. Gruden, T. B. Davidova, M. Mališauskas, R. D. E. Sewell, N. I. Voskresenskaya, K. Wilhelm, E. I. Elistratova, V. V. Sherstnev and L. A. Morozova-Roche, *J. Neuroimmunol.*, 2007, **186**, 181-192.

99. K. K. Papachroni, N. Ninkina, A. Papapanagiotou, G. M. Hadjigeorgiou, G. Xiromerisiou, A. Papadimitriou, A. Kalofoutis and V. L. Buchman, *J. Neurochem.*, 2007, **101**, 749-756.

100. M. A. Gruden, R. D. E. Sewell, K. Yanamandra, T. V. Davidova, V. G. Kucheryanu, E. V. Bocharov, O. R. Bocharova, V. V. Polyschuk, V. V. Sherstnev and L. A. Morozova-Roche, *J. Neuroimmunol.*, 2011, **233**, 221-227.

101. F. Lisdat and D. Schäfer, *Anal. Bioanal. Chem.*, 2008, **391**, 1555-1567.

102. Y. Xiao, R. Y. Lai and K. W. Plaxco, *Nat. Protocols*, 2007, **2**, 2875-2880.

103. U. Oesch and J. Janata, *Electrochim. Acta*, 1983, **28**, 1237-1246.

104. H. Y. Cho, A. Srinivasan, J. Hong, E. Hsu, S. Liu, A. Shrivats, D. Kwak, A. K. Bohaty, H.-j. Paik, J. O. Hollinger and K. Matyjaszewski, *Biomacromolecules*, 2011, **12**, 3478-3486.

105. S. Schilp, A. Rosenhahn, M. E. Pettitt, J. Bowen, M. E. Callow, J. A. Callow and M. Grunze, *Langmuir*, 2009, **25**, 10077-10082.

106. P. Harder, M. Grunze, R. Dahint, G. M. Whitesides and P. E. Laibinis, *J. Phys. Chem. B*, 1998, **102**, 426-436.

107. W. Yang, H. Xue, L. R. Carr, J. Wang and S. Jiang, *Biosensors Bioelectron.*, 2011, **26**, 2454-2459.

108. H. Iwase, M. Kobayashi, M. Nakajima and T. Takatori, *Forensic Sci. Int.*, 2001, **115**, 123-127.

109. A. G. Dobrikova, M. I. Dimitrov, S. G. Taneva and I. B. Petkanchin, *Colloids Surf. B. Biointerfaces*, 2007, **56**, 114-120.

110. X. Song, *J. Chem. Phys.*, 2002, **116**, 9359.

111. Y. Huang, M. C. Bell and I. I. Suni, *Anal. Chem.*, 2008, **80**, 9157-9161.

112. C. G. Goetz, W. Poewe, O. Rascol, C. Sampaio, G. T. Stebbins, C. Counsell, N. Giladi, R. G. Holloway, C. G. Moore, G. K. Wenning, M. D. Yahr and L. Seidl, *Mov. Disord.*, 2004, **19**, 1020-1028.

113. A. Salimi, A. Noorbakhash, E. Sharifi and A. Semnani, *Biosensors Bioelectron.*, 2008, **24**, 792-798.

114. D. Tang, R. Yuan, Y. Chai, J. Dai, X. Zhong and Y. Liu, *Bioelectrochemistry*, 2004, **65**, 15-22.

115. L.-G. Zamfir, I. Geana, S. Bourigua, L. Rotariu, C. Bala, A. Errachid and N. Jaffrezic-Renault, *Sensors Actuators B: Chem.*, 2011, **159**, 178-184.

116. W.-W. Zhao, Z.-Y. Ma, P.-P. Yu, X.-Y. Dong, J.-J. Xu and H.-Y. Chen, *Anal. Chem.*, 2011, **84**, 917-923.

117. X. Chen, Y. Wang, J. Zhou, W. Yan, X. Li and J.-J. Zhu, *Anal. Chem.*, 2008, **80**, 2133-2140.

118. Y. Du, B. Li, H. Wei, Y. Wang and E. Wang, *Anal. Chem.*, 2008, **80**, 5110-5117.

119. J. Wu, D. M. Cropek, A. C. West and S. Banta, *Anal. Chem.*, 2010, **82**, 8235-8243.

120. A. Bogomolova, E. Komarova, K. Reber, T. Gerasimov, O. Yavuz, S. Bhatt and M. Aldissi, *Anal. Chem.*, 2009, **81**, 3944-3949.

121. L. Tao and R. T. Kennedy, *Electrophoresis*, 1997, **18**, 112-117.

122. K.-S. Ma, H. Zhou, J. Zoval and M. Madou, *Sensors Actuators B: Chem.*, 2006, **114**, 58-64.

123. W. M. Hassen, C. Chaix, A. Abdelghani, F. Bessueille, D. Leonard and N. Jaffrezic-Renault, *Sensors Actuators B: Chem.*, 2008, **134**, 755-760.

124. S. M. Radke and E. C. Alocilja, *Biosensors Bioelectron.*, 2005, **20**, 1662-1667.

125. K. L. Prime and G. M. Whitesides, *Science*, 1991, **252**, 1164-1167.

126. S. Pasche, M. Textor, L. Meagher, N. D. Spencer and H. J. Griesser, *Langmuir*, 2005, **21**, 6508-6520.

127. J. M. Harris and R. B. Chess, *Nat Rev Drug Discov*, 2003, **2**, 214-221.

128. L. Li, S. Chen and S. Jiang, *J. Biomater. Sci. Polym. Ed.*, 2007, **18**, 1415-1427.

129. S. D. Lidofsky, T. Imasaka and R. N. Zare, *Anal. Chem.*, 1979, **51**, 1602-1605.

130. D. Grube, *Histochemistry*, 1980, **66**, 149-167.

131. L. R. Carr, H. Xue and S. Jiang, *Biomaterials*, 2011, **32**, 961-968.

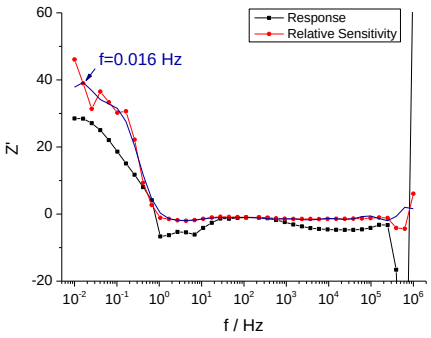
132. L. R. Carr, Y. Zhou, J. E. Krause, H. Xue and S. Jiang, *Biomaterials*, 2011, **32**, 6893-6899.

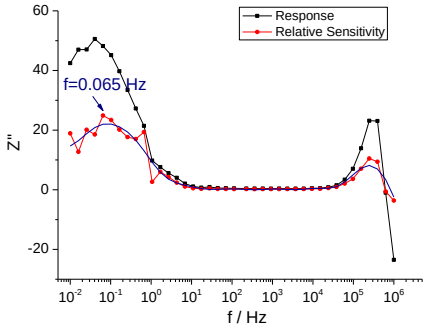
133. A. Papra, A. Bernard, D. Juncker, N. B. Larsen, B. Michel and E. Delamarche, *Langmuir*, 2001, **17**, 4090-4095.

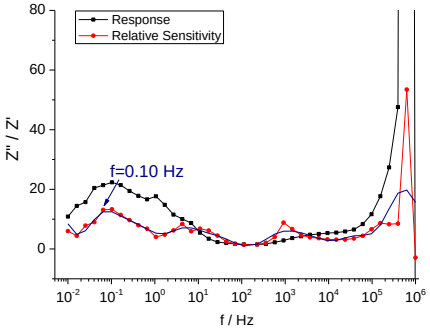
134. A. J. Keefe and S. Jiang, *Nat Chem*, 2012, **4**, 59-63.

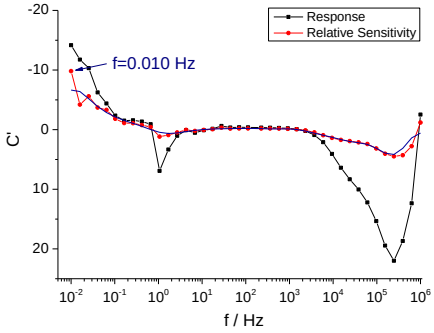
Appendix A. Frequency Spectra (FS)

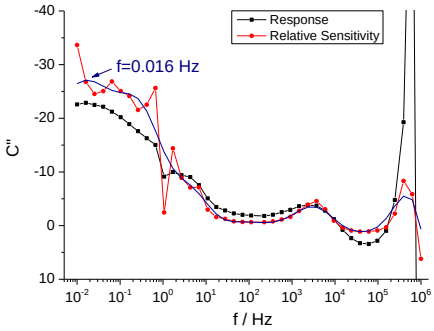
a. Faradaic EIS

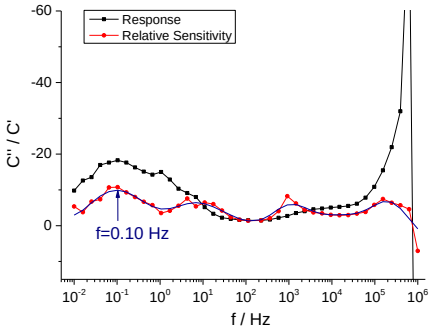












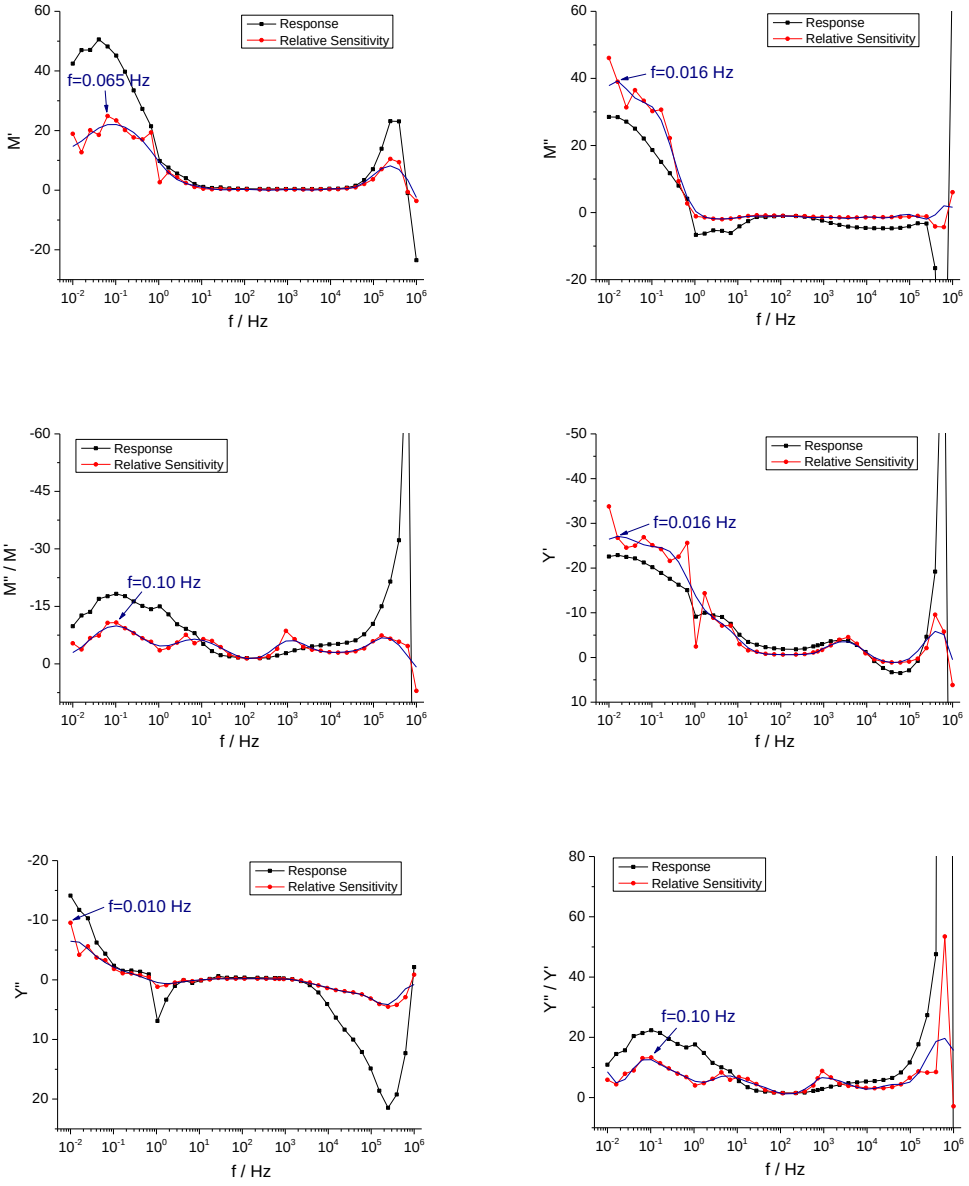
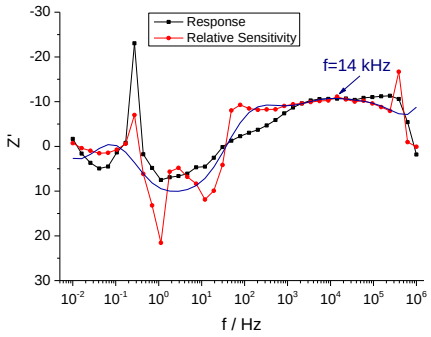
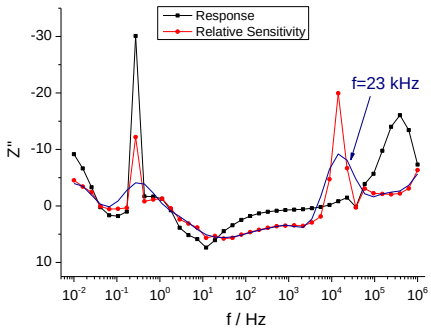
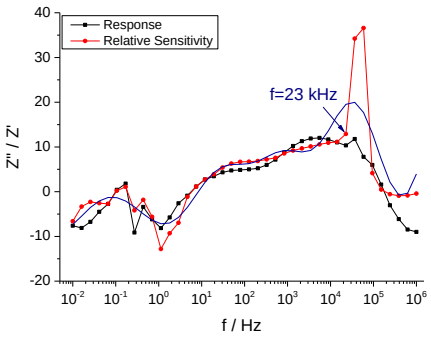


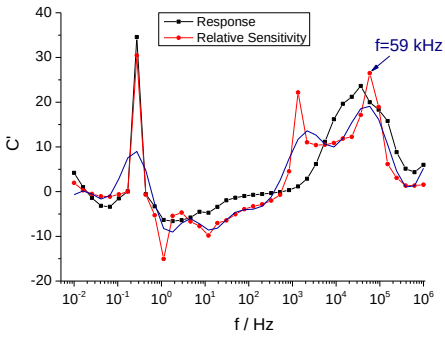
Figure A1. The representative FS of all twelve parameters for Faradaic EIS. Binding-induced response R_n % (black), relative sensitivity *RS* (red), response in *RS* processed by fast Fourier transform (FFT) smoothing in OriginLab (blue).

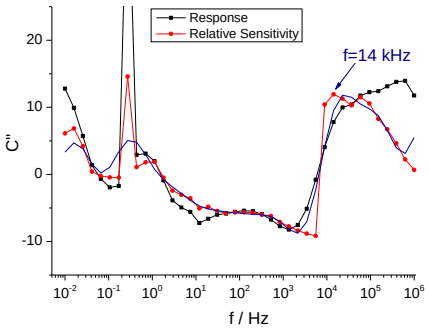
b. Non-Faradaic EIS

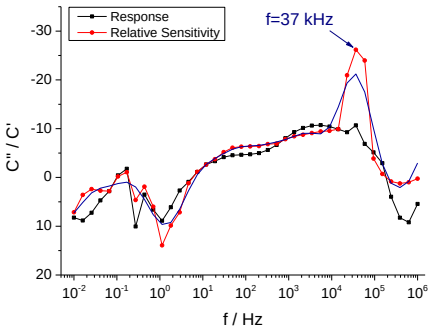












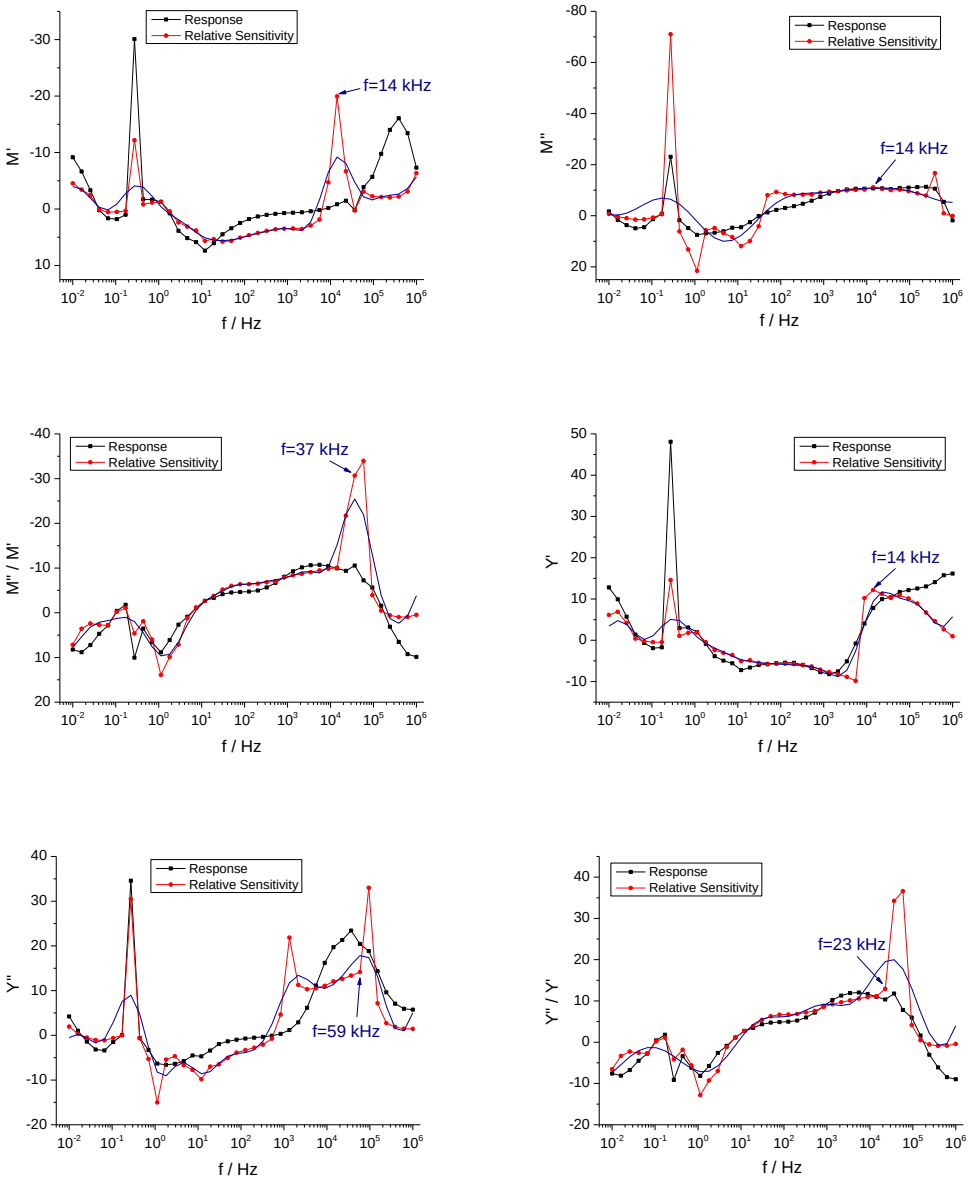


Figure A2. The representative FS of all twelve parameters for non-Faradaic EIS. Binding-induced response R_n % (black), relative sensitivity *RS* (red), response in *RS* processed by fast Fourier transform (FFT) smoothing in OriginLab (blue).

Appendix B. Table of Figures

FIGURE 1.1. ENZYME-LINKED IMMUNE SORBENT ASSAY (ELISA) OVERVIEW FLOWCHART AND SCHEME. 3
FIGURE 1.2. THE THREE TYPES OF ENZYME-LINKED IMMUNE SORBENT ASSAY (ELISA). (A) DIRECT ASSAY, (B) INDIRECT ASSAY, (C) SANDWICH ASSAY. 4
FIGURE 1.3. (A) THE RANDLES EQUIVALENT CIRCUIT OF AN ELECTRIFIED INTERFACE. ELEMENTS IN THE CIRCUIT CORRESPOND TO EACH INTERFACIAL COMPONENT; (WE) WORKING ELECTRODE, (*CDL*) DOUBLE-LAYER CAPACITOR, (R_{CT}) CHARGE TRANSFER RESISTOR, (*Z*) WARBURG IMPEDANCE, (*RS*) RESISTOR OF THE BULK SOLUTION, (CE) COUNTER ELECTRODE. (B) SCHEME OF THE DOUBLE LAYER WHICH FOCUSES AT AN ELECTRIFIED INTERFACE, WHERE THE WORKING ELECTRODE (WE) IS POSITIVELY CHARGED. THE MONOLAYERS OF IONS ABSORBED ONTO THE SURFACE, IN HELMHOLTZ PLANE, CAN BE CONSIDERED AS A SIMPLE CAPACITOR. 11
FIGURE 1.4. A DIAGRAM OF ALTERNATIVE VOLTAGE AND ALTERNATIVE CURRENT. THERE IS A SHIFT BETWEEN THESE TWO SINE WAVES, NAMELY PHASE (ϕ). 12
FIGURE 1.5. A REPRESENTATIVE EXAMPLE OF THE NYQUIST PLOT. 14
FIGURE 1.6. A REPRESENTATIVE EXAMPLE OF THE BODE PLOT. 16
FIGURE 1.7. THE INSULIN MONOMER, FORMED BY CHAIN A (BLUE) AND CHAIN B (MAGENTA), IS PRESENTED. THE BACKBONE IS SHOWN WITH RIBBON, SIDE-CHAINS WITH LINES. TWO DISULFIDE BOUNDS ARE LABELLED IN YELLOW, SHOWN WITH STICKS. 17
FIGURE 1.8. STRUCTURE OF A-SYNUCLEIN IN SODIUM DODECYL SULPHATE. 22
FIGURE 2.1. DETERMINATION OF THE EFFECTIVE SURFACE AREA OF A GOLD SURFACE BY CV SCANS IN 0.5 M H_2SO_4. 29
FIGURE 2.2. REPRESENTATIVE CV CURVE OF A BARE GOLD SURFACE RECORDED IN 10 MM PBS CONTAINING 1.0 MM $[Fe(CN)_6]^{3-/4-}$ AND 0.1 M KCL. THE DIFFERENCE BETWEEN THE ANODIC AND THE CATHODIC PEAK IS AROUND 85 MV, AND THE HALFWAY POTENTIAL IS ABOUT 0.21 V. 30
FIGURE 2.3. STRUCTURAL FORMULA OF PEG THIOL 31
FIGURE 2.4. (A) THE STRUCTURE OF 2-CARBOXYL-*N,N*-DIMETHYL-*N*-(2′-METHACRYLOYLOXYETHYL) ETHANAMINIUM INNER SALT (CBMA). IT IS A ZWITTERIONIC COMPOUND TERMINATED WITH A CARBOXYLIC ACID GROUP. (B) THE STRUCTURE OF ITS POLYMERIC MATERIAL (PCBMA) IS SHOWN IN (A). THE REPRESENTATIVE ILLUSTRATION IN (B) WILL BE USED THROUGHOUT THIS THESIS. 32
FIGURE 2.5. SCHEME FOR THE PROCESS OF THE EDC / NHS ACTIVATION AND SUBSEQUENT IMMOBILISATION OF RECEPTORS (INSULIN ANTIBODY OR A-SYNUCLEIN). THE ANTIBODY INTERFACE BASED ON THE PEG THIOL SAM WAS DEACTIVATED WITH 1.0 M ETHANOLAMINE (PH 8.5) AQUEOUS SOLUTION, WHILE THE ANTIBODY INTERFACE BASED ON POLYMER FILM WAS QUENCHED WITH WATER (IN PBS). 33
FIGURE 2.6. THE CONCENTRATION OF THE REDOX PROBE ($[Fe(CN)_6]^{3-/4-}$) WAS OPTIMISED BY PERFORMING THE DETECTION OF 50 PM INSULIN WITH FRESHLY-PREPARED BIOSENSOR. THREE CONCENTRATIONS, 1.0 MM, 2.0 MM AND 4.0 MM, WERE INVESTIGATED. THE RESPONSE IN R_{CT} WAS RECORDED BEFORE (BLACK) AND AFTER (RED) THE INCUBATION (N = 3 FOR EACH TEST). THE RESULTS DEMONSTRATE THAT THE MOST RESPONSIVE SIGNALS WERE OBSERVED FOR 1.0 MM $[Fe(CN)_6]^{3-/4-}$ 35

FIGURE 2.7. A REPRESENTATIVE EXAMPLE OF DATA FITTING IN FRA. THE BLUE FITTING CURVE WAS OBTAINED BY MARKING THE BEGINNING, CENTRE, AND ENDING POINT OF THE SEMI-CIRCLE, AND MEANWHILE, THE VALUES OF R_S, R_{CT} (R_P), AND *CPE* WERE SHOWN IN THE CORNER WINDOW. 36
FIGURE 2.8. INCUBATION TIME ANALYSIS FOR INSULIN ASSAYS. TWENTY MINUTES WAS CHOSEN TO BE THE INCUBATION TIME. 38
FIGURE 2.9. INCUBATION TIME ANALYSIS FOR SYNUCLEIN ASSAYS. TWENTY MINUTES IS ADOPTED AS THE INCUBATION TIME. 38
FIGURE 2.10. SCHEME OF THE SELF-CALIBRATION METHOD. 46
FIGURE 2.11. SCHEME OF THE STANDARD ADDITION METHOD. 47
FIGURE 2.12. THE EXPLANATION OF BOX-AND-WHISKER PLOT. 48
FIGURE 3.1. (A) FABRICATION OF THE INSULIN BIOSENSOR. (B) NYQUIST PLOTS FOR VARIOUS FILMS, RECORDED IN PBST (10 MM, PH 7.4) SOLUTION (CONTAINS 1.0 MM $[Fe(CN)_6]^{3-/4-}$ AND 0.1 M KCL). A DRAMATIC INCREASE IN R_{CT} WAS OBSERVED AFTER THE IMMOBILISATION OF PEG THIOL AND INSULIN ANTIBODY ONTO THE GOLD SURFACE. (A) BARE GOLD SURFACE (R_{CT} < 160 Ω CM^{-2}); (B) PEG SAM INTERFACE (R_{CT} ~ 4 MΩ CM^{-2}); (C) INSULIN ANTIBODY MODIFIED INTERFACE (R_{CT} ~ 6 MΩ CM^{-2}). 55
FIGURE 3.2. TYPICAL FARADAIC IMPEDANCE SPECTRA, CORRESPONDING TO THE RESPONSE OF THE BIOSENSOR AFTER INCUBATION IN PBST SOLUTION CONTAINING VARYING CONCENTRATIONS OF INSULIN: CURVES FROM (A) TO (F) REPRESENT 0 PM (INSULIN ANTIBODY MODIFIED INTERFACES) (A), 50 PM (B), 100 PM (C), 1 NM (D), 10 NM (E), AND 50 NM (F) INSULIN, RESPECTIVELY. 56
FIGURE 3.3. NORMALISED CHARGE TRANSFER RESISTANCE (R_{CT}) CHANGES OF THE BIOSENSOR AFTER THE INCUBATION WITH DIFFERENT CONCENTRATIONS OF INSULIN PROTEIN IN PBST (10 MM, PH 7.4), CONTAINING 1.0 MM $[Fe(CN)_6]^{3-/4-}$ AND 0.1 M KCL. (A) THE CORRESPONDING CALIBRATION CURVE FOR THE INSULIN BIOSENSORS. (B) BSA WAS USED AS A CONTROL PROTEIN TO SHOW THE SELECTIVITY OF THIS BIOSENSOR. WHEN INCUBATED WITH 500 NM BSA, THE NON-SPECIFIC RESPONSE OF THIS BIOSENSOR IS AROUND 3 %. 57
FIGURE 3.4. CALIBRATION CURVE FOR THE *IN SITU* ASSAY OF INSULIN IN 10 % BLOOD SERUM. THE BIOSENSOR SURFACES WERE INCUBATED IN PBST (10 MM, PH 7.4) SOLUTION, CONTAINING 1.0 MM $[Fe(CN)_6]^{3-/4-}$, 0.1 M KCL AND 10 % BLOOD SERUM, SPIKED WITH DIFFERENT CONCENTRATIONS OF INSULIN. EIS MEASUREMENTS WERE SUBSEQUENTLY CARRIED OUT IN THE SAME SOLUTION. 58
FIGURE 3.5. THE NON-SPECIFIC RESPONSES IN R_{CT} OF THE INSULIN BIOSENSOR AFTER INCUBATION WITH VARIOUS DILUTIONS OF BLOOD SERUM IN PBS. *EX SITU* EIS MEASUREMENTS WERE PERFORMED TO COLLECT THE ORIGINAL R_{CT}, THEN, THE MEASURED DATA WERE CORRECTED BY SUBTRACTION OF RESPONSES THAT CONTRIBUTION FROM THE INSULIN IN THE SERUM ITSELF AS CALCULATED FROM THE CALIBRATION CURVE IN PBS. THIS BIOSENSOR IS LIKELY TO PRESENT SIMILARLY HIGH SENSITIVITY IN UP TO 50 % SERUM. 59
FIGURE 3.6. CALIBRATION CURVE FOR THE EX SITU ASSAYS OF INSULIN IN 50 % BLOOD SERUM. ELECTRODE SURFACES WERE INCUBATED IN PBST (10 MM, PH 7.4) SOLUTION CONTAINING 50 % BLOOD SERUM, SPIKED WITH DIFFERENT CONCENTRATIONS OF INSULIN, AND EIS MEASUREMENTS WERE CARRIED OUT IN PBST (10 MM, PH 7.4) SOLUTION CONTAINING 1.0 MM $[Fe(CN)_6]^{3-/4-}$ AND 0.1 M KCL AFTER RINSING WITH PBST 60
FIGURE 3.7. SENSORY SURFACE REGENERATION BY IMMERSION IN 0.2 M GLY–HCL BUFFER CONTAINING 1 % DMSO FOR 5 MIN PRIOR TO RINSING WITH PBST, AND IMPEDANCE ANALYSIS IN PBST (10 MM, PH 7.4)

SOLUTION CONTAINING 1.0 MM $[Fe(CN)_6]^{3-/4-}$ AND 0.1 M KCL. 'REG 1', 'REG 2', AND 'REG 3' REPRESENT THE REGENERATION NUMBERS. 61

FIGURE 4.1. (A) FABRICATION OF A-SYNUCLEIN ANTIBODY BIOSENSOR. (B) NYQUIST PLOTS OF DIFFERENT FILMS, RECORDED IN PBST (10 MM, PH 7.4) SOLUTION CONTAINING 1.0 MM $[Fe(CN)_6]^{3-/4-}$ AND 0.1 M KCL. DRAMATIC INCREASES IN R_{CT} HAVE BEEN OBSERVED AFTER THE IMMOBILISATIONS OF PEG THIOL AND A-SYNUCLEIN. (A) BARE GOLD SURFACE (R_{CT} < 160 Ω CM^{-2}), (B) PEG SAM INTERFACE (R_{CT} ~ 4 MΩ CM^{-2}), (C) A-SYNUCLEIN MODIFIED INTERFACE (R_{CT} ~ 6 MΩ CM^{-2}). 65

FIGURE 4.2. FARADAIC IMPEDANCE SPECTRA RESPONSIVE TO THE INCUBATION IN PBS SOLUTION WITH DIFFERENT CONCENTRATIONS OF A-SYNUCLEIN ANTIBODY: CURVES REPRESENT 0 PM (A-SYNUCLEIN MODIFIED INTERFACES) (A), 50 PM (B), 100 PM (C), 200 PM (D), 500 PM (E), 1 NM (F), 2 NM (G), 5 NM (H), AND 10 NM (I), RESPECTIVELY. 66

FIGURE 4.3. NORMALISED CHARGE TRANSFER RESISTANCE (R_{CT}) CHANGES OF THE BIOSENSOR AFTER THE INCUBATION WITH DIFFERENT CONCENTRATIONS OF A-SYNUCLEIN ANTIBODY IN PBST (10 MM, PH 7.4). THE MEASUREMENTS OF ORIGINAL R_{CT} WERE CONDUCTED IN 10 MM PBS CONTAINING 1.0 MM $[Fe(CN)_6]^{3-/4-}$ AND 0.1 M KCL. THIS REPRESENTATIVE ANALYTICAL CURVE HAS GOOD LINEARITY (R^2 = 0.99, N = 3 FOR EACH CONCENTRATION) AND A SENSITIVITY OF 13.80 % PER DECADE CONCENTRATION. 67

FIGURE 4.4. *EX SITU* EIS MEASUREMENTS WERE PERFORMED TO DETERMINE THE NON-SPECIFIC RESPONSE OF THE A-SYNUCLEIN ANTIBODY SENSING INTERFACE. THIS BIOSENSOR IS LIKELY TO PRESENT SIMILARLY HIGH SENSITIVITY IN 50 % DILUTED SERUM. 68

FIGURE 4.5. THE CALIBRATION CURVE FOR THE INSULIN ASSAYS, PERFORMED *EX SITU* IN 50 % BLOOD SERUM (R^2 = 0.97). ELECTRODE SURFACES WERE INCUBATED IN PBST (10 MM, PH 7.4) CONTAINING 50 % HUMAN SERUM, SPIKED WITH DIFFERENT CONCENTRATIONS OF A-SYNUCLEIN ANTIBODY, AND EIS MEASUREMENTS WERE CARRIED OUT IN PBST (10 MM, PH 7.4) SOLUTION CONTAINING 1.0 MM $[Fe(CN)_6]^{3-/4-}$ AND 0.1 M KCL AFTER RINSING WITH PBST. 69

FIGURE 4.6. THE ACCURACY OF THESE TWO METHODS, SELF-CALIBRATION AND STANDARD ADDITION, WAS DETERMINED BY PERFORMING THE DETECTION OF A-SYNUCLEIN ANTIBODY IN STANDARD SOLUTIONS, CONTAINING 350 OR 500 PM COMMERCIAL A-SYNUCLEIN ANTIBODY AND 50 % HUMAN SERUM IN PBS. IN REGARD TO THE GIVEN VALUES, THE HIGHEST ERROR OF EXPERIMENTAL VALUES IS DETERMINED TO BE LESS THAN 10 % (318.45 PM COMPARING TO 350 PM), *VIA* SELF-CALIBRATION. 70

FIGURE 4.7. THE VARIATION OF THE DETECTION BETWEEN VARIOUS ELECTRODES WAS DETERMINED BY DETECTING THE SAME SAMPLES, ONE CONTROL (# 7530, BLACK BARS) AND ONE PATIENT SAMPLE (# 8556, RED BARS), ON TWO INDIVIDUAL ELECTRODES (N = 3 FOR EACH TEST). THE COEFFICIENT OF VARIATIONS FOR THE CONTROL AND THE PATIENT SAMPLE ARE 3 % AND 8 %, RESPECTIVELY. 71

FIGURE 4.8. A BOX-AND-WHISKER PLOT OF THE DETECTION OF THE A-SYNUCLEIN AUTO-ANTIBODY CONCENTRATIONS IN THE CONTROL AND H-Y 2 PATIENT SAMPLES. 73

FIGURE 4.9. THE CONCENTRATIONS OF A-SYNUCLEIN AUTO-ANTIBODY IN FOUR H-Y 2 PATIENT SAMPLES, SUPPLIED BY THE *UNIVERSITY OF OXFORD,* RH / 101, RH / 103, RH / 104, AND RH / 105. THE GREY SQUARE HIGHLIGHTS THE CONCENTRATION RANGE OF H-Y 2 PATIENT SAMPLES, IN *UMEÅ UNIVERSITY* PATIENT COHORT. THESE FOUR CONCENTRATIONS ARE COMPLETELY IN THE RANGE. 75

FIGURE 5.1. ASSESSING THE STABILITY OF ZWITTERIONIC POLYMER INTERFACES OVER THE COURSE OF 24 DAYS. RELATIVE RESPONSE (RZ') IS THE RATIO OF RESPONSES IN REAL IMPEDANCE, MEASURED ON DIFFERENT DAYS (Z'_N), TO THOSE OF THE FRESHLY-PREPARED BIOSENSOR (Z'_0). ERROR BARS ARE THE STANDARD DEVIATION OF RZ' AT FOUR FREQUENCIES (0.85, 0.53, 0.11 AND 0.01 HZ), TESTED ON THE SAME DAY. THE POLYMER FILM APPEARS TO BE STABLE FOR AT LEAST 23 DAYS, WITH THE VARIATION OF 3 %. 79

FIGURE 5.2. (A) THE SCHEME OF FABRICATION PROCESS, DEMONSTRATING THE STRUCTURE AND FORMATION OF EACH INTERFACE. THE PHOTO-POLYMERISATION SOLUTION IS AN AQUA SOLUTION, WHICH CONSISTS OF 172 G/L CBMA, 2 G/L ETHYLENE GLYCOL DIMETHACRYLATE AND 11.7 G/L 2-HYDROXYL-2-METHYLPROPIOPHENONE. (B) BODE PLOTS OF VARIOUS INTERFACES RECORDED BY NON-FARADAIC EIS TECHNIQUE IN 10 MM PBS (PH 7.4) SOLUTION. THE EFFECTIVE AREA OF THE ELECTRODE IS ABOUT 0.038 CM^2. (A) BARE GOLD SURFACE, (B) POLYMER FILM (HN TIME 30 MIN), (C) INSULIN ANTIBODY INTERFACE. 81

FIGURE 5.3. THE FREQUENCY-DEPENDENT RESPONSES IN Z', RECORDED ON ANTIBODY FILM INCUBATING WITH DIFFERENT CONCENTRATIONS OF ANTIGEN: (A) 0 PM, THE ANTIBODY INTERFACE, (B) 50 PM, (C) 10 NM, AND (D) 100 NM. 82

FIGURE 5.4. COMPARING THE CONCENTRATION-DEPENDENT RESPONSE IN Z' AT FOUR SELECTED FREQUENCIES (0.010, 0.012, 0.014 AND 0.016). CRITICAL INFORMATION IS SHOWN IN THE TABLE (TOP), SUCH AS SENSITIVITY (THE SLOPE), R^2, LOD AND LINEAR RANGE. LOD, SHOWING THE MOST SIGNIFICANT VARIATION AMONG FREQUENCIES, IS HIGHLIGHTED. ALL THE INFORMATION WAS DETERMINED BASED ON THE ANALYTICAL CURVES (BOTTOM). 84

FIGURE 5.5. THE LANGMUIR ISOTHERM PLOTS OF THE RESPONSES TO THE TARGET, INSULIN, AND THE CONTROL PROTEIN, BSA, AT 0.010 HZ. THE INSERT IS THE CALIBRATION CURVE FOR 0.010 HZ. THE VALUE OF R^2 IS 0.99. THE K_D WAS DETERMINED TO BE 4.2 ± 0.2 NM. 85

FIGURE 5.6. RESPONSE IN Z' % TO VARIOUS SERUM CONCENTRATIONS (1 %, 5 %, 10 %, 20 %, 50 %, 80 %, AND 100 %) IS DISPLAYED. THE BLACK BAR ILLUSTRATES THE SPECIFIC RESPONSE TO 50 PM INSULIN. COMPARING TO THE RESPONSE TO 50 PM INSULIN (~ 10 %), THE NON-SPECIFIC RESPONSE IN 80 % IS STILL TINY (~ 0.5 %); IT SUGGESTS THAT THIS BIOSENSOR IS THEREFORE, LIKELY TO DEMONSTRATE HIGH RESISTANCE TO IRRELEVANT COMPONENTS, EVEN IN 80 % SERUM. 86

FIGURE 5.7. THE BODE PLOTS OBSERVED OF VARIOUS FILMS IN 10 MM PBS (PH 7.4) SOLUTION, UNDER NON-FARADAIC EIS TECHNIQUE: (A) BARE GOLD SURFACE, (B) PEG THIOL SAM, (C) INSULIN ANTIBODY INTERFACE. 87

FIGURE 5.8. THE FREQUENCY-DEPENDENT RESPONSES IN Z' RECORDED ON AN ANTIBODY FILM, INCUBATED WITH FOUR DIFFERENT CONCENTRATIONS OF ANTIGEN: (A) 0 PM, THE ANTIBODY INTERFACE, (B) 50 PM, (C) 10 NM, AND (D) 100 NM. 88

FIGURE 5.9. COMPARING THE CONCENTRATION-DEPENDENT RESPONSE IN Z' AT FOUR SELECTED FREQUENCIES (0.010, 0.012, 0.014 AND 0.016). CRITICAL INFORMATION IS SHOWN IN THE TABLE (TOP), SUCH AS SENSITIVITY (THE SLOPE), R^2, LOD AND LINEAR RANGE. LOD AND R^2, PRESENTING THE MOST SIGNIFICANT VARIATION AMONG FREQUENCIES, ARE HIGHLIGHTED. ALL THE INFORMATION WAS DETERMINED FROM THE ANALYTICAL CURVES (BOTTOM). 89

FIGURE 5.10. THE LANGMUIR ISOTHERM PLOTS OF THE RESPONSES TO THE TARGET, INSULIN, AND THE CONTROL PROTEIN, BSA, AT 0.010 HZ. THE INSERT IS THE CALIBRATION CURVE FOR 0.010 HZ. THE VALUE OF R^2 IS 0.96. THE K_D WAS DETERMINED TO BE 0.69 ± 0.10 NM. 90

FIGURE 5.11. THE RESPONSE IN Z' % TO VARIOUS SERUM CONCENTRATIONS (10 %, 20 %, 50 %, AND 80 %) IN 10 MM PBS SOLUTIONS IS DISPLAYED. THE BLACK BAR ILLUSTRATES THE SPECIFIC RESPONSE TO 50 PM INSULIN. COMPARING TO THE RESPONSE TO 50 PM INSULIN (~ 12.5 %), THE NON-SPECIFIC RESPONSE IN 80 % IS STILL TINY (~ 0.5 %); IT SUGGESTS THAT THIS BIOSENSOR IS CAPABLE OF RESISTING NON-SPECIFIC ADSORPTION IN 50 % SERUM. 91

FIGURE 6.1. ONE EXAMPLE OF FREQUENCY-DEPENDENT RESPONSES IN NORMALISED Z'' (R_N %) (A), NOISE (*CV*) (B) AND THE RELATIVE SENSITIVITY (*RS*) (C). AN FFT SMOOTHED ANALYSIS WAS APPLIED TO FIND THE MAXIMUM. ACCORDING TO (A), 0.04 HZ SEEMS TO BE THE BEST FREQUENCY WHERE DEMONSTRATES THE MOST SENSITIVE RESPONSE. HOWEVER, IF TAKING NOISE INTO ACCOUNT, 0.06 HZ SHOULD BE THE BEST FREQUENCY (C)..... 96

FIGURE 6.2. THE OPTIMUM RESPONSES (RS_{MAX}), FOR 1 NM INSULIN, OF R_{CT} AND ALL INVESTIGATED PARAMETERS BASED ON IMMITTANCE FUNCTIONS, AND THE OPTIMUM FREQUENCY RANGES, WERE DEMONSTRATED ((A) FARADAIC EIS, (B) NON-FARADAIC EIS). THE RESPONSE FOR R_{CT} IS NOT FREQUENCY DEPENDENT, IN THE BLACK BAR. ERROR BARS WERE OBTAINED BY THREE REPETITIONS ON THE SAME ELECTRODE. CORRESPONDING RESULTS HAVE BEEN OBSERVED ON THREE INDIVIDUAL DETECTIONS. THE OPTIMUM PARAMETERS FOR FARADAIC EIS WERE OBSERVED TO BE Z' AND M'' AT LOW FREQUENCY (0.01 – 0.5 HZ), BOTH OF WHICH ARE SIGNIFICANTLY MORE RESPONSIVE THAN R_{CT}, WHILE THOSE FOR NON-FARADAIC EIS ARE C', C''/C', AND M''/M' AT HIGH FREQUENCY (10 – 300 KHZ)..... 97

FIGURE 6.3. ANALYTICAL CURVES OF THE INSULIN ASSAYS, IN THE SELECTED PARAMETERS. THE NUMBERS IN THE BRACKETS ARE THE VALUES OF THE SLOPE OF EACH ANALYTICAL CURVE, WHICH REPRESENTS THE SENSITIVITY. THE VALUES OF SLOPE ARE SHOWN IN THE BRACKETS, EXPRESSED IN % PER DECADE CONCENTRATION. (A) FARADAIC EIS, (B) NON-FARADAIC EIS. ERROR BARS WERE OBTAINED BY THREE REPETITIONS ON THE SAME ELECTRODE. CORRESPONDING RESULTS HAVE BEEN OBSERVED ON THREE INDIVIDUAL DETECTIONS. 100